



NTNU – Trondheim
Norwegian University of
Science and Technology

An Application Prototype for Hydrogen Permeation Data Analysis

Bendik Wendt Simonsen

Master of Science in Engineering and ICT

Submission date: June 2015

Supervisor: Afrooz Barnoush, IPM

Co-supervisor: Martin Steinert, IPM

Norwegian University of Science and Technology
Department of Engineering Design and Materials

THE NORWEGIAN UNIVERSITY
OF SCIENCE AND TECHNOLOGY
DEPARTMENT OF ENGINEERING DESIGN
AND MATERIALS

**MASTER THESIS SPRING 2015
FOR
STUD.TECHN. Bendik Wendt Simonsen**

An application prototype for hydrogen permeation data analysis
En applikasjons prototype for hydrogen gjennomtrengnings dataanalyse

Within this project the candidate will develop an application prototype which can be used by non-expert users to rapidly and simply measure the hydrogen diffusion rate in a given ferritic steel sample. The prototype includes a graphical user interface for automatic evaluation of the data and providing a value of the hydrogen diffusion coefficient and its activation energy.

Formal requirements:


Three weeks after start of the thesis work, an A3 sheet illustrating the work is to be handed in. A template for this presentation is available on the IPM's web site under the menu "Masteroppgave" (<http://www.ntnu.no/ipm/masteroppgave>). This sheet should be updated one week before the master's thesis is submitted.

Risk assessment of experimental activities shall always be performed. Experimental work defined in the problem description shall be planned and risk assessed up-front and within 3 weeks after receiving the problem text. Any specific experimental activities which are not properly covered by the general risk assessment shall be particularly assessed before performing the experimental work. Risk assessments should be signed by the supervisor and copies shall be included in the appendix of the thesis.


The thesis should include the signed problem text, and be written as a research report with summary both in English and Norwegian, conclusion, literature references, table of contents, etc. During preparation of the text, the candidate should make efforts to create a well arranged and well written report. To ease the evaluation of the thesis, it is important to cross-reference text, tables and figures. For evaluation of the work a thorough discussion of results is appreciated.

The thesis shall be submitted electronically via DAIM, NTNU's system for Digital Archiving and Submission of Master's theses.

The contact persons are Afroz Barnoush and Martin Steinert



Torgeir Welo
Head of Division



Afroz Barnoush
Professor/Supervisor

I think that we're all in our private traps, clamped in them, and none of us can ever get out. We scratch and we claw, but only at the air, only at each other, and for all of it, we never budge an inch.

- Norman Bates,

Psycho (1960)

Preface

The application development presented in this Master thesis has been carried out during a period from January to June 2015 at Norwegian University of Science and Technology, Faculty of Engineering Science and Technology, Department of Engineering Design and Materials. It is based on experimental work carried out at the same department, during the period October 2014 to June 2015.

Acknowledgements

This work would be impossible to accomplish without the contribution of multiple people, which I would like to express my gratitude to.

First I wish to thank my supervisor at IPM, Afrooz Barnoush, as well as my co-supervisor, Martin Steinert, for making the realization of this thesis possible.

Secondly, I wish to acknowledge Malin Berglund Hope for her invaluable assistance throughout the entire process, her patience when being encountered with numerous misunderstandings, and her extensive testing of the application editions developed.

I also would like to mention Cristian Torres Rodriguez for showing me the existing software related to an older permeation cell, and my good friend David Alex Borden, for reviewing my code and providing professional advice regarding the architecture of my application.

Finally, I would like to dedicate this work to my parents, for their unwavering support and encouragement.

Abstract

An application has been developed in order to analyze data results from experiments revolving adsorption and diffusion of hydrogen in X70 and Fe 3wt.% Si steel. The experiment was performed under cathodic charging conditions at varying temperatures from 30 degrees to 75 degrees, in custom made equipment designed according to the ASTM standard [1]. The principle of the equipment was based on the article written by Devanathan and Stachurski [2] where a permeation technique is described. Hydrogen is produced electrochemically in one cell, before it diffuses through the specimen and is detected in the other cell. The application developed in this paper reads the result data retrieved from this procedure, and extracts two coherent columns representing the current readings and the elapsed time. By utilizing Fick's laws of diffusion, Iino's numerical methods, and other contributing theoretical work different approaches to compute and display parameters describing material properties is implemented. The ASTM standard engages the analysis of the experiment data according to Fick's laws and the elapsed time method in order to compute the concentrations and the effective diffusion coefficient respectively. These approaches are also represented in the application, but they do not consider the trapping present in the material, and therefore gives an inaccurate approximation of these occurrences. Iino's methods are used to acquire more information concerning reversible and irreversible traps in the material.

Sammendrag

En applikasjon har blitt utviklet for å analysere resultater fra eksperimenter relatert til adsorpsjon og diffusjon av hydrogen i X70 og Fe 3wt.% Si stål. Eksperimentene ble utført ved katodiske ladeforhold, under varierende temperaturer fra 30 til 75 grader celsius, i spesiallaget utstyr utformet i henhold til ASTM standarden [1]. Prinsippet bak utstyret er basert på en artikkel skrevet av Devanathan and Stachurski [2], hvor en diffusjons teknikk blir beskrevet. Hydrogen blir produsert elektrokjemisk i en celle, før den blir diffundert igjennom metallprøven og detektert i den andre cellen. Applikasjonen som ble utviklet i denne oppgaven leser resultatene hentet fra denne prosedyren, og trekker ut to samstemte kolonner som representerer strøm- og tidsavlesningene, henholdsvis. Ved å bruke Ficks lover om diffusjon, lios numeriske metoder og andre medvirkende teoretiske arbeider, ble forskjellige tilnærmings metoder for å utregne og vise parameterne som beskriver materialets egenskaper implementert. ASTM standarden utfører analysen av eksperimentdataen etter Ficks lover og forløpt tid metoden for å utregne konsentrasjoner og den effektive diffusjonskoeffisienten, respektivt. Disse tilnærmingsmetodene blir også representert i applikasjonen, men de tar ikke hensyn til fellene i materialet, og gir derfor en unøyaktig approksimasjon av disse forekomstene. Iios metoder blir brukt for å tilegne mer informasjon vedrørende reversible og irreversible feller i materialet.

Background

Hydrogen embrittlement and associated failures is a big problem in different industries, such as offshore, aircraft, and nuclear. Both hydrogen sources and stress contributors must be present, in order for a failure to occur from hydrogen embrittlement. The experimental work described in this paper focuses on hydrogen evolving from cathodic protection systems in the offshore industry. The subsea equipment used during oil and gas exploration and production often operates in extreme conditions at considerable depths. When this equipment fails, the consequences are safety risks, environmental pollution, and costly shutdowns. The offshore industry relies on high strength steels, in order to withstand the forces experienced under operation. The microstructure related to high strength steel is very susceptible to hydrogen failure, and applied stresses related to the problem are applied during the production of the equipment. Various conditions need to be taken into account when designing the different components, and should be reliable over longer operating periods. The first descriptions of hydrogen embrittlement were in 1874, before the submerged oil wells in water were developed. The earliest theories revolving around hydrogen induced failure did therefore not consider the conditions related to the offshore industry, and the problem is still not fully understood. The objective of this paper is to map the problems related to hydrogen embrittlement, elaborate different mathematical models developed to describe the procedure of hydrogen diffusion, create an application analyzing retrieved data from experiments reenacting hydrogen diffusion based on the mathematical approaches, and presenting the results in a manageable manner, describing the influence of the different retrieved parameters extracted from the data.

Contents

<i>Preface</i>	iv
<i>Acknowledgements</i>	vi
<i>Abstract</i>	viii
<i>Sammendrag</i>	x
<i>Background</i>	xii
<i>List of Figures</i>	xvi
<i>List of Tables</i>	xxii
<i>Nomenclature</i>	xxiii
<i>List of Symbols</i>	xxiv
1 Introduction.....	1
2 Theory	3
2.1 Hydrogen Embrittlement	3
2.2 Hydrogen Sources.....	5
2.2.1 Cathodic Protection	5
2.2.2 Phosphating	6
2.2.3 Pickling.....	6
2.2.4 Electroplating	6
2.2.5 Welding	6
2.2.6 Hydrogen Sulfide	7
2.3 HE Mechanisms.....	7
2.3.1 HELP.....	7
2.3.2 HEDE	8
2.4 Hydrogen Diffusion.....	9
2.4.1 X70 Steel	10
2.4.2 FeSi Steel.....	12
2.4.3 Main Mechanisms	12
2.4.4 Electrochemical Hydrogen Permeation Technique	13
2.5 Trapping.....	15
2.5.1 Properties.....	15
2.5.2 Reversible and Irreversible Traps	15
3 Calculations.....	16
3.1 Fick's Laws of Diffusion	16

3.2	Analysis of Permeation Transient.....	16
3.2.1	Steady State Permeation Flux	17
3.2.2	Time Dependent Permeation Flux.....	17
3.2.3	Elapsed Time Method	17
3.2.4	Breakthrough Time Method	18
3.2.5	Slope Method	18
3.3	Sub-Surface Hydrogen Concentration.....	19
3.4	Numerical Solutions	20
3.4.1	Numerical Approach to Fick's Laws	21
3.4.2	Caskey and Pillinger.....	22
3.4.3	Thomas and Stern.....	24
3.4.4	Iino	27
3.4.5	Curve Fitting	29
4	Software	31
4.1	Software Architecture.....	31
4.1.1	Architectural Pattern	31
4.1.2	Model-View-Controller.....	31
4.2	Framework.....	33
4.2.1	Software Framework	33
4.2.2	Swing.....	33
4.2.3	JFreeChart	34
4.3	Implementation.....	35
4.3.1	Functional Requirements.....	35
4.3.2	Non-functional Requirements	38
4.3.3	System	39
5	Results.....	44
5.1	Functional properties	44
5.1.1	File Reader	44
5.1.2	Data Display.....	45
5.1.3	Chart Generator	46
5.1.4	Curve Fitter	48
5.1.5	Noise Reduction	50
5.2	Iino's Method	62

5.3	Non-functional Properties.....	86
5.3.1	Usability	86
5.3.2	Modifiability.....	86
5.3.3	Performance	87
6	Discussion	89
6.1	System Functionalities.....	89
6.2	Iino's Results	91
6.3	Software Attributes.....	92
7	Conclusion	94
8	Future work.....	95
	<i>Bibliography</i>	97
	<i>Appendix A: Class Diagram</i>	100
	<i>Appendix B: Diffusion Calculator User Guide</i>	102
	<i>Step 1: Choosing a File</i>	102
	<i>Step 2: Input a Starting Point</i>	102
	<i>Step 3: Input the Duration</i>	102
	<i>Step 4: Input Correct Parameters</i>	103
	<i>Step 5: Calculating Values and Plotting</i>	103
	<i>Step 6: Current/Time Chart</i>	104
	<i>Step 7: Save</i>	105
	<i>Step 8: Add Transient</i>	105
	<i>Step 9: Restore</i>	106
	<i>Step 10: Fick's Lattice and Elapsed Time Curve</i>	106
	<i>Step 11: Fick's Curve Fitting</i>	107
	<i>Step 12: Iino's Curve Fitting</i>	107
	<i>Step 13: Iino's filter</i>	108
	<i>Step 14: Custom Pass Filter</i>	108
	<i>Step 15: Zooming and Mouse Clicking</i>	109
	<i>Step 16: Permeation Chart</i>	110
	<i>Step 17: Update Button</i>	111
	<i>Appendix C: Application Editions</i>	112
	<i>Appendix D: Hope Data</i>	118

List of Figures

Figure 2-1: The three main factors of HE, and their properties. Obtained from Barnoush [5].	4
Figure 2-2: Display of the HELP mechanism, figure from Lynch [16]	8
Figure 2-3: Displaying the HEDE mechanism, taken from Lynch [16]	9
Figure 2-4: A graph retrieved from Park <i>et al</i> [21] describing the processes performed in order to make the different steel tested	11
Figure 2-5: Optical microstructures for the steel tested by Park <i>et al</i> [21]. (a) and (c) shows ferrite/degenerated pearlite, (b) is ferrite/acicular ferrite, and (d) shows ferrite/bainite.	11
Figure 2-6: Base centered cubic structure (BCC) and face centered cubic structure (FCC) shows the lattice structure for ferritic and austenitic microstructure respectively, while body centered tetragonal structure (BCT) and hexagonal close packed structure (HCP) are different types of martensitic microstructure.	12
Figure 2-7: Illustration of Devanathan and Stachurski 's cell, adopted from their publication [2]. It displays the specimen tested (6) in the middle of two cells, one anodic and one cathodic side.	13
Figure 2-8: Illustration of Hope's set up, borrowed from her paper [19].	14
Figure 3-1: Graphical representation of the elapsed time method, adapted from Fallamohamadi <i>et al</i> [26]. Here j_{∞} represents the hydrogen steady state flux, and the left chart is a close up of the region marked in the right chart.	18
Figure 3-2: Experimental transients plotted together with theoretical solutions, derived from Fick's second law. Left and right chart represents F22 and X65 steel samples respectively. Figure adopted from Fallahmohammadi <i>et al</i> [26]	21
Figure 3-3: Permeation graphs adapted from Caskey and Pillinger [29]. they represent tendencies when individual parameters are increased. Explanations included in illustration. x-axis parameter a equals sample thickness L in this paper	23
Figure 3-4: Normalized flux plotted against reduced time, with different β increments to the left, and ν increments to the right. Charts adapted from Thomas and Stern [30]	26
Figure 3-5: Illustration of the influence from κ and λ/μ on the permeation flux. Chart adapted from Iino [31]	29
Figure 4-1: Sketch displaying a traditional Model-View-Controller structure, with the relations between the components.	32
Figure 4-2: The three main class types in a MVC structure. Adapted from Buschmann <i>et al</i> [32]	32
Figure 4-3: A sequence diagram describing some of the interactions between the classes in a Model-View-Controller architectural pattern. Diagram copied from Buschmann <i>et al</i> [32]	33
Figure 4-4: Containment hierarchy in a Swing application. Adopted from Sharan's book [34]	34
Figure 4-5: Example chart, built with the JFreeChart framework. Adopted from Gilbert [35]	35
Figure 4-6: Use-case diagram illustrating an user selecting a file to read, who gets prompted with range selection, and selects appropriate range. the System reads data from file	36
Figure 4-7: Use case diagram illustrating a user receiving a display of data, making an input that updates the data, which in turn enables calculations to be made	36

Figure 4-8: Use case diagram showing a user choosing a chart type, and processing the display by zooming, copying or retrieving data. An extension to the charts will be to apply additional plots	37
Figure 4-9: Use case showing a user initiate a curve fitting, which then updates and displays the results. The user is also able to apply filter, or double click on unwanted noise	37
Figure 4-10: Small class diagram presenting all the classes and their relations. bigger class diagrams depicting all the belonging methods and fields is included in Appendix A: <i>Class Diagram</i>	39
Figure 4-11: Example .dta file. The columns read are the time column (T) in seconds (s), and the charging current column (Vu) in ampere (A).....	40
Figure 5-1: JFreeChart component from the swing framework 4.2.2), letting the user select a file from the device he is using	44
Figure 5-2: JFrame container from the swing framework4.2.2), containing columns with data both extracted and computed from the .dta file, results from effective diffusion coefficient and concentration calculation, and parameters from performed curve fittings.....	46
Figure 5-3: JFreeChart chart from the JFreeChart framework(4.2.3), displaying the experimental data, Fick's lattice diffusion and effective diffusion curve, and two extra transients all illustrating the normalized flux as a function of normalized time	47
Figure 5-4: JFreeChart chart displaying the same data as Figure 5-3 illustrating the permeation current as a function of time.....	47
Figure 5-5: Chart displaying normalized flux as a function of normalized time for a ferrosilicon sample, Tested at 50 degrees. Iino's and Fick's curve fittings are plotted together with the experimental data	48
Figure 5-6: Chart displaying cathodic current as a function of time for a ferrosilicon sample, Tested at 50 degrees. Iino's and Fick's curve fittings are plotted together with the experimental data	49
Figure 5-7 : Chart displaying normalized flux as a function of normalized time for an X70 sample, Tested at 30 degrees. Iino's and Fick's curve fittings are plotted together with the experimental data	49
Figure 5-8: Chart displaying cathodic current as a function of time for an X70 sample, Tested at 30 degrees. Iino's and Fick's curve fittings are plotted together with the experimental data.....	50
Figure 5-9: Chart displaying normalized flux as a function of normalized time for a ferrosilicon sample, Tested at 50 degrees. The Iino approximation has low deviation before noise reduction, but the highest point is determined by an interference	51
Figure 5-10: Chart displaying normalized flux as a function of normalized time for a ferrosilicon sample, Tested at 50 degrees. The noise have been reduced manually, which gives a slightly better Iino approximation	51
Figure 5-11: Chart displaying normalized flux as a function of normalized time for a ferrosilicon sample, Tested at 50 degrees. The noise have been reduced by Iino's filter, giving the same approximation as in Figure 5-10	52
Figure 5-12: Chart displaying normalized flux as a function of normalized time for a ferrosilicon sample, Tested at 50 degrees. The noise have been reduced using the low pass filter, giving a bit better approximation, but failing at removing the worst noise	52

Figure 5-13: Chart displaying normalized flux as a function of normalized time for a ferrosilicon sample, Tested at 50 degrees. Noise reduced using low pass filter and manual data removal, resulting in the same approximation as Figure 5-10 and Figure 5-11..... 53

Figure 5-14: Chart displaying cathodic current as a function of time for a ferrosilicon sample, Tested at 50 degrees. The Iino approximation has low deviation before noise reduction, but the highest point is determined by an interference..... 53

Figure 5-15: Chart displaying cathodic current as a function of time for a ferrosilicon sample, Tested at 50 degrees. The noise have been reduced manually, which gives a better Iino approximation..... 54

Figure 5-16: Chart displaying cathodic current as a function of time for a ferrosilicon sample, Tested at 50 degrees. The noise have been reduced using the Iino's method, which removes to much data, giving a wrong approximation by Iino's method 54

Figure 5-17: Chart displaying cathodic time as a function of time for a ferrosilicon sample, Tested at 50 degrees. The noise have been reduced using the low pass filter, giving slightly better approximation 55

Figure 5-18: Chart displaying cathodic current as a function of time for a ferrosilicon sample, Tested at 50 degrees. Noise reduced by applying the low pass filter, and using the data remover function, yielding the same approximation as in Figure 5-17 55

Figure 5-19: Chart displaying normalized flux as a function of normalized time for an X70 sample, Tested at 50 degrees. The experimental data is very noisy, and the Iino approximation is not accurate..... 57

Figure 5-20: Chart displaying normalized flux as a function of normalized time for an X70 sample, Tested at 50 degrees. The noise have been reduced manually, which gives a better Iino approximation 57

Figure 5-21: Chart displaying normalized flux as a function of normalized time for an X70 sample, Tested at 50 degrees. The noise have been reduced using Iino's low pass filter, removing to much experimental data, giving an wrong approximation by Iino's method 58

Figure 5-22: Chart displaying normalized flux as a function of normalized time for an X70 sample, Tested at 50 degrees. The noise have been reduced using the low pass filter multiple times, giving a better representation of the experimental data, but still giving an wrong approximation by Iino's method 58

Figure 5-23: Chart displaying normalized flux as a function of normalized time for an X70 sample, Tested at 50 degrees. The noise have been reduced using the low pass filter one time to reduce the small differences, and then manually removing the biggest deviations. This gives the best approximation..... 59

Figure 5-24: Chart displaying cathodic current as a function of time for an X70 sample, Tested at 50 degrees. The experimental data is very noisy, and the Iino approximation is not accurate..... 59

Figure 5-25: Chart displaying cathodic current as a function of time for an X70 sample, Tested at 50 degrees. The noise have been reduced manually, which gives a better Iino approximation..... 60

Figure 5-26: Chart displaying cathodic current as a function of time for an X70 sample, Tested at 50 degrees. The noise have been reduced using Iino's low pass filter, removing to much experimental data, giving an wrong approximation..... 60

Figure 5-27: Chart displaying cathodic time as a function of time for an X70 sample, Tested at 50 degrees. The noise have been reduced using the low pass filter multiple times, giving a better representation of the experimental data, but still giving an wrong approximation by Iino’s method..... 61

Figure 5-28: Chart displaying cathodic current as a function of time for an X70 sample, Tested at 50 degrees. The noise have been reduced using the low pass filter one time to reduce the small differences, and then manually removing the biggest deviations. This gives the best approximation..... 61

Figure 5-29: Chart displaying normalized flux as a function of normalized time for an X70 sample, Tested at 75 degrees. The Iino numerical curve fitting is fairly accurate 63

Figure 5-30: Chart displaying cathodic current as a function of time for an X70 sample, Tested at 75 degrees. The Iino numerical curve fitting is fairly accurate 63

Figure 5-31: Chart displaying normalized flux as a function of normalized time for an X70 sample, Tested at 75 degrees. The Iino numerical curve fitting with kappa set to 1 is added . 64

Figure 5-32: Chart displaying normalized flux as a function of normalized time for an X70 sample, Tested at 75 degrees. The Iino numerical curve fitting with kappa set to 10 is added 64

Figure 5-33: Chart displaying normalized flux as a function of normalized time for an X70 sample, Tested at 75 degrees. The Iino numerical curve fitting with kappa set to 100 is added 65

Figure 5-34: Chart displaying cathodic current as a function of time for an X70 sample, tested at 75 degrees. The Iino numerical curve fitting with kappa set to 1 is added 65

Figure 5-35: Chart displaying cathodic current as a function of time for an X70 sample, tested at 75 degrees. The Iino numerical curve fitting with kappa set to 10 is added 66

Figure 5-36: Chart displaying cathodic current as a function of time for an X70 sample, tested at 75 degrees. The Iino numerical curve fitting with kappa set to 100 is added 66

Figure 5-37: Chart displaying normalized time as a function of normalized time for an X70 sample, tested at 75 degrees. The Iino numerical curve fitting with D_{eff} set to 0 is added 67

Figure 5-38: Chart displaying normalized time as a function of normalized time for an X70 sample, tested at 75 degrees. The Iino numerical curve fitting with D_{eff} set to 1 is added 68

Figure 5-39: Chart displaying normalized time as a function of normalized time for an X70 sample, tested at 75 degrees. The Iino numerical curve fitting with D_{eff} set to the elapsed time D_{eff} divided by 10 is added 68

Figure 5-40: Chart displaying normalized time as a function of normalized time for an X70 sample, tested at 75 degrees. The Iino numerical curve fitting with D_{eff} set to the elapsed time D_{eff} divided by 100 is added 69

Figure 5-41: Chart displaying normalized time as a function of normalized time for an X70 sample, tested at 75 degrees. The Iino numerical curve fitting with D_{eff} set to the elapsed time D_{eff} multiplied by 10 is added..... 69

Figure 5-42: Chart displaying normalized time as a function of normalized time for an X70 sample, tested at 75 degrees. The Iino numerical curve fitting with D_{eff} set to the elapsed time D_{eff} multiplied by 100 is added..... 70

Figure 5-43: Chart displaying normalized time as a function of normalized time for an X70 sample, tested at 75 degrees. The Iino numerical curve fitting with D_{eff} set to the lattice diffusion coefficient D_l is added..... 70

Figure 5-44: Chart displaying cathodic current as a function of time for an X70 sample, tested at 75 degrees. The Iino numerical curve fitting with D_{eff} set to 0 is added 71

Figure 5-45: Chart displaying cathodic current as a function of time for an X70 sample, tested at 75 degrees. The Iino numerical curve fitting with D_{eff} set to 1 is added 71

Figure 5-46: Chart displaying cathodic current as a function of time for an X70 sample, tested at 75 degrees. The Iino numerical curve fitting with D_{eff} set to the elapsed time D_{eff} divided by 10 is added..... 72

Figure 5-47: Chart displaying cathodic current as a function of time for an X70 sample, tested at 75 degrees. The Iino numerical curve fitting with D_{eff} set to the elapsed time D_{eff} divided by 100 is added..... 72

Figure 5-48: Chart displaying cathodic current as a function of time for an X70 sample, tested at 75 degrees. The Iino numerical curve fitting with D_{eff} set to the elapsed time D_{eff} multiplied by 10 is added..... 73

Figure 5-49: Chart displaying cathodic current as a function of time for an X70 sample, tested at 75 degrees. The Iino numerical curve fitting with D_{eff} set to the elapsed time D_{eff} multiplied by 100 is added..... 73

Figure 5-50: Chart displaying cathodic current as a function of time for an X70 sample, tested at 75 degrees. The Iino numerical curve fitting with D_{eff} set to the lattice diffusion coefficient D_l is added 74

Figure 5-51: Chart displaying normalized time as a function of normalized time for an X70 sample, tested at 75 degrees. The Iino numerical curve fitting with lambda set to 0 is added 75

Figure 5-52: Chart displaying normalized time as a function of normalized time for an X70 sample, tested at 75 degrees. The Iino numerical curve fitting with lambda set to 1 is added 75

Figure 5-53: Chart displaying normalized time as a function of normalized time for an X70 sample, tested at 75 degrees. The Iino numerical curve fitting with lambda set to 10 is added 76

Figure 5-54: Chart displaying normalized time as a function of normalized time for an X70 sample, tested at 75 degrees. The Iino numerical curve fitting with lambda set to 100 is added 76

Figure 5-55: Chart displaying normalized time as a function of normalized time for an X70 sample, tested at 75 degrees. The Iino numerical curve fitting with lambda set to 1000 is added 77

Figure 5-56: Chart displaying normalized time as a function of normalized time for an X70 sample, tested at 75 degrees. The Iino numerical curve fitting with lambda set to 10000 is added 77

Figure 5-57: Chart displaying cathodic current as a function of time for an X70 sample, tested at 75 degrees. The Iino numerical curve fitting with lambda set to 0 is added..... 78

Figure 5-58: Chart displaying cathodic current as a function of time for an X70 sample, tested at 75 degrees. The Iino numerical curve fitting with lambda set to 1 is added..... 78

Figure 5-59: Chart displaying cathodic current as a function of time for an X70 sample, tested at 75 degrees. The Iino numerical curve fitting with lambda set to 10 is added..... 79

Figure 5-60: Chart displaying cathodic current as a function of time for an X70 sample, tested at 75 degrees. The Iino numerical curve fitting with lambda set to 100 is added..... 79

Figure 5-61: Chart displaying cathodic current as a function of time for an X70 sample, tested at 75 degrees. The Iino numerical curve fitting with lambda set to 1000 is added..... 80

Figure 5-62: Chart displaying cathodic current as a function of time for an X70 sample, tested at 75 degrees. The Iino numerical curve fitting with lambda set to 10000 is added..... 80

Figure 5-63: Chart displaying normalized time as a function of normalized time for an X70 sample, tested at 75 degrees. The Iino numerical curve fitting with my set to 1 is added..... 81

Figure 5-64: Chart displaying normalized time as a function of normalized time for an X70 sample, tested at 75 degrees. The Iino numerical curve fitting with my set to 10 is added..... 82

Figure 5-65: Chart displaying normalized time as a function of normalized time for an X70 sample, tested at 75 degrees. The Iino numerical curve fitting with my set to 100 is added... 82

Figure 5-66: Chart displaying normalized time as a function of normalized time for an X70 sample, tested at 75 degrees. The Iino numerical curve fitting with my set to 1000 is added. 83

Figure 5-67: Chart displaying normalized time as a function of normalized time for an X70 sample, tested at 75 degrees. The Iino numerical curve fitting with my set to 10000 is added83

Figure 5-68: Chart displaying cathodic current as a function of time for an X70 sample, tested at 75 degrees. The Iino numerical curve fitting with my set to 1 is added..... 84

Figure 5-69: Chart displaying cathodic current as a function of time for an X70 sample, tested at 75 degrees. The Iino numerical curve fitting with my set to 10 is added..... 84

Figure 5-70: Chart displaying cathodic current as a function of time for an X70 sample, tested at 75 degrees. The Iino numerical curve fitting with my set to 100 is added..... 85

Figure 5-71: Chart displaying cathodic current as a function of time for an X70 sample, tested at 75 degrees. The Iino numerical curve fitting with my set to 1000 is added..... 85

Figure 5-72: Chart displaying cathodic current as a function of time for an X70 sample, tested at 75 degrees. The Iino numerical curve fitting with my set to 10000 is added..... 86

List of Tables

Table 5-1: Table displaying results from the curve fittings in Figure 5-5 to Figure 5-8.....	50
Table 5-2: Results from noise reduction procedures for normalized flux chart data from ferrosilicon material experiments depicted in Figure 5-9 to Figure 5-13.....	56
Table 5-3: Results from noise reduction procedures for cathodic current chart data from ferrosilicon material experiments depicted in Figure 5-14 to Figure 5-18.....	57
Table 5-4: Results from noise reduction procedures for normalized flux chart data from x70 material experiments depicted in Figure 5-19 to Figure 5-28.....	62
Table 5-5: Results from the curve fitting of an X70 material experimental data set, depicted by the chart in Figure 5-29 and Figure 5-30.....	63
Table 5-6: Overview of the initial conditions and boundary conditions for the effective diffusion coefficient	67
Table 5-7: Overview of the initial conditions and boundary conditions for the lambda variable	74
Table 5-8: Overview of the initial conditions and boundary conditions for the my variable ..	81
Table 5-9: Old and new software running Iino's method on the same experimental data. Results displayed for both runs, and the difference is computed. The old software use the brute force technique, with untrained boundaries and iniital conditions, resulting in bad runtime and accuracy. The new software includes an initial and boundary condition method evovling throughout the analysis, which gives better accuracy and decreased runtime. The old software's kappa value was changed in order to match the new software.....	87
Table 5-10 : Old and new software running Iino's method on the same experimental data. Results displayed for both runs, and the difference is computed. The old software uses the brute force technique, with untrained boundaries and initial conditions, resulting in bad runtime and accuracy. The new software includes an initial and boundary condition method evolving throughout the analysis, which gives better accuracy and decreased runtime. The old software's kappa value was changed in order to match the new software.....	88

Nomenclature

BCC	Body centered cubic
BCT	Body centered cubic
BM	Base material
CP	Cathodic protection
FCC	Face centered cubic
FW	Framework
H ₂	Hydrogen molecule
H ₂ S	Hydrogen Sulphide
HAZ	Heat affected zone
HCP	Hexagonal close packed
HE	Hydrogen embrittlement
HEDE	Hydrogen enhanced decohesion
HELP	Hydrogen enhanced localized plasticity
HIC	Hydrogen induced cracking
HSC	Hydrogen stress cracking
SEM	Scanning Electron Microscope
MVC	Model-View-Controller
GUI	Graphical user interface

List of Symbols

D	Diffusion coefficient
D_0	Maximum diffusion coefficient
E	Activation energy
T	Absolute temperature
R	Gas constant
J_{SS}	Steady state flux
D_l	Lattice diffusion coefficient
C	Concentration
x	Distance variable
t	Time
I_{SS}	Steady state permeation current
A	Exposed area of specimen
F	Faraday's constant
C_0	Sub-surface concentration
L	Thickness of the specimen
$J(t)$	Time dependent flux
$I(t)$	Time dependent permeation current
t_{lag}	Elapsed time at $J(t)/J_{SS}$
D_{eff}	Effective diffusion coefficient
t_b	Breakthrough time
Q	Lattice jump energy

\check{C}_0	Sub-surface concentration
M_h	Molar mass of hydrogen
\dot{C}_0	Sub-surface concentration
ρ_{steel}	Steel density
N	Density of trap sites
Θ	Fraction of occupied traps
k	Capture rate per trap
p	Release rate per trap
τ	Normalized time
λ, μ, ν	Capture and release per trap rates
β	Number of traps per input hydrogen atom
h	x-step
a	Time-step
φ	Mesh ratio
ζ	Relative Distance
S	Least squares sum
y	Actual value in least squares method
$f(t)$	Predicted value in least squares method
r	Residual in least squares method

1 Introduction

This work seeks to aid electrochemical experiments, investigating hydrogen diffusion properties in steel. By developing a user friendly analysis tool, heavy numerical approaches to data extracted from the experiment will be more intuitive to perform, quicker and more accessible, and easier to present in a straightforward way.

Chapter 2 covers the theory behind the hydrogen induced failure caused by hydrogen diffusion. In section 2.1 hydrogen embrittlement will be elaborated, discussing the different properties and factors. Section 2.2 presents the different sources of hydrogen normal for materials affected by hydrogen embrittlement, describing Cathodic Protection, Phosphating, Electroplating, Welding, and Hydrogen Sulfide. Section 2.3 comprises the two mechanisms of hydrogen embrittlement, HELP and HEDE. Section 2.4 presents the reader with the concept of hydrogen diffusion, by first informing about the two materials experimented on in relation to this work, X70 Steel and FeSi Steel, before disclosing the Main Mechanisms of the process, and presenting the Electrochemical Hydrogen Permeation Technique used during experiments. The last part of the chapter, section 2.5, revolves around trapping, discussing its Properties and its two types, namely Reversible and Irreversible Traps.

Chapter 3 presents the different mathematical calculations, methods, models, and analysis techniques studied in order to implement the software correctly. Section 3.1 will focus on Fick's laws of diffusion, which most of the other approaches are based on. Section 3.2 will introduce the reader with the analysis methods of permeation flux as described in the ASTM standard [1]. This includes the computation of Steady State Permeation Flux and Time Dependent Permeation Flux, and three common approaches to calculate the effective diffusion coefficient; the Elapsed Time Method, the Breakthrough Time Method, and the Slope Method. Section 3.3 involves the calculation of sub-surface hydrogen concentration. In the end of the chapter at section 3.4, there will be derivations of the different numerical solutions approached through this work. A Numerical Approach to Fick's Laws gives the user the theory behind several functions in the software, before more comprehensive methods, taking traps into account, are presented. Caskey and Pillinger, and Thomas and Stern have extensive methods which will be deduced, before Iino's model which is used in the software, is elaborated. In the end of the section the least squares method, utilized to perform Curve Fittings in the software is enclosed.

Chapter 4 will cover the software properties and specifics. Section 4.1 presents software architecture, and discusses the definition and use of an Architectural Pattern, before the chosen pattern Model-View-Controller will be described. Section 4.2 contains theory about frameworks, introducing the concept of Software Framework to the user, and then presenting the frameworks Swing and JFreeChart. Section 4.3 covers the implementation process of the software, enclosing the predefined Functional Requirements, and the Non-functional Requirements given to the software, and then describing the System parts which were implemented according to the requirements.

Chapter 5 presents the results obtained during the work with this paper. Section 5.1 presents the finished software and its compliance according to the functional requirements predefined in subsection 4.3.1. It will also present the initial and boundary conditions implemented for Iino's method, and depict the influence from the different parameters in the model. Section 5.3 covers the attributes of the system, and the fulfillment of the non-functional requirements from subsection 4.3.2.

Chapter 6 discusses the results and the work done in the master thesis. Section 6.1 covers functional properties, potential improvements and advantages of the functionalities. Section 6.2 discuss all results related to Iino's method. Section 6.3 aims to establish the systems attributes.

Chapter 7 concludes the paper, and gives a summary of the discussion from chapter 6.

Chapter 8 displays unfinished functionalities, possible improvements, and other recommended future work concerning the software.

2 Theory

In this chapter the theory behind hydrogen induced failure is covered. First hydrogen embrittlement will be presented, different hydrogen sources causing hydrogen embrittlement is discussed, two mechanisms of hydrogen will be elaborated, hydrogen diffusion and its mechanisms will be described, and lastly theory around traps and its properties will be reviewed.

2.1 Hydrogen Embrittlement

Hydrogen embrittlement (HE) is an undesirable effect, happening to different materials under contact with single hydrogen atoms. This process, especially important in high-strength steels, causes the metal to crack. Oriani [3] discusses the agreement that the phenomenon is due to structural imperfections developed during manufacture operations or operational processes, and interactions with dissolved hydrogen atoms. HE has been a persistent problem in different material design processes, in industries like offshore, aircraft, and nuclear.

Okwudiri [4] looks at some of the processes where HE occurs in his thesis. Operations include cathodic protection, phosphating, pickling, electroplating and welding. These operations causes movement among the atoms in the metal to relieve stress, thus resulting in dislocations or traps inside the material presented in section 2.5. The material could from these operations be exposed to hydrogen atoms on the surface. This could also be due to galvanic corrosion or other chemical reactions. Hydrogen sources are discussed further in section 2.2.

Some of the small diffusing hydrogen ions will be trapped inside micro cracks in the material, unable to escape due to high traffic of hydrogen, causing a jam. By removing the hydrogen source, actions could be performed to remove the hydrogen from the traps, if executed shortly after the disclosure. In oil and gas industries Sulfide Stress Cracking (SSC) is a notable problem, where alloys react with hydrogen sulfide, making the hydrogen either combining to hydrogen molecules (H_2) or diffusing into the metal matrix. SSC is a form of hydrogen embrittlement, but should not be confused with Stress Corrosion Cracking (SCC). This happens when the specimen is subjected to tensile mechanical stresses and a corrosive environment, sometimes caused by hydrogen embrittlement [4].

Stepwise Cracking (SWC) is when hydrogen atoms combines inside the traps into hydrogen molecules, and therefore becomes too big to be removed from the material. This phenomenon

creates blisters on the surface of the material, which will eventually create cracks. Stress Oriented Hydrogen Induced Cracking (SOHIC) and Soft Zone Cracking (SZC) are cracking events which are in the scope between SSC and SWC [4].

The three main factors of HE, as indicated by the paragraphs above, is mechanical, material, and environmental. The mechanical part consists of applied load and other forces affecting the material. The material part is what kind of microstructure the specimen has. Lastly the environmental part consists of how the material is exposed to hydrogen. All of these factors are illustrated in Figure 2-1, further discussed by Barnoush [5].

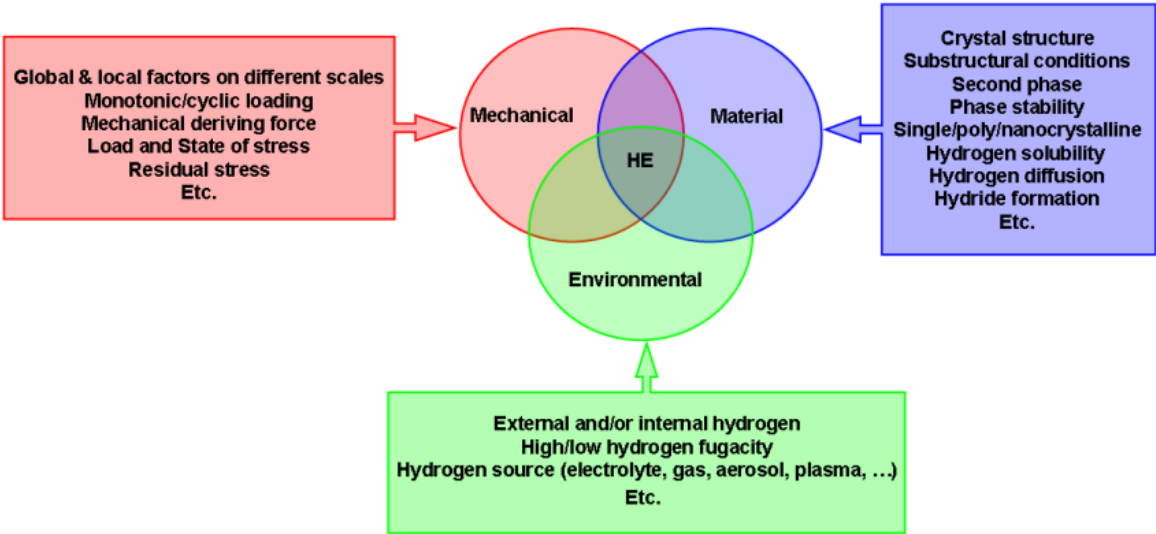


FIGURE 2-1: THE THREE MAIN FACTORS OF HE, AND THEIR PROPERTIES. OBTAINED FROM BARNOUSH [5]

In the first descriptions of HE back in 1874, Johnson [6] publishes his findings concerning an iron wire immersed in acid. He discovered that the wire, enduring bending on itself and back again up to three times without breaking, breaks after being bent only once after immersion into the acid. He weighed the wire after immersion, and found it to gain weight from the reaction. He hoped to figure out in future time, if this gain in weight was entirely due to occluded hydrogen, but he was speculating if the wire also absorbed some of the acid. His examinations gave him two reasons to believe that hydrogen was the sole cause, or inseparably connected with the changes in the iron. Firstly, only acids evolving reactions between hydrogen and iron creates these changes in the wire. Secondly, setting fire to the gas evolving from the reaction creates a flame burning with the same characteristics as that for hydrogen. While the definitions and properties of hydrogen embrittlement still are up for

discussion, Johnson's works made the discovery of similar effects in different structural material possible.

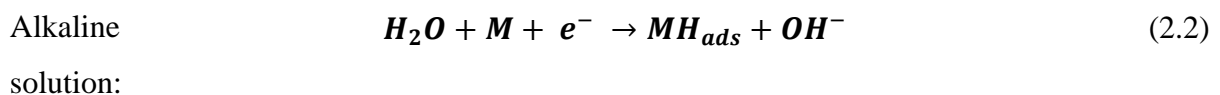
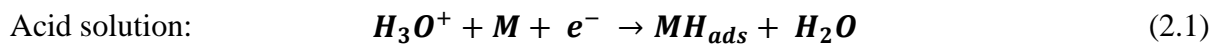
2.2 Hydrogen Sources

This section will present the most common sources of hydrogen, causing HE. As stated by Olden *et al* [7] the main sources of hydrogen in pipelines and installations are through cathodic protection, and welding, but phosphating, pickling, electroplating, and hydrogen sulfide will also be described briefly as sources.

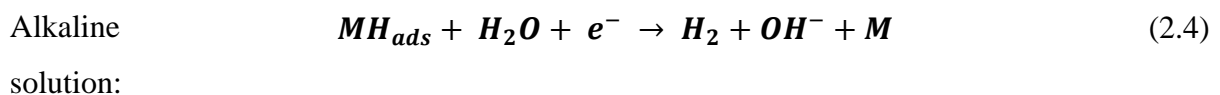
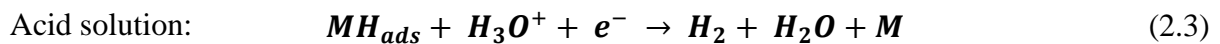
2.2.1 Cathodic Protection

Cathodic protection is applied to control corrosion of metal in several different environments. It is a well-known procedure in offshore industries, used to protect steel pipes and other constructions. The metal gets the role as a cathode in an electrochemical cell, by attaching another sacrificial metal to appear as the anode in the reaction. The sacrificial metal needs to be more easily exposed to corrosion, than the material of the construction. This could be done by attaching a chunk of the sacrificial metal, often zinc or aluminum, onto the construction, or make a coating on the construction. Steel pipes will sometimes require a current source to make the electrochemical cell more effective, due to its length.

Okwudiri [4] describes the hydrogen evolution in two stages, first by hydrogen adsorption in acid and alkaline solution.



Secondly he describes electrochemical desorption in acid and alkaline solution.



In these reactions M represents the metal. Smirnova [8] addresses the hydrogen atom generation, and concludes that hydrogen formation by water reduction becomes considerable, at low negative potentials (below 800-900 mV). This statement is supported by Okstad *et al*

[9], who documents experiments showing results which satisfies this assumption. In addition, they propose that calcareous deposits act as a catalyst for the forming of hydrogen on the metal.

2.2.2 Phosphating

Phosphating is a type of coating applied to metal, for corrosion resistance, lubricity, or as foundation for further coating or painting. A dilute solution of phosphoric acid and phosphate salts are sprayed or immersed on the metal part, where the chemicals react to form a layer of insoluble, crystalline phosphates.

The acid and metal reaction forms hydrogen gas bubbles, which sticks to the surface of the material. Kumar and Gaur [10] states that the risk for HE to occur is medium for the phosphating process. A preventive action could be to bake the material after applying the coating, but this effectiveness reduces over time.

2.2.3 Pickling

Pickling is a method used to remove any impurities on the surface of metals. The process consists of dipping the metal part in pickle liquor. This liquor contains strong acids, and one of the primary acids commonly used is hydrochloric acid. This acid pickles quickest while minimizing base metal loss. HE becomes a problem when pickling some alloys and high-carbon steels. For these materials, it is sometimes necessary to use acids such as phosphoric, nitric and hydrofluoric acid. It is also normal for the process to go over multiple steps.

2.2.4 Electroplating

Electroplating is analogous with a reverse galvanic cell, and the method is called electro deposition. The cathode in the process gets its coating from the oxidation of the anode, and is used to give the cathode corrosion protection, lubricity, abrasion, wear resistance, or other properties. The two electrodes are placed in an electrolyte, and then ions either from the anode or the electrolyte cover the cathode. Hillier and Robinson [11] investigates the effect of hydrogen embrittlement in high strength steel plated with a zinc-cobalt, and a cadmium layer. While the cadmium caused more embrittlement than the zinc-cobalt, the latter was not fully recovered after baking for several days at 200 °C.

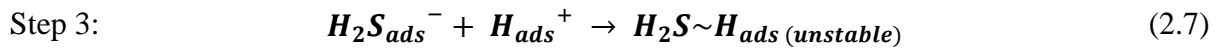
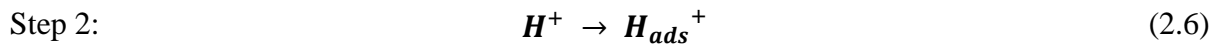
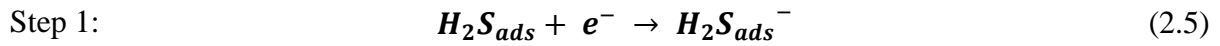
2.2.5 Welding

Welding is another source of hydrogen, which is critical for hydrogen embrittlement in pipelines and other subsea equipment. The temperature change during welding processes

creates stress in the material, and gives rise to hydrogen manifesting on the work piece. Some welding operations are performed on site, on equipment currently in use. In these processes, hydrogen could be accumulated from different sources, and the temperature changes acquired from the welding will magnify the hydrogen uptake. Louthan explains in his paper [12] how cracks from welding could occur weeks after the operation has been performed, due to residual stress applied by the welding, and hydrogen uptake.

2.2.6 Hydrogen Sulfide

Absorption of hydrogen could also be promoted if the environment is exposed to cathodic poisons, for example ionic sulphur. Hydrogen sulfide (H₂S) reacts with the iron in the material, to form hydrogen atoms. Kim and Kim [13] discuss this issue further, and disclose the following reaction model in their paper, containing the four steps, where the sulfide creates hydrogen atoms which in turn attach to the metal.



2.3 HE Mechanisms

The mechanisms of HE are not fully understood yet, and several theories are proposed. The two properties crack tip stress and hydrogen affected process zone strain, are not fully covered by any of the existing models. Below two of the most renowned hypotheses are presented, and described further by accompanying figures.

2.3.1 HELP

Hydrogen enhanced localized plasticity is a model proposed by Beachem [14] in 1972 and developed by Birnbaum and Sofronis [15] in 1994. The theorem proposes that hydrogen creates softening locally in front of cracks resulting in, as the name suggests, enhanced plasticity in the material, eventually causing ductile fracture. This mechanism could be spotted on the surface as small dimples.

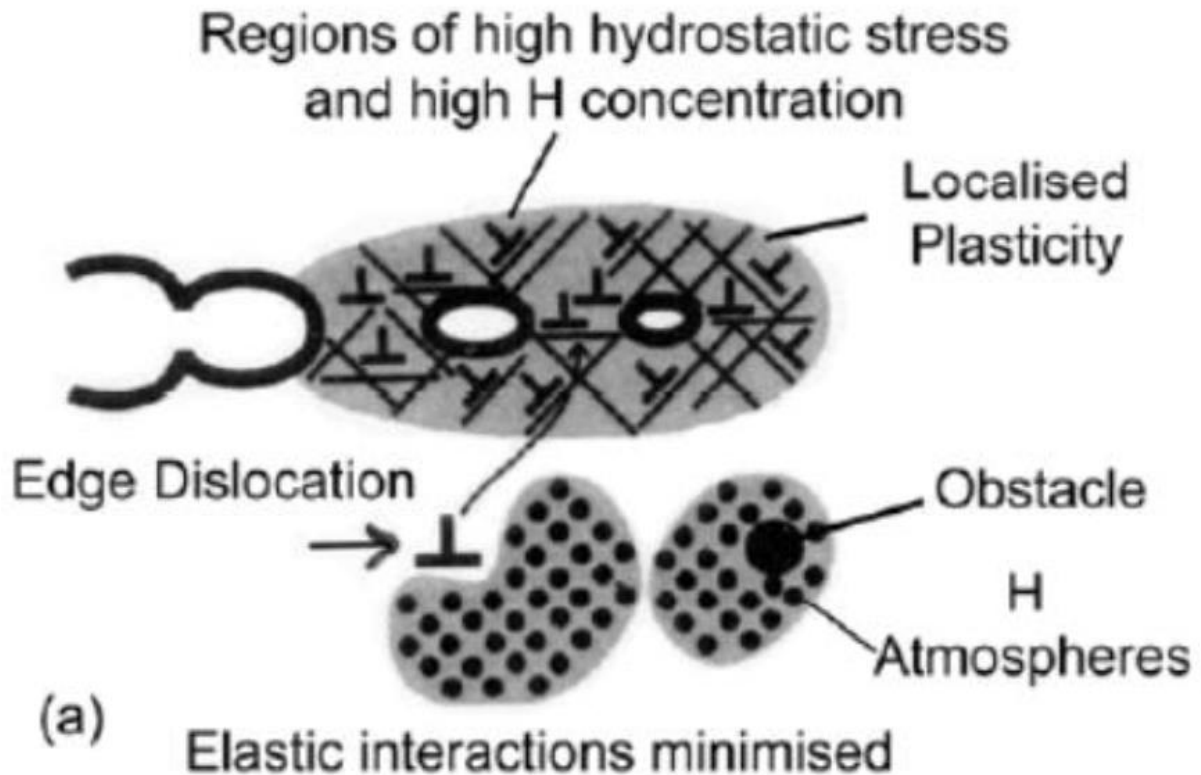


FIGURE 2-2: DISPLAY OF THE HELP MECHANISM, FIGURE FROM LYNCH [16]

Barnoush [5] mentions the controversy of this theorem in his paper, with opposing results reported for the same type of alloys, and other weaknesses supporting the evidence.

2.3.2 HEDE

The Hydrogen enhanced decohesion model was first proposed by Troiano *et al* [17] in 1960, before Oriani [3] made further developments to the theory in 1970. They state that a localized high concentration of hydrogen atoms, affect the inter-metal bonds at crack tips, so that the cohesion reduces significantly. The thought is that the presence of hydrogen decreases the electron charged density binding the metals together.

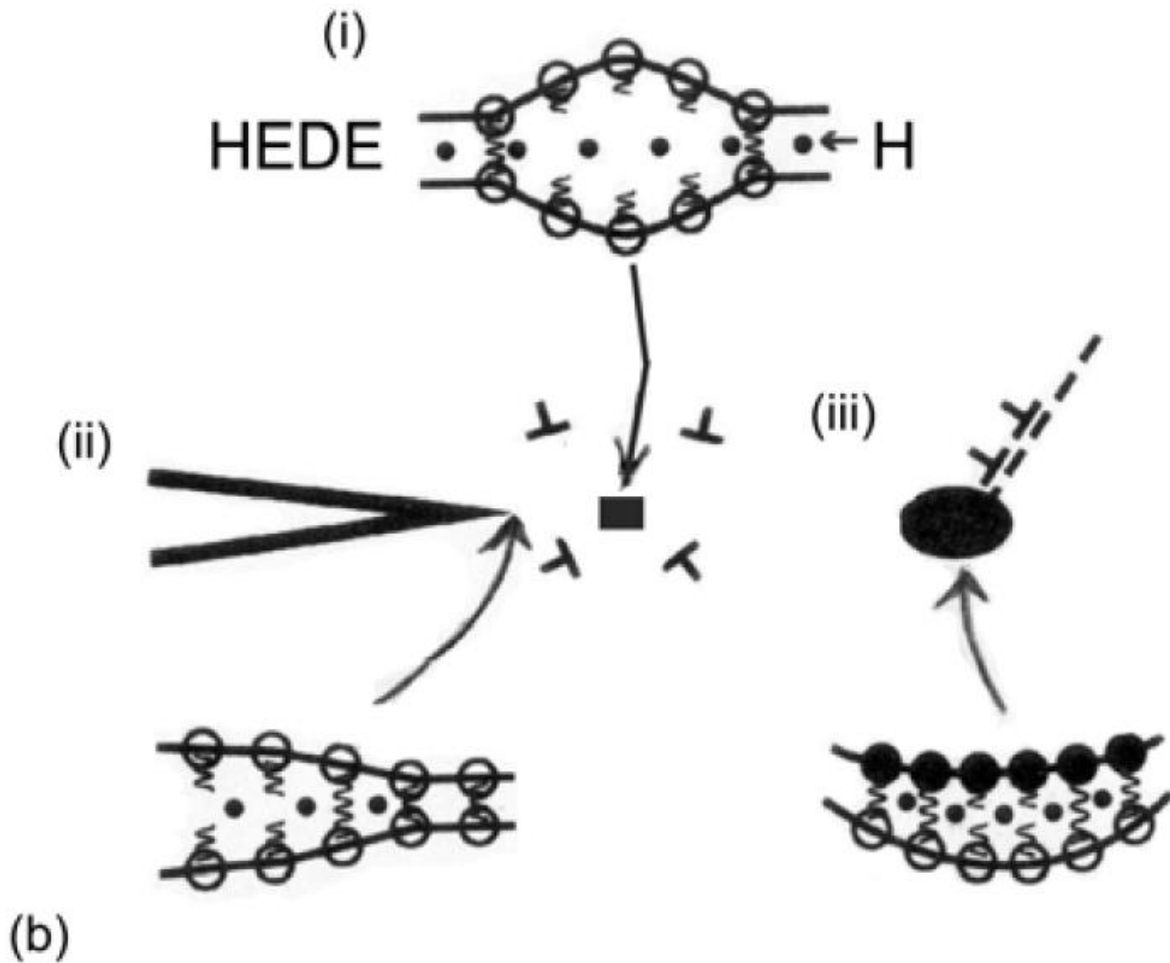


FIGURE 2-3: DISPLAYING THE HEDE MECHANISM, TAKEN FROM LYNCH [16]

The skepticism around this model is discussed by Barnoush in his paper [5], where he states that there is still no experiments confirming that the presence of hydrogen lowers interatomic force-displacement relationships, or in any way alters such bindings.

2.4 Hydrogen Diffusion

Diffusion is the movement of a substance from a region of high concentration to a region of low concentration. Diffusion in solids has been used for a long time, for example in cementation processes where steel was produced from iron through carbon diffusion.

However, the first systematic experimental studies were performed by Thomas Graham. He focused on diffusion in gases, but he described the main phenomenon in 1829 [18] with the following quote:

Fruitful as the miscibility of the gases has been in interesting speculations, the experimental information we possess on the subject amounts to little more than the well established fact, that gases of different nature, when brought into contact, do not arrange themselves according to their density, the heaviest undermost, and the lighter uppermost, but they spontaneously diffuse, mutually and equally, through each other, and so remain in the intimate state of mixture for any length of time.

In this section a brief introduction to X70 steel will be given, the main mechanisms of hydrogen diffusion will be elaborated, and the permeation technique used throughout this paper will be explained.

2.4.1 X70 Steel

All experiments referred to in this paper, are performed on either ferritic FeSi steel described below, or ferritic X70 steel specimens. It is a high strength, low-alloy steel which is often used in subsea pipelines. Hope [19] states in her paper that the hydrogen properties obtained for X70 is assumed to be applicable for X65 steel as well. As manufacturing techniques evolved through time, pipelines could be made out of high strength steel, which allowed for higher pressures and other benefits. In Thaulow and Valbergs compendium [20] it is mentioned that new stainless steel is developed to withstand buckling corrosion in chloride environments. The low carbon content and other properties makes X70 better suited as a material in such environments than most austenitic steel, and gives it better weldability. The X65 steel made by TMCP rolling, the same way the X70 used in this paper is made, where tested by Park *et al* [21]. Their results are assumed to be applicable for X70 steel. Figure 2-4 and Figure 2-5, shows which microstructure occurs.

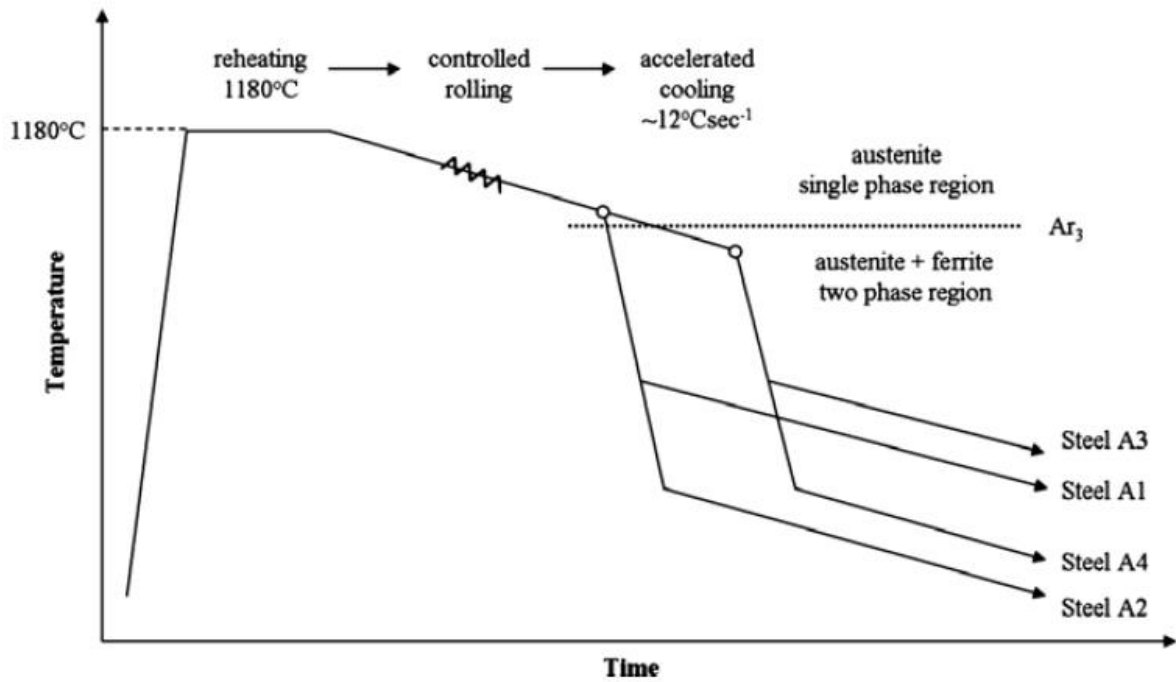


FIGURE 2-4: A GRAPH RETRIEVED FROM PARK *ET AL* [21] DESCRIBING THE PROCESSES PERFORMED IN ORDER TO MAKE THE DIFFERENT STEEL TESTED

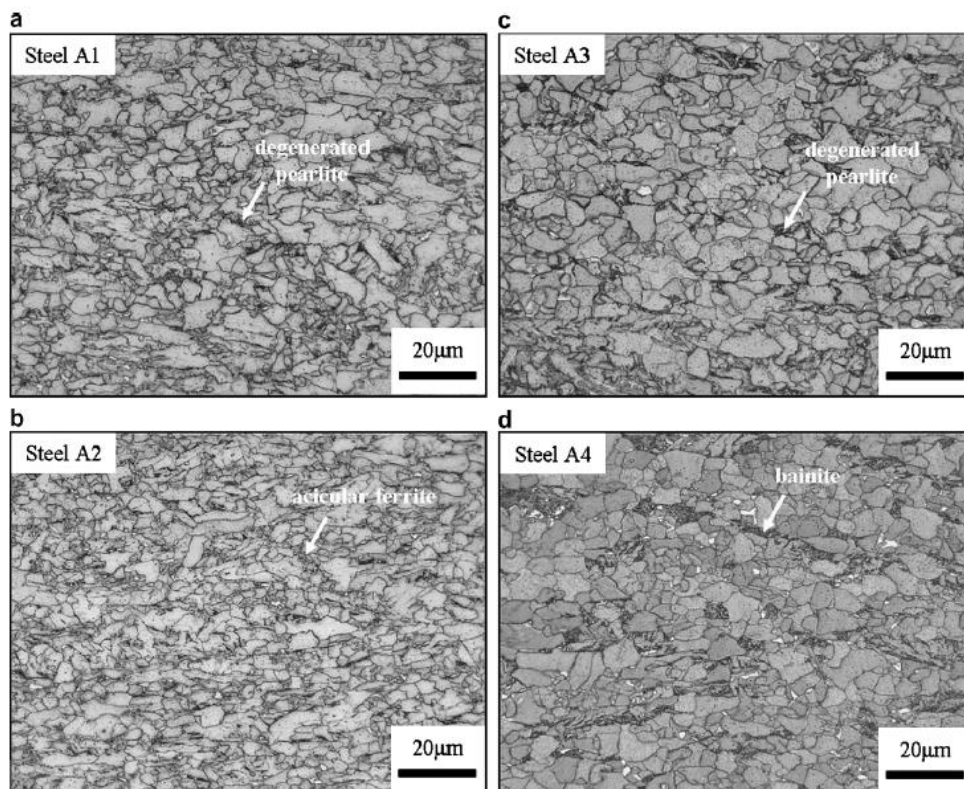


FIGURE 2-5: OPTICAL MICROSTRUCTURES FOR THE STEEL TESTED BY PARK *ET AL* [21]. (A) AND (C) SHOWS FERRITE/DEGENERATED PEARLITE, (B) IS FERRITE/ACICULAR FERRITE, AND (D) SHOWS FERRITE/BAINITE.

2.4.2 FeSi Steel

The iron-silicon alloy is called ferrosilicon, and is often used in transformer cores, which require the use of soft magnetic materials, mentioned in Callister and Rethwisch's book [22]. Single crystals of this alloy are magnetically anisotropic, which minimizes energy losses of transformers. Since the production of single crystals are an expensive venture, the alloy are more commonly fabricated as polycrystalline sheets through rolling as for the X65 material discussed in subsection 2.4.1. The alloy used in these experiments consists of 3 wt. % of silicon.

2.4.3 Main Mechanisms

The main diffusion mechanism for hydrogen in steel is lattice diffusion by interstitial jumps. In the subsections 2.4.1 and 2.4.2 microstructures was discussed, and Figure 2-6 will show some of the corresponding lattice structures.

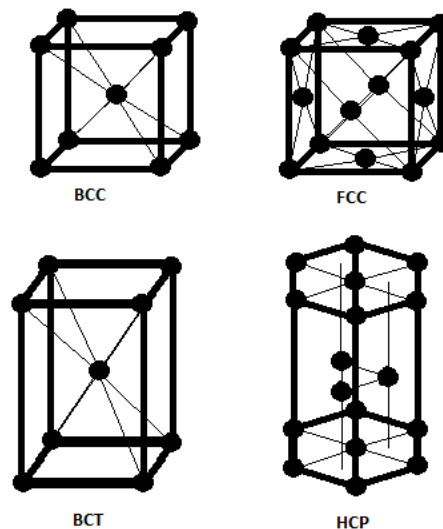


FIGURE 2-6: BASE CENTERED CUBIC STRUCTURE (BCC) AND FACE CENTERED CUBIC STRUCTURE (FCC) SHOWS THE LATTICE STRUCTURE FOR FERRITIC AND AUSTENITIC MICROSTRUCTURE RESPECTIVELY, WHILE BODY CENTERED TETRAGONAL STRUCTURE (BCT) AND HEXAGONAL CLOSE PACKED STRUCTURE (HCP) ARE DIFFERENT TYPES OF MARTENSITIC MICROSTRUCTURE.

Olden *et al* [7] describes in their work how the different lattice structures affects the diffusion in the material. A ferritic BCC is an open lattice structure, which gives a high diffusion rate, and a low solubility. The austenitic FCC structure got a much denser packed lattice, which in turn gives a lower diffusion rate, and a higher solubility. The martensitic structures BCT and HCP lies in between BCC and FCC regarding their lattice structure, and their diffusion rate

and solubility are therefore medium. The diffusion rate can be calculated by the following equation, based on Arrhenius formula for temperature dependence of reaction rates.

$$D = D_0 e^{-E/RT} \quad (2.9)$$

The diffusion coefficient D tells us at which rate a substance diffuses in another substance (cm^2/s). D_0 is the maximum diffusion coefficient at infinite temperature (cm^2/s), reported in the range 0.076-0.22 mm^2/s for ferrite and 1.1-1.5 mm^2/s for austenite by Olden *et al* [7]. The activation energy E could be looked at as an interstitial barrier, and is given in the same report as 12.5 J/mol for ferrite and about 42 J/mol for austenite. T is the temperature in Kelvin, and R is the gas constant (8.314 J/molK). Fick's laws of diffusion describe the diffusion of hydrogen from an area of high concentration to an area of lower concentration. These equations are discussed further in chapter 3, together with other calculations taking trapping (section 2.5) into account.

2.4.4 Electrochemical Hydrogen Permeation Technique

The permeation technique mentioned in this paper was developed by Devanathan and Stachurski, who published the method in 1962 [2].

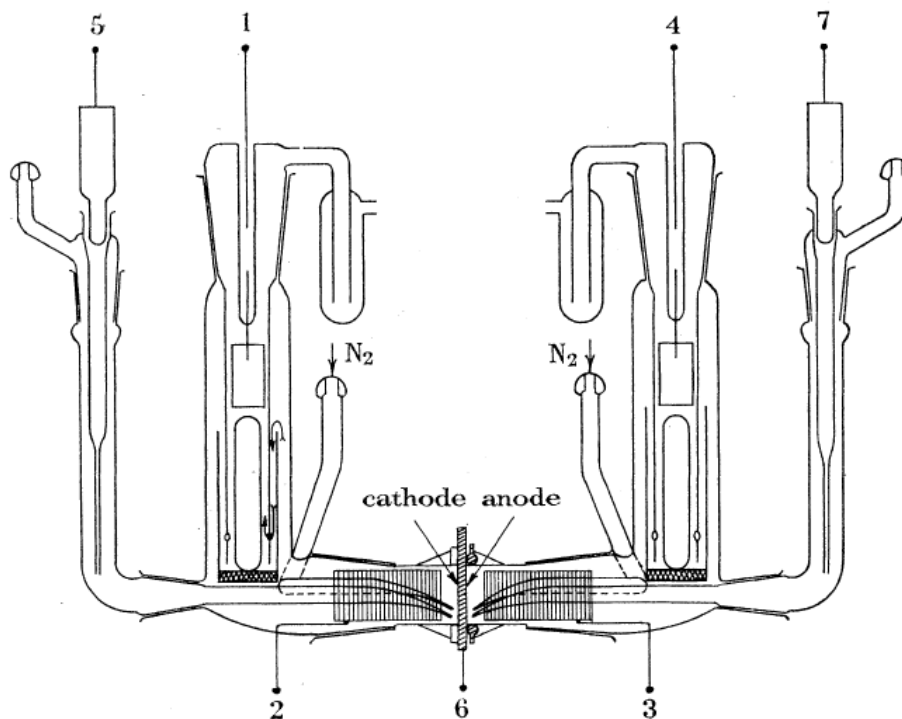


FIGURE 2-7: ILLUSTRATION OF DEVANATHAN AND STACHURSKI 'S CELL, ADOPTED FROM THEIR PUBLICATION [2]. IT DISPLAYS THE SPECIMEN TESTED (6) IN THE MIDDLE OF TWO CELLS, ONE ANODIC AND ONE CATHODIC SIDE.

This method is now described in the standard [1], for measuring hydrogen flux through a specimen. Hope shows her own design in her paper [19], and she performs all the experiments related to this work using her own cell.

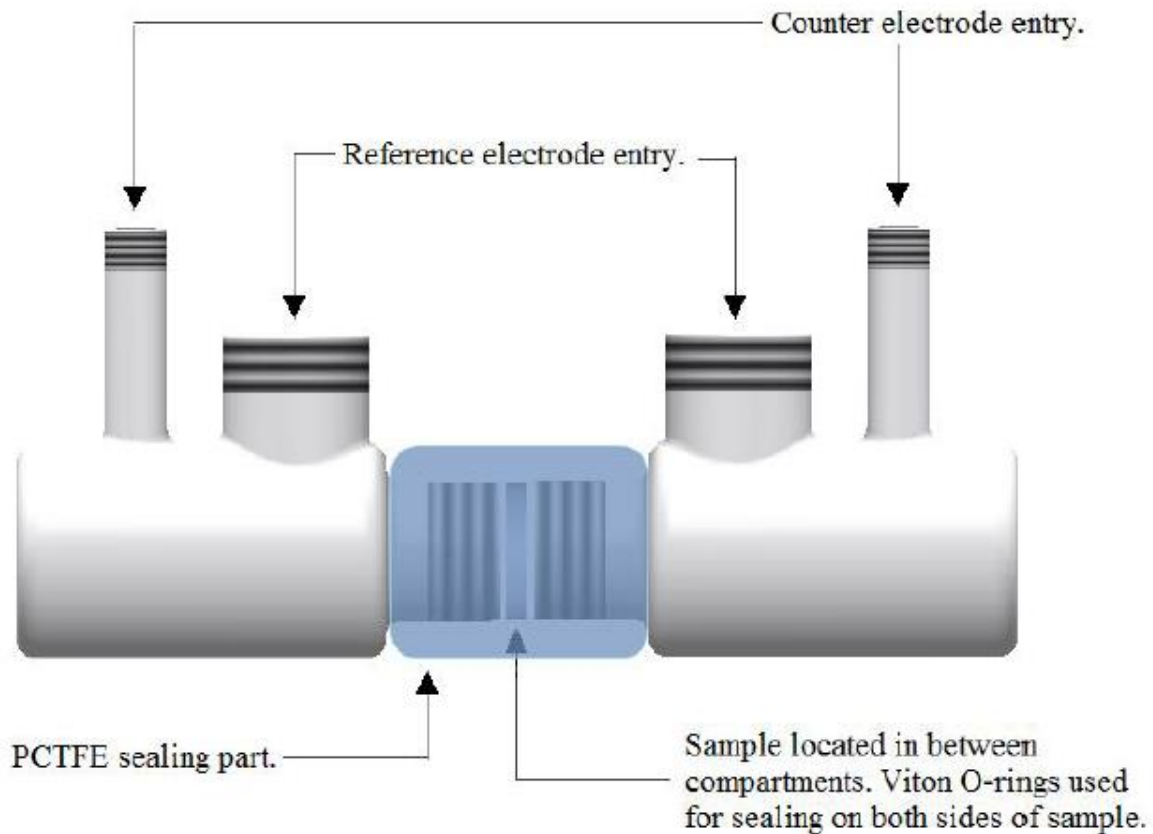


FIGURE 2-8: ILLUSTRATION OF HOPE'S SET UP, BORROWED FROM HER PAPER [19].

Hope's design shown in Figure 2-8 is a bit simpler than Devanathan and Stachurski's cell but the basic principles are the same. The specimen is attached between a cathodic hydrogen charging cell and an anodic, oxidizing cell. Both cells are then filled with an electrolyte. By cathodically polarizing with a potentiostat, hydrogen atoms are generated from the electrolyte and adhere to the specimen surface. The small hydrogen atoms will then be absorbed by the specimen and diffuse to the other side. Here the hydrogen will be oxidized, by anodically polarizing this side with another potentiostat. The oxidation current can then be measured, thus giving data of how much hydrogen were successfully diffused through the specimen, enabling calculations on how much were trapped.

2.5 Trapping

In Fallahmohammadi's dissertation [23] he defines a trap as a localized region where a hydrogen atom spend more time than in a normal interstitial lattice site. In this section a short introduction to trapping will be made, and the two different main types of trapping will be elaborated.

2.5.1 Properties

Hydrogen atoms can diffuse quickly in most metals, particularly in BCC microstructures as mentioned in subsection 2.4.3. Commercial metals and alloys are more complicated than the lattice structures illustrated in this subsection. Hydrogen's extreme mobility allows it to accumulate in different imperfections in the materials like grain boundaries, inclusions, voids, dislocations, and solute atoms, which exists locally in microstructures. Although hydrogen induced fracture are usually considered as brittle, many materials exposed to hydrogen experience ductile fractures. Fick's laws which are described in section 3.1 describes relations between flux and concentrations, but they do not take trapping into account, thus giving a simple approximation of the reality based on ideal conditions regarding hydrogen diffusion. Turnbull *et al* [24] states in their report, that since the traps will act as sinks and sources of hydrogen, more comprehensive treatment is required.

2.5.2 Reversible and Irreversible Traps

Usually traps are categorized into reversible and irreversible traps. The ASTM standard [1] defines reversible traps as microstructural sites where hydrogen atoms resides longer than in lattice sites, but because of low binding energy the residence time is shorter than the time to attain steady state permeation. It continues to define irreversible traps as microstructural sites where the residence time is infinite or extremely long compared to the time to attain steady state permeation, due to high binding energy compared to migration energy for diffusion. By tempering the material the hydrogen atoms in the reversible traps could be removed, but the hydrogen in the irreversible traps are as the name implies unable to be removed by this procedure. Arrhenius equation (2.9) gives the relation between the diffusion rate and activation energy needed for hydrogen to perform interstitial jumps between lattices. To describe these relations while considering the reversible and irreversible traps, more complex mathematical models have been proposed. Some of these models are presented later in section 3.4 about numerical approaches.

3 Calculations

In this chapter all the calculations related to the software developed will be presented, alongside mathematical models studied during this work. In the first section Fick's laws of diffusion will be reviewed, making a basis for the analysis of permeation transients, computation of sub-surface hydrogen concentration, and numerical approaches to hydrogen diffusion.

3.1 Fick's Laws of Diffusion

Fick's laws of diffusion were reported already in 1855 [25], and are inspired by Thomas Graham's experiments revolving around diffusion by salts in water [18]. His first law assumes a steady state environment, and makes the relation between diffusive flux and the concentration.

Fick's first law:

$$J_{ss} = -D_l \frac{\partial C}{\partial x} \quad (3.1)$$

It describes the flow of atom from high to low concentrated areas. J_{ss} is the steady state flux (mol/cm²s), D_l is the lattice diffusion coefficient (cm²/s), C is the concentration (mol/cm³), and x is the position (cm). The first law can be used to derive Fick's second law.

Fick's second law:

$$\frac{\partial C}{\partial t} = D_l \frac{\partial^2 C}{\partial x^2} \quad (3.2)$$

His second law can be used when it is impossible to assume steady state. It is also called the diffusion equation and predicts how diffusion makes the concentration change over time t (s). Both of Fick's laws are applicable when describing hydrogen diffusion, but they do not take trapping, which is described in section 2.5, directly into account.

3.2 Analysis of Permeation Transient

By analyzing permeation transients retrieved from various experiments, it is possible to determine a material hydrogen diffusion rate, by calculating the effective diffusion coefficient already discussed in subsection 2.4.3. This could be used to tell us something about the materials trapping, and if they are reversible or irreversible. In the standard [1] three different methods are mentioned, used to retrieve the diffusion coefficient. Steady state and time dependent flux, are two parameters used to plot normalized flux ($J(t)/J_{ss}$).

3.2.1 Steady State Permeation Flux

Steady state permeation flux (J_{SS}) could be used to calculate the effective diffusion coefficient. The standard [1] states that it gives information on the subsurface concentration of hydrogen atoms at the charging surface, and it is calculated from the following equation.

Steady state permeation flux:

$$J_{SS} = \frac{I_{SS}/A}{F} = \frac{D_l C_0}{L} \quad (3.3)$$

Here J_{SS} is the hydrogen flux at steady state (mol/cm²s), I_{SS} is the steady-state atomic hydrogen permeation current (μA), A is the exposed area of the specimen in the oxidation cell (cm²), F is faraday's constant (9.6485 x 10⁴ coulombs/mol), D_l is the lattice diffusion coefficient of atomic hydrogen (cm²/s), C_0 is the sub-surface concentration of atomic hydrogen at the charging side of the specimen (mol/cm³), and L is the thickness of the specimen (cm). According to the standard [1], the equation may be inadequate for highly alloyed or multiphase metals. When reversible trapping is the only noteworthy trapping type, Fick's first law can be used to find the steady state flux (equation (3.1)).

3.2.2 Time Dependent Permeation Flux

Time dependent permeation flux ($J(t)$) is used to verify the applicability of Fick's second law, and could also be used to calculate the effective diffusion coefficient. The standard [1] gives us the equation below to compute the flux.

Time dependent permeation flux:

$$J(t) = \frac{I(t)/A}{F} \quad (3.4)$$

$J(t)$ is the hydrogen flux (mol/cm²s), $I(t)$ is the time dependent atomic hydrogen permeation current (μA), A is the exposed area of the specimen in the oxidation cell (cm²), and F is Faraday's constant (9.6485 x 10⁴ coulombs/mol).

3.2.3 Elapsed Time Method

The effective diffusion coefficient can be calculated, by finding the elapsed time (t_{lag}) at $J(t)/J_{SS} = 0.63$ according to standard [1].

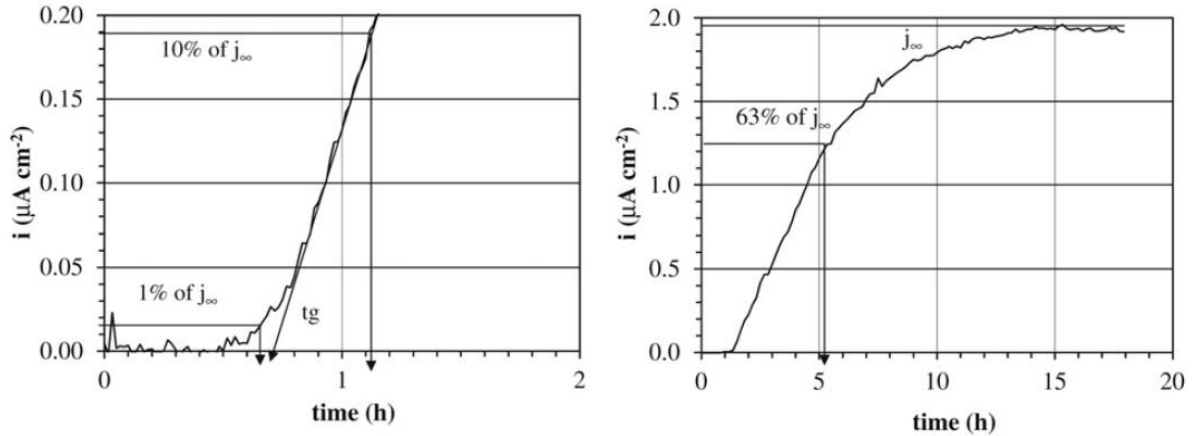


FIGURE 3-1: GRAPHICAL REPRESENTATION OF THE ELAPSED TIME METHOD, ADAPTED FROM FALLAMOHAMADI *ET AL* [26]. HERE J_{∞} REPRESENTS THE HYDROGEN STEADY STATE FLUX, AND THE LEFT CHART IS A CLOSE UP OF THE REGION MARKED IN THE RIGHT CHART.

The following equation should be used based on the elapsed time.

$$D_{eff} = \frac{L^2}{6t_{lag}} \quad (3.5)$$

D_{eff} is the effective diffusion coefficient (cm^2/s), L is the thickness of the specimen (cm), and t_{lag} is the elapsed time (s).

3.2.4 Breakthrough Time Method

The breakthrough time method calculates the effective diffusion by using the elapsed time (t_b (s)) measured extrapolating the linear portion of the rising permeation flux transient to $J(t) = 0$. It measures the time it takes for the first atom to diffuse through the material and appear on the anodic site. This method could be unreliable if the material contains a lot of trapping sites. The standard [1] gives the equation below to compute the coefficient.

$$D_{eff} = \frac{L^2}{15.3t_b} \quad (3.6)$$

Here D_{eff} is the effective diffusion coefficient (cm^2/s), L is the thickness of the specimen (cm), and t_b is the breakthrough time.

3.2.5 Slope Method

The slope method calculates the effective diffusivity from the slope of a plot of $\log (|J_{SS} - J(t)|)$ versus $1/t$ which is linear with a slope of $L^2 \log(e)/4D$.

3.3 Sub-Surface Hydrogen Concentration

When the cathodic polarization on the charging side starts, the hydrogen atom concentration on the charging side has the value C_0 . As long as the applied charging current is constant, C_0 is supposed to remain constant as well. At the anodic side the hydrogen atoms are supposed to oxidize, so the hydrogen concentration attains the value 0. The sub-surface hydrogen concentration on the charging side could be calculated, using equation (3.3) for steady state permeation flux.

Sub-surface
hydrogen
concentration:

$$C_0 = \frac{I_{SS}/A L}{D_l F} \quad (3.7)$$

C_0 is the hydrogen atom concentration on the charging side (mol/cm³), I_{SS} is the steady-state atomic hydrogen permeation current (μA), A is the exposed area of the specimen (cm²), L is the thickness (cm), D_l is the lattice diffusion coefficient of atomic hydrogen (cm²/s), and F is Faraday's constant (9.6485 x 10⁴ coulombs/mol).

Kiuchi and McLellan [27] derived three equations for D_l after analyzing hydrogen permeation data for different measurement methods, based on the environments temperature range. For the electrochemical measurement method, in temperature range -40°C to 80°C, the following equation applies.

$$D_l = 7.23 \times 10^{-4} e^{\frac{-Q}{RT}} \text{ cm}^2 \text{ s}^{-1} \quad (3.8)$$

D_l is the lattice diffusion coefficient (cm²/s), Q is the energy hydrogen atoms needs in order to jump between two lattice sites (5.69 kJ/mol), R is the gas constant (8.314 J/molK), and T is the absolute temperature in Kelvin (K).

When hydrogen concentration (3.7) is calculated using D_l , it measures the concentration in lattice sites in the metal. Since trapping is involved in the experiments connected to this paper, the effective diffusion coefficient (D_{eff}) needs to be used instead of D_l , which gives the following equations.

$$C_0 = \frac{I_{SS}/A L}{D_{eff} F} \quad (3.9)$$

$$\check{C}_0 = C_0 M_h \quad (3.10)$$

$$\dot{C}_0 = \frac{\check{C}_0}{\rho_{steel}} 1000000 \quad (3.11)$$

Here \check{C}_0 is the hydrogen atom concentration given in g/cm^3 , M_h is the molar mass of hydrogen (1.0079 g/mol), \dot{C}_0 is the hydrogen atom concentration given in parts per million, and ρ_{steel} is the density of the steel used (7.9 g/cm^3).

3.4 Numerical Solutions

Since Fick's laws of diffusion falls short when dealing with traps, other attempts have been made to make up models handling trapping. McNabb and Foster published the model below in 1963 [28].

$$\frac{\partial C}{\partial t} + N \frac{\partial \theta}{\partial t} = D_l \frac{\partial^2 C}{\partial x^2} \quad (3.12)$$

$$\frac{\partial \theta}{\partial t} = kC(1 - \theta) - p\theta \quad (3.13)$$

Here C is the concentration (mol/cm^3), t is time (s), D_l is the lattice diffusion coefficient (cm^2/s), x is the distance into the thickness of the specimen tested (cm), N is the density of trap sites (traps/cm^3), θ is the fraction occupied of N traps, k is the capture rate per trap, and p is the release rate per trap. This system takes reversible trapping into account. Turnbull *et al* [24] modified McNabb and Foster's model to make it apply to irreversible traps as well. They express their continuity equations in one-dimensional form with the following mathematical model.

$$\frac{\partial C}{\partial t} = D_l \frac{\partial^2 C}{\partial x^2} - N_r \frac{\partial \theta_r}{\partial t} - N_i \frac{\partial \theta_i}{\partial t} \quad (3.14)$$

$$\frac{\partial \theta_r}{\partial t} = k_r C(1 - \theta_r) - p\theta_r \quad (3.15)$$

$$\frac{\partial \theta_i}{\partial t} = k_i C(1 - \theta_i) \quad (3.16)$$

The subscripts r and i represent reversible and irreversible traps respectively. The non-linear systems have been proven troublesome to solve analytically, which has led to considerable interest in numerical solutions of the models. In this section an approach to a numerical

solution of Fick's laws will be displayed, and then the more comprehensive methods will be elaborated.

3.4.1 Numerical Approach to Fick's Laws

In Fallahmohammadi *et al*'s article [26] they compare their data from hydrogen diffusion experiments, with theoretical solutions derived from Fick's second law (equation (3.2)).

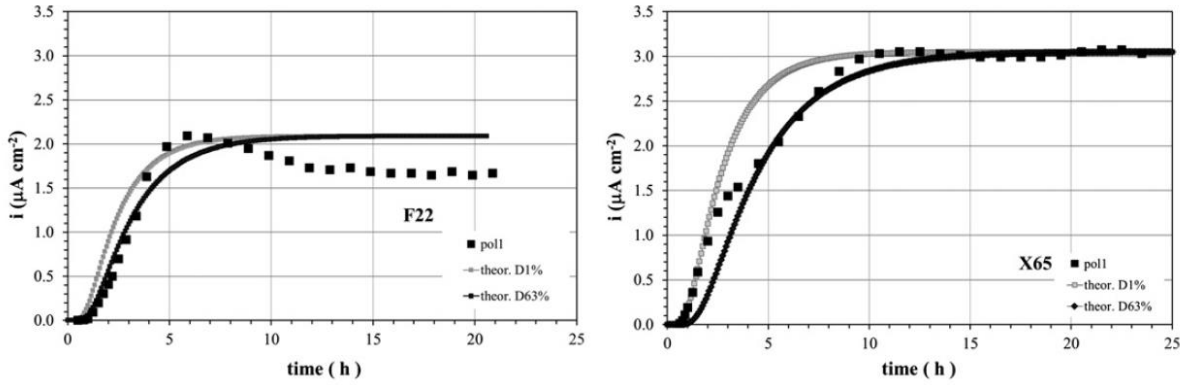


FIGURE 3-2: EXPERIMENTAL TRANSIENTS PLOTTED TOGETHER WITH THEORETICAL SOLUTIONS, DERIVED FROM FICK'S SECOND LAW. LEFT AND RIGHT CHART REPRESENTS F22 AND X65 STEEL SAMPLES RESPECTIVELY. FIGURE ADOPTED FROM FALLAHMOHAMMADI *ET AL* [26]

The plots in Figure 3-2 show some of their experimental data. In their article they state that they use one of the following numerical equations derived from Fick's second law (Fourier equation corrected according to the standard [1]).

Laplace:
$$\frac{J(t)}{J_{SS}} = \frac{2}{\sqrt{(\pi\tau)}} \sum_{n=0}^{\infty} e^{-\frac{(2n+1)^2}{4\tau}} \quad (3.17)$$

Fourier:
$$\frac{J(t)}{J_{SS}} = 1 + 2 \sum_{n=1}^{\infty} (-1)^n e^{-n^2\pi^2\tau} \quad (3.18)$$

$J(t)$ is the hydrogen flux (mol/cm²s), J_{SS} is the hydrogen flux at steady state (mol/m²s), τ is the normalized time parameter defined as follows.

Normalized time:
$$\tau = D \frac{t}{L^2} \quad (3.19)$$

Here D could either be the effective or the lattice diffusion coefficient (cm²/s), t is time (s), and L is the membrane thickness (cm). This procedure could replace the lattice diffusion coefficient in Fick's second law, with the effective diffusion coefficient, which will implicitly

include traps in the numerical approximation. Fallahmohammedi *et al* computes the effective diffusion coefficient from the elapsed time method, explained in subsection 3.2.3. From equation (3.3) and (3.4) we can deduce the relation below.

$$\frac{J(t)}{J_{SS}} = \frac{I(t)}{I_{SS}} \quad (3.20)$$

$I(t)$ is the time dependent atomic hydrogen permeation current (μA), and I_{SS} is the steady-state atomic hydrogen permeation current (μA). Using this relation, a numerical expression for the hydrogen permeation current could be achieved, used in the theoretical transients in Figure 3-2.

3.4.2 Caskey and Pillinger

Caskey and Pillinger gives an approximate solution of McNabb and Foster's system (equations (3.12) and (3.13)) in their article [29], using the finite difference method. To make the system more adaptive to the method they begin with one of McNabb and Fosters dimensionless forms.

$$\frac{\partial u}{\partial \tau} + \frac{\partial \omega}{\partial \tau} = \nabla u^2 \quad (3.21)$$

$$\frac{\partial \omega}{\partial \tau} = \lambda u - \mu \omega - \nu u \omega \quad (3.22)$$

All the variables in this model are dimensionless, and the following equations define them.

Relative concentration:

$$u = \frac{C}{C_0} \quad (3.23)$$

C is the concentration of the diffusant (mol/cm^3), and C_0 is the surface concentration (mol/cm^3).

Relative trapped concentration:

$$\omega = N \frac{\theta}{C_0} \quad (3.24)$$

N is the density of trap sites (traps/cm^3), and θ is the fraction of traps occupied.

τ is the reduced time defined the same way as in equation (3.19).

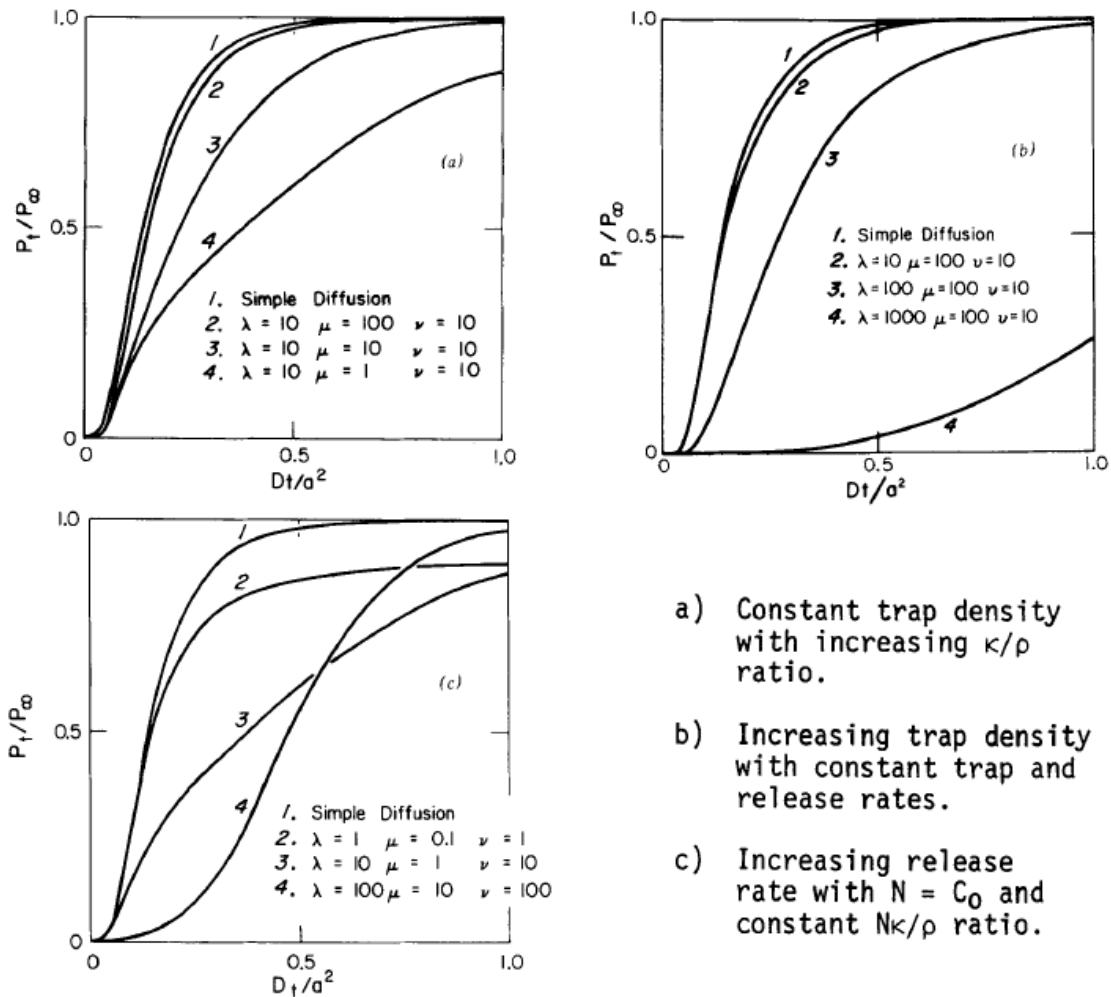
The parameters λ , μ , and ν describe the rates as which atoms are captured and released from the traps and are defined by the following equations:

$$\lambda = N\kappa \frac{L^2}{D_l} \quad (3.25)$$

$$\mu = \rho \frac{L^2}{D_l} \quad (3.26)$$

$$\nu = C_0 k \frac{L^2}{D_l} \quad (3.27)$$

k and ρ are defined such that the rate of capture of diffusing atoms in a volume (δV) is $kCN(I - \theta) \delta V$, and the rate of release in the volume is $\rho\theta N\delta V$. If all three parameters λ , μ and ν equals to zero equation (3.21) computes simple diffusion, and if only μ is zero the system represents irreversible traps or chemical reactions.



- a) Constant trap density with increasing κ/ρ ratio.
- b) Increasing trap density with constant trap and release rates.
- c) Increasing release rate with $N = C_0$ and constant $N\kappa/\rho$ ratio.

FIGURE 3-3: PERMEATION GRAPHS ADAPTED FROM CASKEY AND PILLINGER [29]. THEY REPRESENT TENDENCIES WHEN INDIVIDUAL PARAMETERS ARE INCREASED. EXPLANATIONS INCLUDED IN ILLUSTRATION. X-AXIS PARAMETER a EQUALS SAMPLE THICKNESS L IN THIS PAPER

The tendencies of the theoretical plots, when altering different parameters are showed in Figure 3-3. Caskey and Pillingers work makes interpretation of experimental data possible in a more general way, by using the finite differential method on McNabb and Fosters model [28]. Their approach was replicated by Thomas and Stern [30] in their article in 1981, described in the next subsection.

3.4.3 Thomas and Stern

Thomas and Stern [30] approaches a numerical model to McNabb and Fosters system (equations (3.12) and (3.13)), in order to make it as efficient as possible, by utilizing minimum computing time and storage. They acknowledge Caskey and Pillingers work, and their method facilitates comparison. However, they start out with another dimensionless system from McNabb and Fosters work [28].

$$\frac{\partial u}{\partial \tau} + \beta \frac{\partial \gamma}{\partial \tau} = \nabla u^2 \quad (3.28)$$

$$\frac{\partial v}{\partial \tau} = v u - \mu v - v u \gamma \quad (3.29)$$

Here τ , u , μ and v are defined by the equations (3.19), (3.23), (3.26) and (3.27) respectively. The difference from the system used by Caskey and Pillinger ((3.21) and (3.22)), is the introduction of β which is the number of traps per input hydrogen atom.

$$\beta = \frac{N}{K} \quad (3.30)$$

λ is replaced by βv , and ω is replaced by $\beta \gamma$. γ could be deduced from equation (3.24) using equation (3.30).

$$\gamma = K \frac{\theta}{C_0} \quad (3.31)$$

Thomas and Stern state that these dimensionless quantities reflect the physical parameters N , ρ , and κ with the greatest fidelity. The finite-difference replacement of equation (3.28) and (3.29) is displayed in the following system.

$$\begin{aligned} u_m^{n+1} - u_m^n + \beta(v_m^{n+1} - v_m^n) & \\ = \frac{r}{2}(u_{m-1}^{n+1} - 2u_m^{n+1} + u_{m+1}^{n+1}) & \\ + \frac{r}{2}(u_{m-1}^n - 2u_m^n + u_{m+1}^n) & \end{aligned} \quad (3.32)$$

$$v_m^{n+1} - v_m^n = \frac{a}{2} (\nu u_m^{n+1} - \mu v_m^{n+1} - \nu u_m^{n+1} v_m^{n+1}) \quad (3.33)$$

$$+ \frac{a}{2} (\nu u_m^n - \mu v_m^n - \nu u_m^n v_m^n)$$

Here u_m^n , and v_m^n denotes $u(mh, na)$, $v(mh, na)$ in the range $m \in \mathcal{M} = \{1 \dots M-1\}$, and $n=0,1, \dots$. $M = 1/h$, h denotes the x -step, a is the time-step, and φ is the mesh ratio given by the following equation.

$$\varphi = \frac{a}{h^2} \quad (3.34)$$

Equation (3.32) is the bottleneck this far, because of the non-linearity. In the next step Thomas and Stern performs Taylor expansions to remove the non-linearity parts of the equation and gives the following boundary conditions for u .

$$(n = 0, 1, \dots) \quad \mathbf{u}_0^n = \mathbf{1}, \mathbf{u}_M^n = \mathbf{0} \quad (3.35)$$

The initial conditions for u and v are given below.

$$(m \in \mathcal{M}) \quad \mathbf{u}_m^0 = \mathbf{v}_m^0 = \mathbf{0} \quad (3.36)$$

They then modify equation (3.32) and (3.33), in a similar structure as Caskey and Pillinger did in their paper [29].

$$-\frac{r}{2} \mathbf{u}_{m-1}^{n+1} + K_m \mathbf{u}_m^{n+1} - \frac{r}{2} \mathbf{u}_{m+1}^{n+1} = C_m \quad (3.37)$$

$$\mathbf{v}_m^{n+1} = R_m \mathbf{u}_m^{n+1} + S_m \quad (3.38)$$

Coefficients are defined in the following equations.

$$R_m = \frac{z_m}{d_m} \quad (3.39)$$

$$d_m = 2 + a(\mu + \nu u_m^n) \quad (3.40)$$

$$z_m = a\nu(1 - v_m^n) \quad (3.41)$$

$$K_m = 1 + r + \beta R_m \quad (3.42)$$

$$C_m = \frac{r}{2} (\mathbf{u}_{m-1}^n + \mathbf{u}_{m+1}^n) + (2 - K_m) \mathbf{u}_m^n + \frac{2a\beta\mu\nu v_m^n}{d_m} \quad (3.43)$$

$$S_m = \frac{(2 - a\mu)v_m^n + avu_m^n}{d_m} \quad (3.44)$$

By the recurrence relation, equation (3.37) could be simplified by using the boundary equations (3.35).

$$(m = 1 \dots M) \quad u_m^{n+1} = A_m u_{m-1}^{n+1} + B_m \quad (3.45)$$

Evaluating equation (3.38) directly by inserting equation (3.45) reveals the final equations in Thomas and Sterns efficient system.

$$(m \in \mathcal{M}) \quad A_m = \frac{r}{2K_m - rA_{m+1}} \quad (3.46)$$

$$(m \in \mathcal{M}) \quad B_m = \frac{2C_m + rB_{m+1}}{2K_m - rA_{m+1}} \quad (3.47)$$

In their paper Thomas and Stern claims that this system yields more accurate results using approximately 20% of the computer time, and less than 1/3 of the storage of the Caskey and Pillinger system.

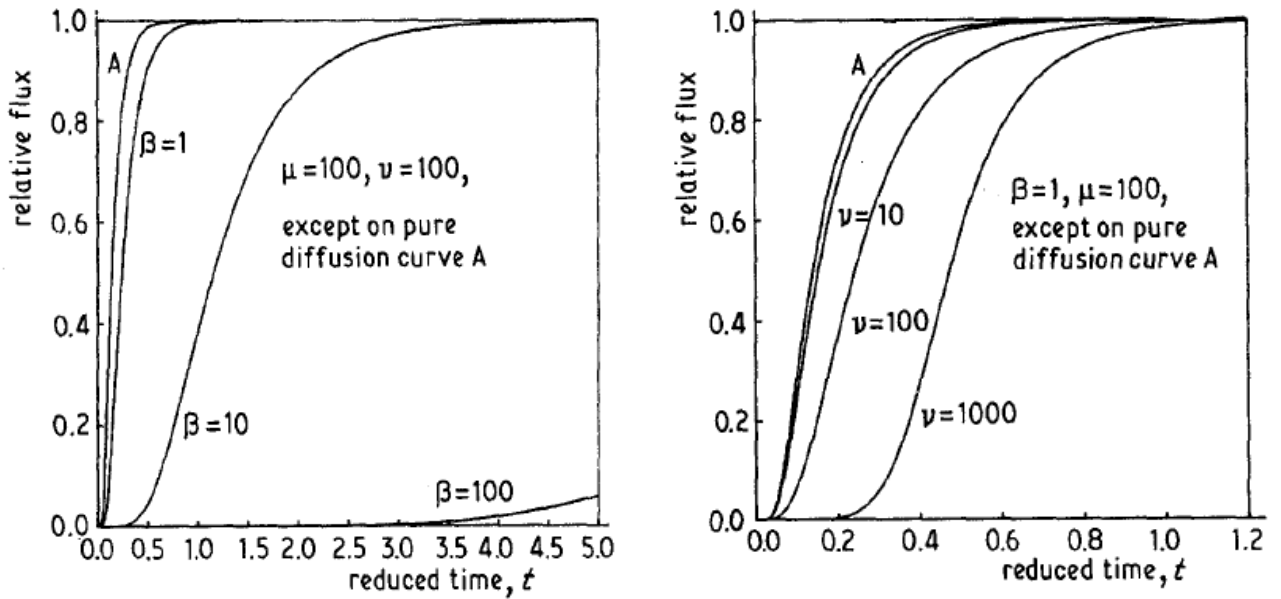


FIGURE 3-4: NORMALIZED FLUX PLOTTED AGAINST REDUCED TIME, WITH DIFFERENT B INCREMENTS TO THE LEFT, AND ν INCREMENTS TO THE RIGHT. CHARTS ADAPTED FROM THOMAS AND STERN [30]

3.4.4 Iino

Iino [31] was not content with McNabb and Fosters assumption [28] that filled traps had no influence on the diffusion of a system. Therefore he based their calculations of flux on a dimensionless model which include an irreversible trapping part. It bears resemblance to Turnbull *et al*'s system presented in equations (3.14)-(3.16).

$$\frac{\partial u}{\partial \tau} + \frac{\partial \omega_r}{\partial \tau} + \frac{\partial \omega_i}{\partial \tau} = \frac{\partial^2 u}{\partial \xi^2} \quad (3.48)$$

$$\frac{\partial \omega_r}{\partial \tau} = \lambda u - \mu \gamma \quad (3.49)$$

$$\frac{\partial \omega_i}{\partial \tau} = \kappa u(1 - \theta_i) \quad (3.50)$$

Here τ and u are defined by the equation (3.19) and (3.23) respectively. Iino introduces us with the variables ω_r , λ , μ , ω_i , κ , and ξ defined by the equations below.

$$\omega_r = N_r \frac{\theta_r}{C_0} \quad (3.51)$$

$$\lambda = N_r k_r \frac{L^2}{D_l} \quad (3.52)$$

$$\mu = \rho \frac{L^2}{D_l} \quad (3.53)$$

$$\omega_i = N_i \frac{\theta_i}{C_0} \quad (3.54)$$

$$\kappa = N_i k_i \frac{L^2}{D_l} \quad (3.55)$$

Relative distance: $\xi = \frac{x}{L} \quad (3.56)$

N is the density of trap sites (traps/cm³), θ is the fraction of traps occupied, C_0 is the hydrogen atom concentration on the charging side (mol/cm³), k is the capture rate per trap, ρ is the release rate per trap, L is the thickness of the membrane (cm), D_l is the lattice diffusion coefficient, and x is the position (cm). The subscripts r and i represents reversible and irreversible variables respectively.

The initial and boundary conditions are as follows.

$$\text{For } \tau < 0 \quad \mathbf{u} = \omega_r = \omega_i = \mathbf{0} \quad (3.57)$$

$$\begin{aligned} \text{For } \xi = 0 \text{ at} \\ \tau > 0 \end{aligned} \quad \mathbf{u} = \omega_r = \omega_i = \mathbf{0} \quad (3.58)$$

$$\begin{aligned} \text{For } \xi = 1 \text{ at} \\ \tau > 0 \end{aligned} \quad \mathbf{u} = \mathbf{1} \quad (3.59)$$

Applying the Laplace transformation and using a simplified version of equation (3.50), when $\theta_i \ll 1$, gives the system below.

$$\left(\kappa + s + \frac{\lambda s}{s + \mu} \right) \bar{u} = \frac{\partial^2 \bar{u}}{\partial \xi^2} \quad (3.60)$$

$$\text{At } \xi = 0 \quad \bar{u} = \bar{\omega}_r = \bar{\omega}_i \quad (3.61)$$

$$\text{At } \xi = 1 \quad \bar{u} = \frac{1}{s} \quad (3.62)$$

The behaviors of $\bar{\omega}_r$, and $\bar{\omega}_i$ in relation to \bar{u} are represented by the following equations.

$$\bar{\omega}_r = \frac{\lambda}{s + \mu} \bar{u} \quad (3.63)$$

$$\bar{\omega}_i = \frac{\kappa}{s} \bar{u} \quad (3.64)$$

By using the boundary conditions from equations (3.61) and (3.62), and doing an inverse transformation, we compute the following from equation (3.60).

$$\mathbf{u} = \frac{1}{2\pi i} \int ds e^{s\tau} \frac{1}{s} \frac{\sinh \sqrt{\kappa + s + \frac{\lambda}{s + \mu}} \xi}{\sinh \sqrt{\kappa + s + \frac{\lambda}{s + \mu}}} \quad (3.65)$$

s is defined as where the integrand has conjugate simple poles.

$$\begin{aligned} s = -s^\mp = -\frac{1}{2} \left[n^2 \pi^2 + \kappa + \lambda + \mu \right. \\ \left. \mp \sqrt{(n^2 \pi^2 + \kappa + \lambda - \mu)^2 + 4\lambda\mu} \right] \end{aligned} \quad (3.66)$$

Iino then solves equation (3.65) by using equation (3.66) and differentiates it with respect to ζ and lets $\zeta = 0$, to get his numerical expression for the permeation flux.

$$\frac{J(t)}{J_{SS}} = \frac{\sqrt{\kappa}}{\sinh \sqrt{\kappa}} + \sum_{n=1}^{\infty} (-1)^n \frac{2n^2 \pi^2}{s_n^- \left[\frac{\lambda \mu}{(s_n^- - \mu)^2} \right]} e^{-s_n^- \tau} \quad (3.67)$$

$$+ \sum_{n=1}^{\infty} (-1)^n \frac{2n^2 \pi^2}{s_n^+ \left[\frac{\lambda \mu}{(s_n^+ - \mu)^2} \right]} e^{-s_n^+ \tau}$$

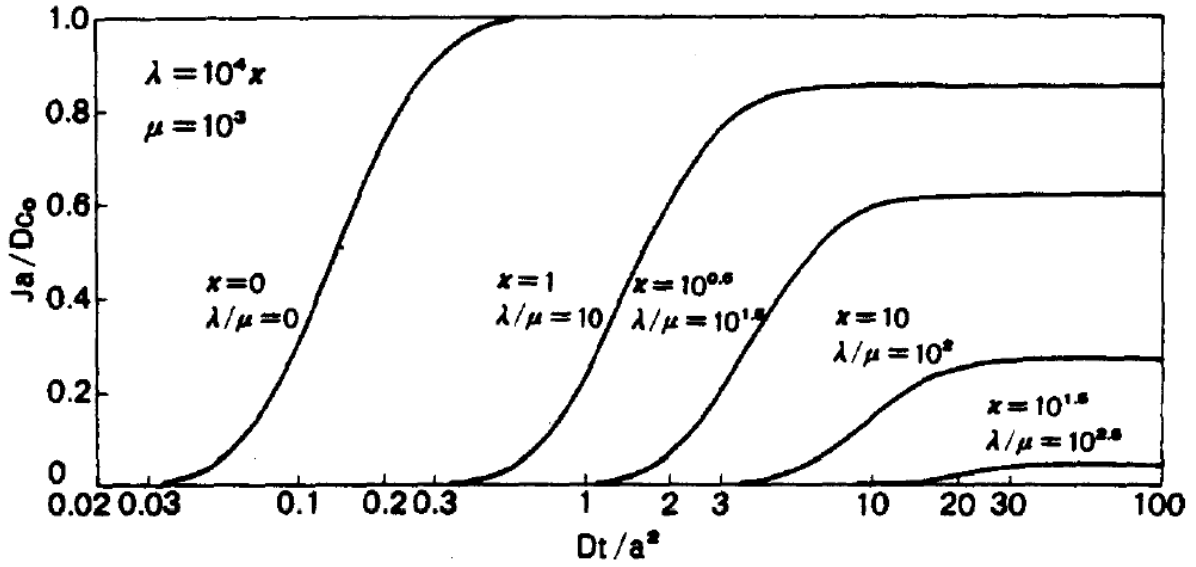


FIGURE 3-5: ILLUSTRATION OF THE INFLUENCE FROM κ AND λ/μ ON THE PERMEATION FLUX.

CHART ADAPTED FROM IINO [31]

3.4.5 Curve Fitting

By utilizing the equations mentioned throughout section 3.4, different parameters could be determined by curve fitting. A standard approach to perform a data fitting is by applying the least squares method. The following equation describes the procedure.

$$S = \sum_{i=1}^n (y_i - f(t)) = \sum_{i=1}^n r_i^2 \quad (3.68)$$

S represents the final sum, y is the actual time, $f(t)$ is the predicted value based on time, and r is the residual of the latter. The subscript i represents every point in the data set. To make a prediction the numerical approaches are performed with a predefined value of one or more of the parameters. The entire method should then be repeated, incrementing one of the

parameters at the time by a given value. This method requires some sort of threshold to end the iterations when the residuals are small enough.

4 Software

The main objective of the work related to this paper, is to develop an analysis tool, which could be used together with a hydrogen diffusion cell based on the procedure described in subsection 2.4.4. In this chapter the architecture of the software will be explained, before the different frameworks used will be presented, and lastly the implementation itself will be elaborated.

4.1 Software Architecture

This section will explain what an architectural pattern is, and describe Model-View-Controller (MVC) as a solution to the architectural approach in this work.

4.1.1 Architectural Pattern

An architectural pattern is a solution to a general problem which commonly occurs in different contexts. Design patterns builds on the same principle, but are solutions to specific parts of software. Buschmann *et al* describes an architectural pattern in their book [32] as an expression of the fundamental structural organization schema for software systems. They specify the structural properties of an application, and the impact of the selection of design patterns for the subsystems. The concept behind using a predefined architecture pattern is relatively acknowledged by software engineers as a time saving procedure. Different patterns address different abilities, which could be utilized to achieve the desired functionality in a program. The focus of a software could be to implement high modifiability, easier usability, better security, less risk, reliable availability, increased performance, or other attributes. An architectural pattern is not defined for one particular programming language or platform. The Model-View-Controller (MVC) pattern is one of the best known architectural patterns, and provides a structure for interactive software systems.

4.1.2 Model-View-Controller

Model-View-Controller (MVC) is an architectural pattern, which is commonly used when developing user interfaces. Buschmann *et al* [32] summarizes an user-interface of a long-lived system as a moving target, since menus need to be modified to access new functions, and visual properties need to match all the platforms the application is connected to. A system revolving around a user friendly interface requires flexibility, which is error-prone and expensive if the functionality of the program is to tightly interwoven with the user interface. To solve this issue, MVC architecture divides the application into three areas representing processing, output and input subsequently:

- The model components encapsulate core data and functionality. It should be independent of specific output and input representations.
- The view components obtain data from the model, and display it to the user.
- Each view should have an associated controller component, which receive input, usually as events that denote mouse or keyboard actions. The events are translated to service requests, which are sent to the model. The user should interact with the system solely through the controllers.

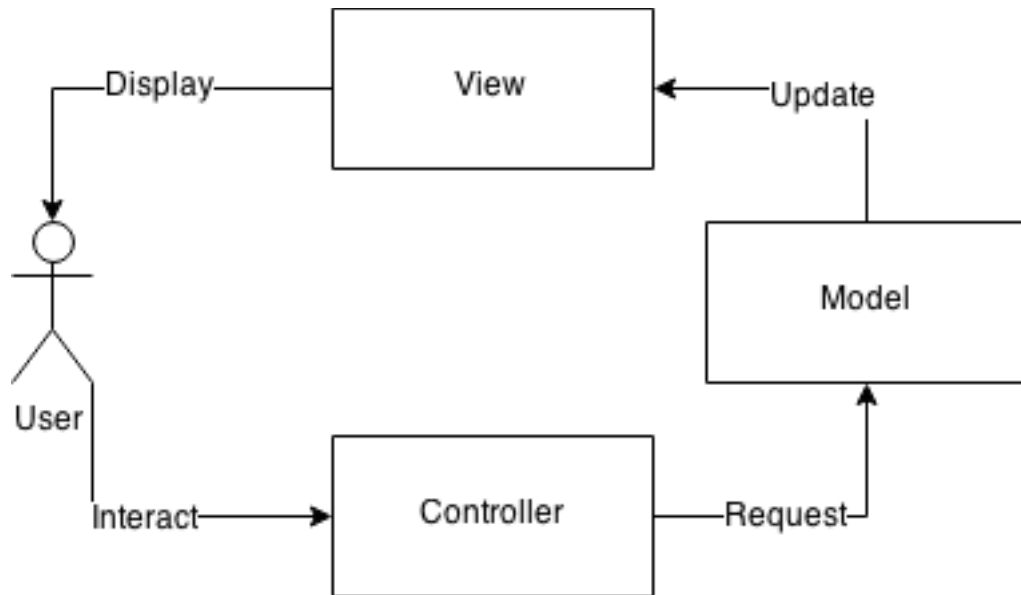


FIGURE 4-1: SKETCH DISPLAYING A TRADITIONAL MODEL-VIEW-CONTROLLER STRUCTURE, WITH THE RELATIONS BETWEEN THE COMPONENTS

By separating the model from the view and controller, several views of the same model could be initiated. Change of a model through one controller, should reflect all the views dependent on this data. This solution allows change in a small part of the application, without causing too many errors in the other subsystems. A change-propagation mechanism ensures consistency between the user interface and the model.

Class Controller	Collaborators <ul style="list-style-type: none"> • View • Model 	Class Model	Collaborators <ul style="list-style-type: none"> • View • Controller 	Class View	Collaborators <ul style="list-style-type: none"> • Controller • Model
Responsibility <ul style="list-style-type: none"> • Accepts user input as events. • Translates events to service requests for the model or display requests for the view. • Implements the update procedure, if required. 		Responsibility <ul style="list-style-type: none"> • Provides functional core of the application. • Registers dependent views and controllers. • Notifies dependent components about data changes. 		Responsibility <ul style="list-style-type: none"> • Creates and initializes its associated controller. • Displays information to the user. • Implements the update procedure. • Retrieves data from the model. 	

FIGURE 4-2: THE THREE MAIN CLASS TYPES IN A MVC STRUCTURE. ADAPTED FROM BUSCHMANN

ET AL [32]

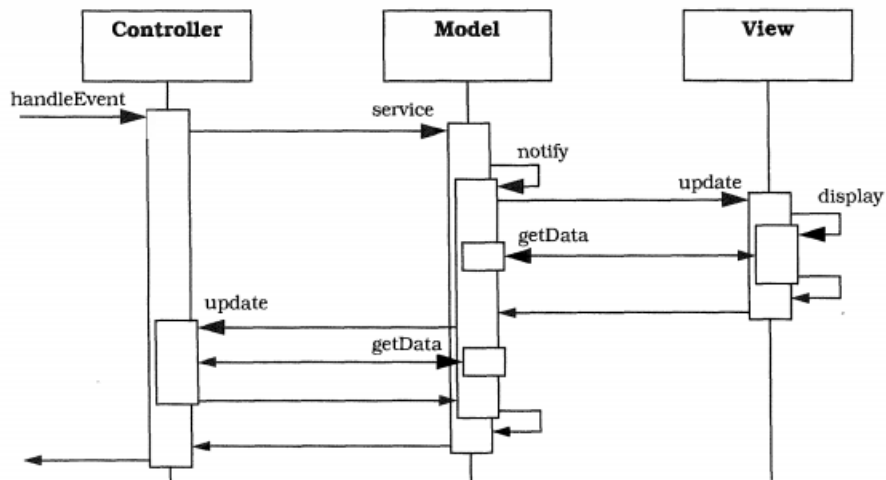


FIGURE 4-3: A SEQUENCE DIAGRAM DESCRIBING SOME OF THE INTERACTIONS BETWEEN THE CLASSES IN A MODEL-VIEW-CONTROLLER ARCHITECTURAL PATTERN. DIAGRAM COPIED FROM BUSCHMANN *ET AL* [32]

4.2 Framework

This section will describe what a framework is, and some of the different frameworks used in the software development process in this paper.

4.2.1 Software Framework

Kuchana describes frameworks in his book [33] as a group of components that cooperate with each other to provide a reusable architecture for applications with a given domain. The primary goal of a framework is to help improve the quality of the software, by making it reusable, maintainable, extensible, etc. By using a framework the user will reduce the development time. These principles compares to those of architectural patterns as described in section 4.1, but the concept differ entirely since frameworks exist in the physical form of software. This feature makes them implementation specific, and gives them domain specific functionality. They are not complete applications on their own, and needs to be inherited or used directly by software.

4.2.2 Swing

Swing is a platform-independent, Model-View-Controller (MVC) implemented graphical user interface (GUI) framework for Java. This means that it is independent of which platform it is implemented in. Sharan [34] describes Swing as a provider of GUI components to develop Java applications with a rich set of graphics such as windows, buttons, checkboxes, etc. These different user interface components enable the means for information exchange between the

user and the program. Swing is built in a containment hierarchy, since every component must be hold by a container component. At the root of the containment hierarchy is a top-level container, and every Swing application needs at least one top-level container to function properly.

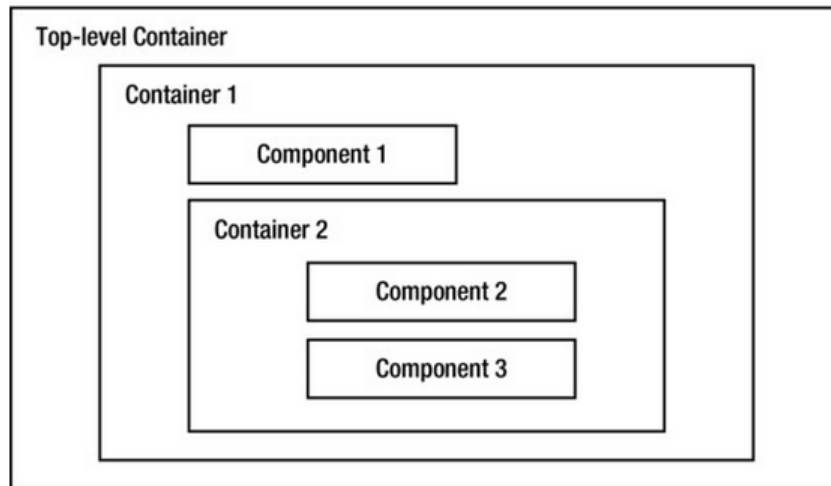


FIGURE 4-4: CONTAINMENT HIERARCHY IN A SWING APPLICATION. ADOPTED FROM SHARAN'S BOOK [34]

4.2.3 JFreeChart

JFreeChart is an open-source framework for the programming language Java, which allows the creation of a wide variety of both interactive and non-interactive charts. Gilbert tells us in a reference document [35] accompanying an older version of the framework, that JFreeChart supports pie charts, bar charts, line charts, scatter plots, time series charts, Gantt charts, meter charts, symbol charts, wind plots, combination charts and more. JFreeChart provides interactive zooming, event listeners, tooltips, accessible data, and the ability to export charts to JPEG, PNG, SVG, and PDF. It works in applications, servlets and applets, and the complete source code is available from the website. It is written in Java, and should run on any implementation of the Java platform, but it requires the open-source framework JCommon to be installed as well.

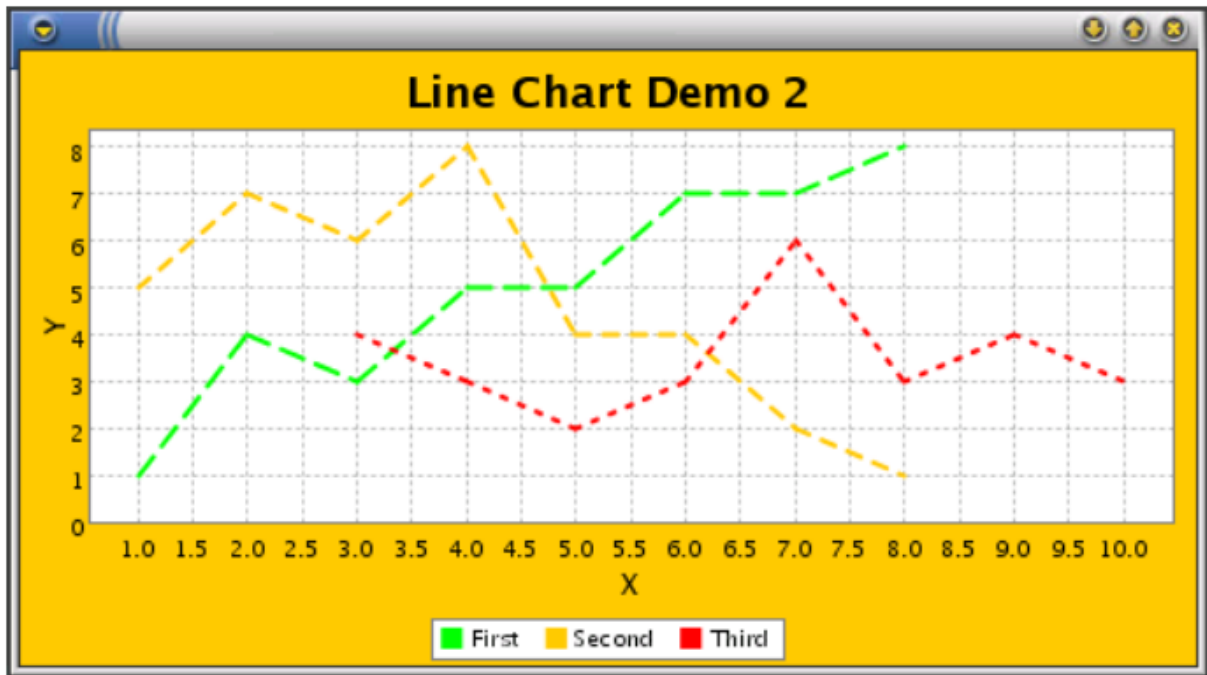


FIGURE 4-5: EXAMPLE CHART, BUILT WITH THE JFREECHART FRAMEWORK. ADOPTED FROM GILBERT [35]

4.3 Implementation

In this section the software developed in this work will be presented. First the functional and non-functional requirements will be discussed, before the system itself will be elaborated.

4.3.1 Functional Requirements

There are different functionalities which are needed to perform the analysis described in this paper. The main requirements will be explained below and illustrated with use-cases.

4.3.1.1 Read File

The experiment data is generated from a Gamry potentiostat, and will be available in a .dta format. The program must let the user browse a file to read, select the desired range of applicable information, and extract the appropriate time and current data from the file.

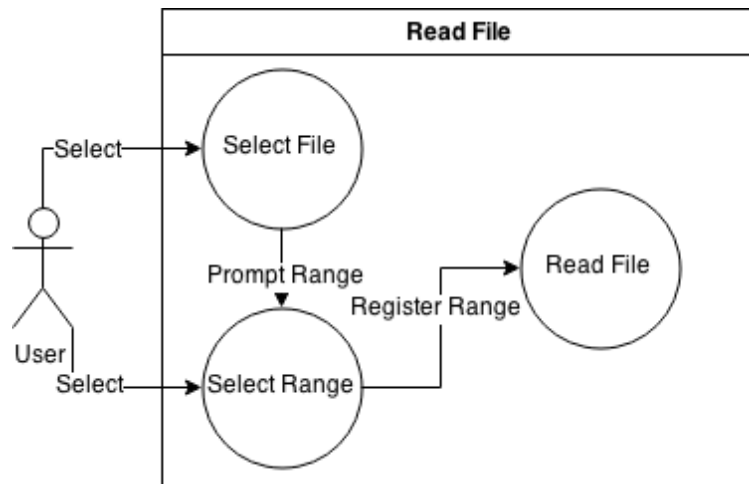


FIGURE 4-6: USE-CASE DIAGRAM ILLUSTRATING AN USER SELECTING A FILE TO READ, WHO GETS PROMPTED WITH RANGE SELECTION, AND SELECTS APPROPRIATE RANGE. THE SYSTEM READS DATA FROM FILE

4.3.1.2 Show Data and Calculations

The application must display the current and time data read from the file. The system must then receive thickness of the sample tested, testing temperature and the background current in order to compute the normalized flux and the normalized time. Then the program must calculate the elapsed time diffusion coefficient, concentration of hydrogen and other results needed to draw charts later.

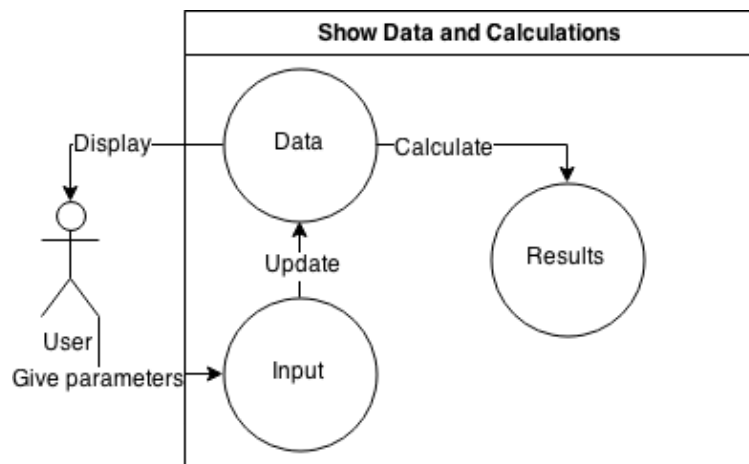


FIGURE 4-7: USE CASE DIAGRAM ILLUSTRATING A USER RECEIVING A DISPLAY OF DATA, MAKING AN INPUT THAT UPDATES THE DATA, WHICH IN TURN ENABLES CALCULATIONS TO BE MADE

4.3.1.3 Generate Charts

To perform analysis of the experiment data, the software must generate charts, graphing the oxidation current as a function of time, and the normalized permeation flux as a function of

normalized time. The user must be able to interact with the generated graphs, retrieving values, zooming in on areas, and export an image of the chart.

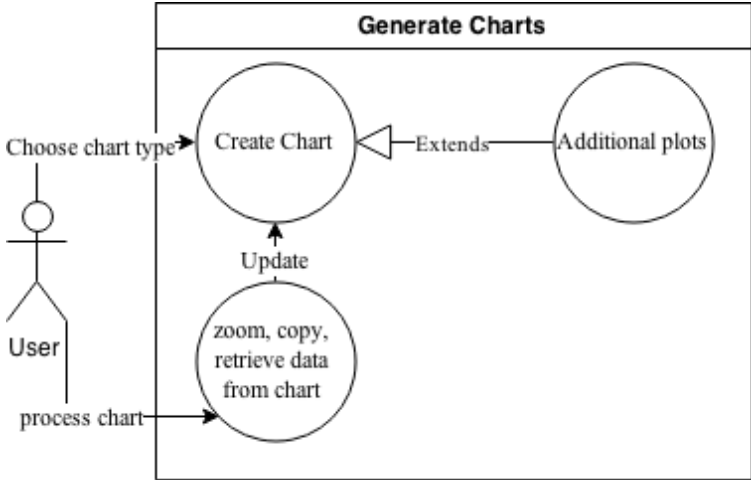


FIGURE 4-8: USE CASE DIAGRAM SHOWING A USER CHOOSING A CHART TYPE, AND PROCESSING THE DISPLAY BY ZOOMING, COPYING OR RETRIEVING DATA. AN EXTENSION TO THE CHARTS WILL BE TO APPLY ADDITIONAL PLOTS

4.3.1.4 Perform Curve Fittings

The last functional requirement for the software is to perform curve fittings, by utilizing numerical methods. This way the user will be able to extract parameters from a function, describing the properties of the material. The user must be able to use different filter functionalities, in order to remove noise from the experimental data.

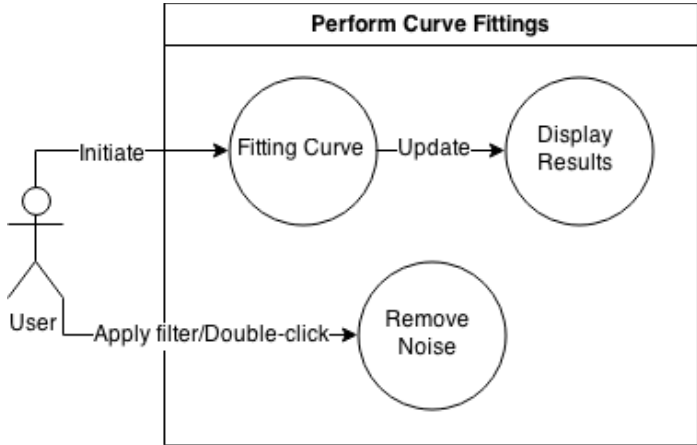


FIGURE 4-9: USE CASE SHOWING A USER INITIATE A CURVE FITTING, WHICH THEN UPDATES AND DISPLAYS THE RESULTS. THE USER IS ALSO ABLE TO APPLY FILTER, OR DOUBLE CLICK ON UNWANTED NOISE

4.3.2 Non-functional Requirements

It was decided to focus on three quality attributes during the software development. They are presented below, sorted after importance of the attribute.

4.3.2.1 Usability

Usability describes the ease of use of a system. It was decided that usability was the most important trait of the software, because one of the requirements is that a complete stranger to the procedure of hydrogen diffusion, should be able to operate the software. The software should outmatch the standard approach to do the analysis in Microsoft Excel. To achieve a graphical user interface (GUI) which is intuitive, it is important to have an architecture which focuses on good user interface. By choosing the Model-View-Controller (MVC) architectural pattern described in subsection 4.1.2, the GUI will be handled explicitly, thus ensuring a focus on the usability quality. Potential users of the software have also received releases of the software throughout the development. Their feedback enabled continuous adjustments of the GUI, to ensure that the software was customized to be user friendly, and also be efficient and accurate for all users.

4.3.2.2 Modifiability

Modifiability was chosen to be the second most important feature for the software, because more functionality will probably be added later in development. Another software developer should be able to continue working on the software after this work has been finished, to make modifications, and additions of future properties (see chapter 8). It is also important that the program is able to run on different platforms. The Model-View-Controller (MVC) architectural pattern described in subsection 4.1.2 makes a base structure for the software. The MVC structure recommends logical partitions of the code, making it easy to comprehend, especially for programmers who are familiar with the MVC pattern. The Swing framework mentioned in subsection 4.2.2 is platform-independent, making the software runnable on systems different from the system it was developed in. The JFreeChart framework presented in subsection 4.2.3 is also compatible with different systems, but could cause problems for UNIX systems (for example OS X) if the X11 window system handling bitmap displays are not installed.

4.3.2.3 Performance

Performance is very important in analysis programs, and requires a lot of work in order to make the program useful. To achieve good performance the system needs short response time,

high throughput, low utilization of resources, and high availability, so this requirement implies a lot of other requirements as well. The Model-View-Controller (subsection 4.1.2) structure’s modifiability enables quick location of bottlenecks in the program, and the frameworks (subsection 4.2.2 and 4.2.3) handles the graphical user interface (GUI) components efficiently. The software developed through this assignment, involves a lot of heavy calculations during its numerical approaches to theoretical solutions, which has the biggest impact on the performance of the system. The methods need training in order to select the approaches with the smallest runtime, highest accuracy, and lowest storage use. Correct initial and boundary conditions for all materials being tested needs to be implemented or inputted from the users. Noise removal application is essential to acquire acceptable levels of accuracy.

4.3.3 System

This subsection will introduce the structure of the software, before the different implemented parts will be described.

4.3.3.1 Structure

The structure of the system is based upon the Model-View-Controller (MVC) structure described in subsection 4.1.2, but some modifications have been made. To simplify the quantity of classes, and since every view will only display one type of model, the controller part and the view part of a traditional MVC structure have been fused together. This makes it easier to create several charts, where every frame controls its own data. The complete structure of the program is depicted in the class diagram below.

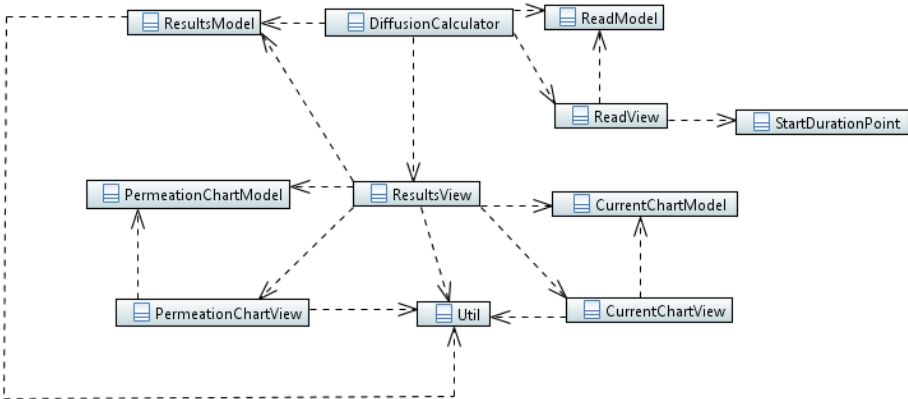
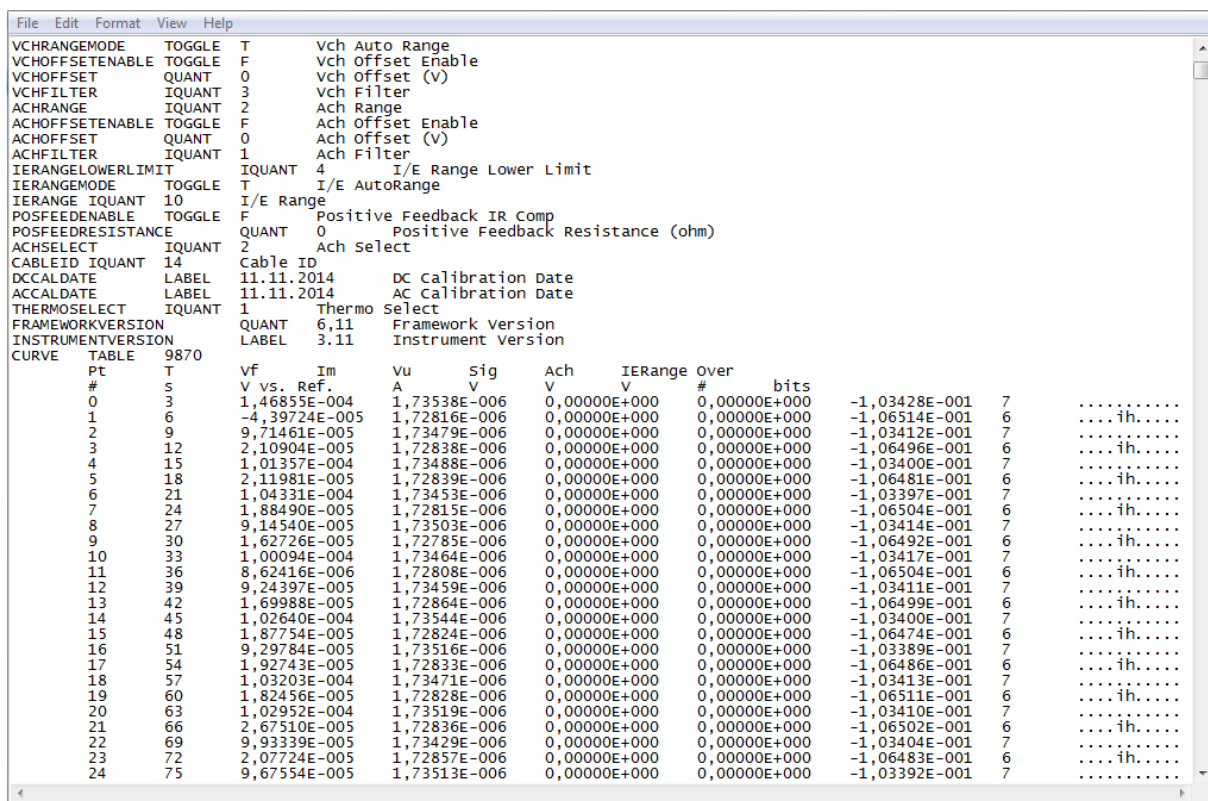


FIGURE 4-10: SMALL CLASS DIAGRAM PRESENTING ALL THE CLASSES AND THEIR RELATIONS. BIGGER CLASS DIAGRAMS DEPICTING ALL THE BELONGING METHODS AND FIELDS IS INCLUDED IN APPENDIX A: CLASS DIAGRAM

As seen from the class diagram in Figure 4-10, the *DiffusionCalculator* class is the main class of the program, initiating all the other classes. It starts out by creating a *ReadModel*, and a *ReadView* which uses the created *ReadModel* to display data. The *ReadView* class utilizes the class *StartDurationPoint*. Then the *DiffusionCalculator* initiates the *ResultsModel* with data collected from the *ReadModel*, and uses this class to initiate the *ResultsView*. The *ResultsView* accede the role as main menu, initiating the different chart models and views upon request. The *Util* class is a helper class which defines global constants, utilized by the other classes.

4.3.3.2 Reading

The file to be read is made from a Gamry potentiostat, which produces a .dta file, with similar properties as a .txt file. The file tends to have the same structure, so in order to save the columns showing the time and current, the reader was programmed to skip the lines above the valuable ones.



The screenshot shows a text-based configuration window for a DiffusionCalculator application. The top section lists various settings such as VCHOFFSETENABLE, VCHOFFSET, VCHFILTER, ACHRANGE, ACHOFFSETENABLE, ACHOFFSET, ACHFILTER, IERANGELOWERLIMIT, IERANGEMODE, IERANGE, POSFEEDENABLE, POSFEEDRESISTANCE, ACHSELECT, CABLEID, DCCALDATE, ACCALDATE, THERMOSELECT, FRAMEWORKVERSION, INSTRUMENTVERSION, and CURVE. The bottom section is a data table with columns: #, T, V vs. Ref., Vu, Sig, Ach, IERange, Over, #, bits, and a final column with dots. The data rows show time (T) increasing from 0 to 24 seconds and current (Vu) fluctuating around 1.73538E-006 A.

#	T	V vs. Ref.	Vu	Sig	Ach	IERange	Over	#	bits	
0	3	1,46855E-004	1,73538E-006	0,00000E+000	0,00000E+000	0,00000E+000	-1,03428E-001	7	
1	6	-4,39724E-005	1,72816E-006	0,00000E+000	0,00000E+000	0,00000E+000	-1,06514E-001	6ih.....	
2	9	9,71461E-005	1,73479E-006	0,00000E+000	0,00000E+000	0,00000E+000	-1,03412E-001	7	
3	12	2,10904E-005	1,72838E-006	0,00000E+000	0,00000E+000	0,00000E+000	-1,06496E-001	6ih.....	
4	15	1,01357E-004	1,73488E-006	0,00000E+000	0,00000E+000	0,00000E+000	-1,03400E-001	7	
5	18	2,11981E-005	1,72839E-006	0,00000E+000	0,00000E+000	0,00000E+000	-1,06481E-001	6ih.....	
6	21	1,04331E-004	1,73453E-006	0,00000E+000	0,00000E+000	0,00000E+000	-1,03397E-001	7	
7	24	1,88490E-005	1,72815E-006	0,00000E+000	0,00000E+000	0,00000E+000	-1,06504E-001	6ih.....	
8	27	9,14540E-005	1,73503E-006	0,00000E+000	0,00000E+000	0,00000E+000	-1,03414E-001	7	
9	30	1,62726E-005	1,72785E-006	0,00000E+000	0,00000E+000	0,00000E+000	-1,06492E-001	6ih.....	
10	33	1,00094E-004	1,73464E-006	0,00000E+000	0,00000E+000	0,00000E+000	-1,03417E-001	7	
11	36	8,62416E-006	1,72808E-006	0,00000E+000	0,00000E+000	0,00000E+000	-1,06504E-001	6ih.....	
12	39	9,24397E-005	1,73459E-006	0,00000E+000	0,00000E+000	0,00000E+000	-1,03411E-001	7	
13	42	1,69988E-005	1,72864E-006	0,00000E+000	0,00000E+000	0,00000E+000	-1,06499E-001	6ih.....	
14	45	1,02640E-004	1,73544E-006	0,00000E+000	0,00000E+000	0,00000E+000	-1,03400E-001	7	
15	48	1,87754E-005	1,72824E-006	0,00000E+000	0,00000E+000	0,00000E+000	-1,06474E-001	6ih.....	
16	51	9,29784E-005	1,73516E-006	0,00000E+000	0,00000E+000	0,00000E+000	-1,03389E-001	7	
17	54	1,92743E-005	1,72833E-006	0,00000E+000	0,00000E+000	0,00000E+000	-1,06486E-001	6ih.....	
18	57	1,03203E-004	1,73471E-006	0,00000E+000	0,00000E+000	0,00000E+000	-1,03413E-001	7	
19	60	1,82456E-005	1,72828E-006	0,00000E+000	0,00000E+000	0,00000E+000	-1,06511E-001	6ih.....	
20	63	1,02952E-004	1,73519E-006	0,00000E+000	0,00000E+000	0,00000E+000	-1,03410E-001	7	
21	66	2,67510E-005	1,72836E-006	0,00000E+000	0,00000E+000	0,00000E+000	-1,06502E-001	6ih.....	
22	69	9,93339E-005	1,73429E-006	0,00000E+000	0,00000E+000	0,00000E+000	-1,03404E-001	7	
23	72	2,07724E-005	1,72857E-006	0,00000E+000	0,00000E+000	0,00000E+000	-1,06483E-001	6ih.....	
24	75	9,67554E-005	1,73513E-006	0,00000E+000	0,00000E+000	0,00000E+000	-1,03392E-001	7	

FIGURE 4-11: EXAMPLE .dta FILE. THE COLUMNS READ ARE THE TIME COLUMN (T) IN SECONDS (S), AND THE CHARGING CURRENT COLUMN (Vu) IN AMPERE (A)

The *ReadModel* class holds the current and time lists, ending up with containing the data, and *ReadView* prompts the user with a browse window using the Swing framework presented in subsection 4.2.2, enabling selection of which file to read. The view class then utilizes the

StartDurationPoint class to ask the user when the experiment starts, and how long it lasts. The initialization of the reading procedure happens in the view class, but the formatting and saving of each line into the lists occurs in the model class.

4.3.3.3 Main Menu

The *ResultModel* and *ResultView* classes create the main menu of the application. The view class creates a frame with several containers, as depicted in Figure 4-4, using the Swing framework presented in subsection 4.2.2. In these containers a table presenting the current and time lists discussed above is displayed. By entering additional data, a new current column subtracted by the background current is added to the table, along with a normalized flux and normalized time column.

The normalized flux is calculated by dividing the time dependent permeation flux (equation 3.4) with the steady state permeation flux (equation (3.3)). The steady-state atomic hydrogen permeation current used in these calculations are taken as the maximum value from the current list subtracted by initial background current, the time dependent atomic hydrogen permeation current is taken from the current list subtracted by initial background current, and the specimen areal and Faraday's constant are predefined values gathered from the *Util* helper class. The normalized time is calculated from equation (3.19), where the time list and the user input sample thickness is used. It also needs the lattice diffusion coefficient, which is defined by the Arrhenius equation (2.9). It utilizes the predefined values for maximum diffusion coefficient, gas constant and activation energy gathered from the *Util* helper class, and the user input value for temperature.

After the additional columns are generated, the diffusion coefficient could be computed from the elapsed time method, followed by the concentration values. The elapsed time method is defined by equation (3.5), using the user input thickness and the time when the normalized flux is closest to 0.63. The sub-surface hydrogen concentration is calculated with equation (3.9) using fields from the *Util* helper class, the diffusion coefficient from the elapsed time method, and the maximum current value giving mol per volume. This value is multiplied with the hydrogen molar mass, gathered from the *Util* class, in order to get mass per volume as described in equation (3.10). The last value computed with equation (3.11) and displayed is the sub-surface hydrogen concentration given in parts per million, using the density of the steel received from the *Util* class.

4.3.3.4 Current Charts

The *CurrentChartModel* and the *CurrentChartView* classes create the chart displaying the current as a function of time. By using the Swing framework presented in subsection 4.2.2, the frame is constructed with layers of containers, panels and buttons. The JFreeChart framework from subsection 4.2.3 is imported to handle the chart creation, plots and graph rendering. A crosshair layer is also added over the chart, which is dynamically tracking the data representing the current, in order to display the specific values the user moves the mouse pointer over.

The main transient graph is generated in the model class from the lists with current and time values, gathered from the *ResultsModel* class. In addition to this curve the user is able to add two more transients, Fick's curve depicting the ideal graph for ferritic steel without traps, Fick's curve based on the elapsed time method, Fick's curve fitted numerically, and Iino's curve fitted numerically.

In order to add earlier transients, it needs to be a way to save the current transient. The view class adds a save button which prompts the user with a destination folder and a name field. The button uses a method in the model class to save the data to a text file. The view class implements two transient buttons, which let the user choose between earlier saved text file, which upon selection gets generated in the chart by a method in the model class.

Fick's ideal material curve is made from the numerical approach to Fick's second law based on Fourier series (equation (3.18)) and the relation given in equation (3.20). It utilizes parameters inputted from the *ResultsModel* class, including the lattice diffusion coefficient computed from Arrhenius equation (2.9). Fick's curve based on the elapsed time method is made the same way as the curve without trapping, but the lattice diffusion coefficient is switched out with the effective diffusion coefficient computed from the elapsed time equation (3.5). The numerical approach to Fick's curve loops through incremental values of the diffusion coefficient, and uses the least squares method (equation (3.68)) to determine when the curve fitting is as close as it gets.

The last curve is also a curve fitting, which uses Iino's numerical approaches, described in subsection 3.4.4. It also utilizes the *ResultsModel* parameters, the relation from equation (3.20), and the least squares method to do the fitting, but the equation used to calculate the permeation flux (equation (3.67)) got 4 unknown variables. The kappa variable does not vary too much between the materials tested in this paper, so it is kept constant for now. Firstly the

diffusion coefficient is approximated, by using initial values of the other unknowns. Afterwards the lambda variable is iterating between some boundary conditions, while the my variable is iterating through boundary conditions for every increment of the lambda value.

Two different types of filters where also implemented, one custom made, and another based on Iino's curve. The custom filter exclusively utilizes the data from the experiment, to recognize trends, and respond to noise by removing points either over or under a given limit, represented by two buttons. The Iino's filter works in the same way, but compares the experiment data to the theoretical Iino's data, and removes abnormalities. In addition the user is able to remove unwanted data by double clicking on transient points. Edited charts needs to be updated in the main menu, before reinitialized to be represented correctly.

4.3.3.5 Flux Chart

The permeation flux chart is developed mostly in the same way as the current chart, but it displays the normalized flux as a function of normalized time, instead of the current. These values are retrieved from the *ResultsModel* class as well as most of the parameters. As advised in the standard [1] the normalized flux is plotted against the logarithm of the normalized time.

5 Results

In this chapter the finished software will be presented as a product, by describing the properties of the program in relation to the requirements defined in section 4.3. The functional properties will be elaborated first, and then the properties of Iino's method will be explained, before the non-functional properties will be reviewed.

5.1 Functional properties

This section covers the different functionalities of the finished software, based on the predefined functional requirements from subsection 4.3.1. Descriptions below will include file reading functionality, data displaying functionality, chart creating functionality, curve fitting functionality, and the noise reduction functionality.

5.1.1 File Reader

The software requirement regarding file reading is illustrated by the use case diagram in Figure 4-6. The Swing library presented in subsection 4.2.2 includes a component called *JFileChooser*, which lets the user browse after a file to read, by prompting the frame displayed in Figure 5-1 below. It sets the initial directory path to the user desktop for convenience.

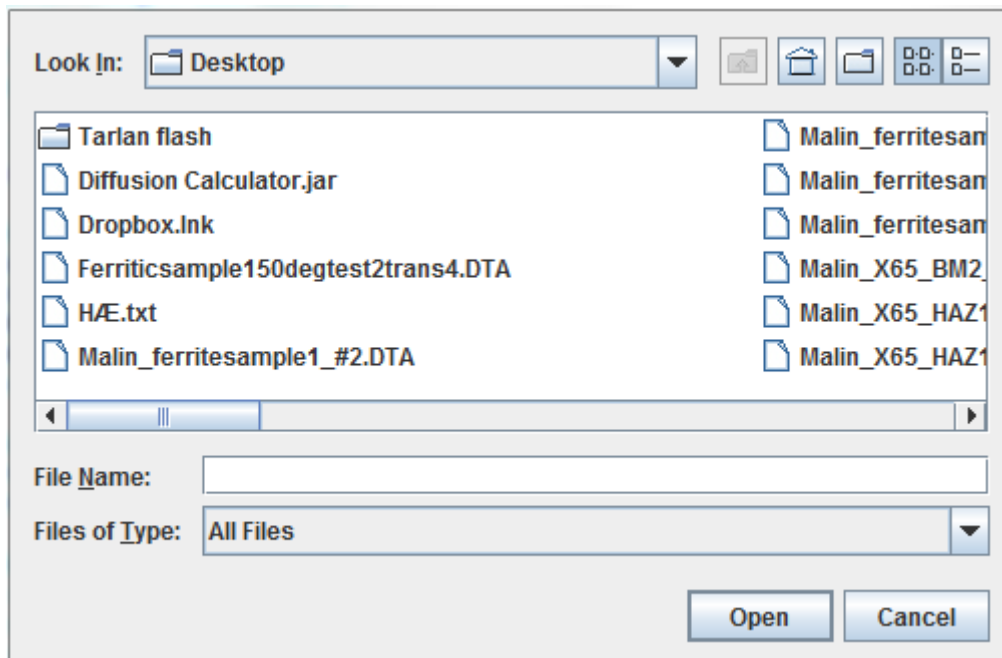


FIGURE 5-1: JFREECHART COMPONENT FROM THE SWING FRAMEWORK 4.2.2), LETTING THE USER SELECT A FILE FROM THE DEVICE HE IS USING

In addition the helper class prompts the user with a Swing component, called a *JOptionPane*, asking when the experimental current is applied, and the duration of the experiment. This information lets the file reader shorten the information needed to read, decreasing runtime, accuracy and storage needed.

5.1.2 Data Display

Displaying of data is defined by the use case diagram in Figure 4-7. The relevant data presented to the user is the time and current data retrieved by the reader classes, current subtracted by the initial background current, computed normalized flux, and computed normalized time. In addition results from computation of the effective diffusion and concentration is displayed including index of where the normalized flux is closest to 0.63, the lattice diffusion coefficient, the maximal current value, the normalized time and regular time when the normalized flux is closest to 0.63, the effective diffusion coefficient computed from equation (3.5) and concentrations computed from equations (3.9),(3.10), and (3.11). After the curve fitting methods have been run from the charts the effective diffusion coefficient from Fick's curve fitting method and Iino's curve fitting method, the kappa, lambda, my, residual, and runtime from Iino's curve fitting method could be presented.

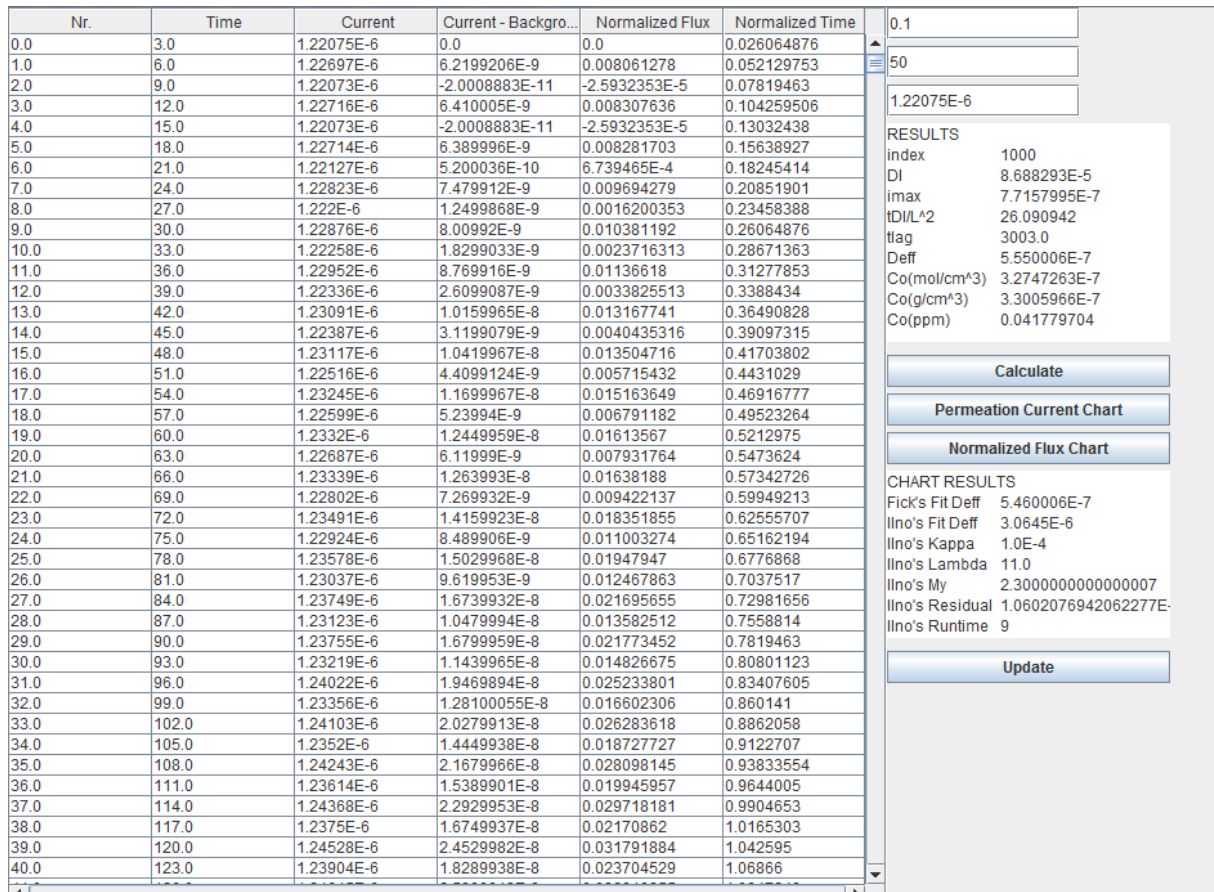


FIGURE 5-2: JFrame CONTAINER FROM THE SWING FRAMEWORK 4.2.2), CONTAINING COLUMNS WITH DATA BOTH EXTRACTED AND COMPUTED FROM THE .DTA FILE, RESULTS FROM EFFECTIVE DIFFUSION COEFFICIENT AND CONCENTRATION CALCULATION, AND PARAMETERS FROM PERFORMED CURVE FITTINGS

The user is prompted with fields where he must enter the thickness of the specimen from the experiment, temperature during the experiment, and the initial background current which needs to be subtracted.

5.1.3 Chart Generator

Requirements regarding the chart generation is depicted by the use case diagram in Figure 4-8. The two types of charts included in the software plots current as a function of time, and normalized flux as a function of the logarithmic normalized time. In addition to the experimental data, Fick's lattice diffusion and effective diffusion curve could be added, and the experimental data could be saved in order to add additional transients later.

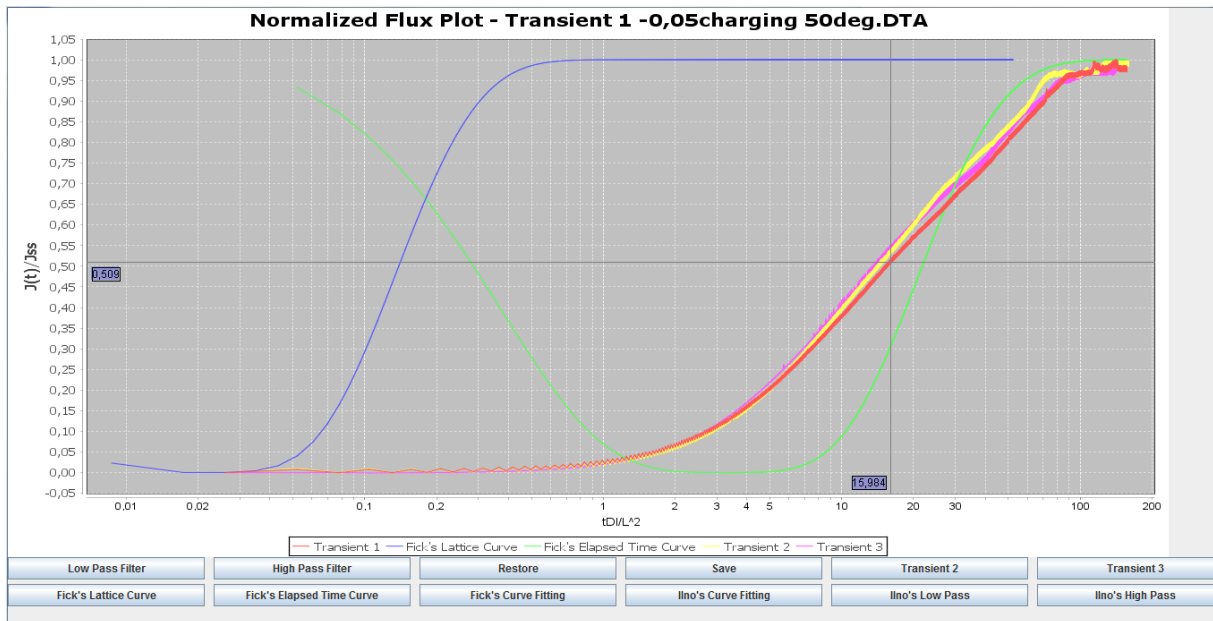


FIGURE 5-3: JFREECHART CHART FROM THE JFREECHART FRAMEWORK(4.2.3), DISPLAYING THE EXPERIMENTAL DATA, FICK'S LATTICE DIFFUSION AND EFFECTIVE DIFFUSION CURVE, AND TWO EXTRA TRANSIENTS ALL ILLUSTRATING THE NORMALIZED FLUX AS A FUNCTION OF NORMALIZED TIME

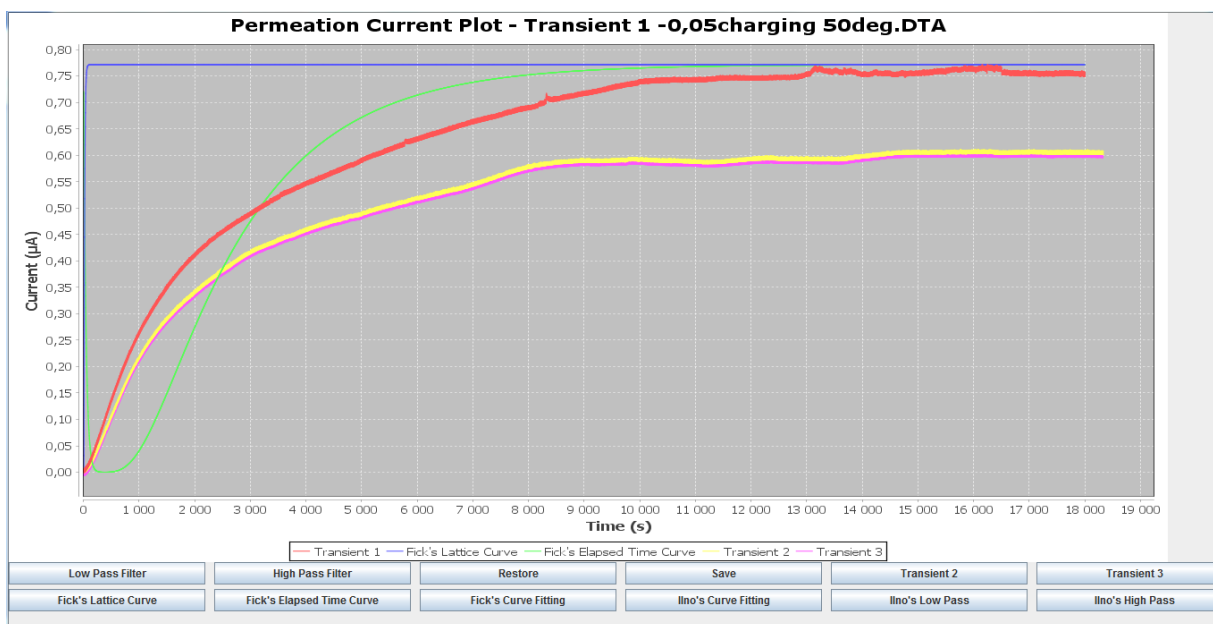


FIGURE 5-4: JFREECHART CHART DISPLAYING THE SAME DATA AS FIGURE 5-3 ILLUSTRATING THE PERMEATION CURRENT AS A FUNCTION OF TIME

The charts illustrated in Figure 5-3 and Figure 5-4, displays the same curves from the same experiment, plotted in the two different charts available in the software. The first transient differs from the following transients, which is more distinguishable in the permeation current

plot. Fick's lattice curve is better represented in the normalized flux chart, and the effective diffusion curve shows equally good tendencies in both illustrations.

5.1.4 Curve Fitter

Figure 4-9 sketches a use case diagram covering the wanted functionalities related to curve fitting. Each of the charts has the ability to perform two different types of curve fitting. Fick's curve fitting has limited significance, because the output gives approximately the same result as Fick's elapsed time curve. Iino's approach gives a much better estimation of the experiment data for both material types. The following charts display the two different curve fitting approaches on experimental data from the two material types.

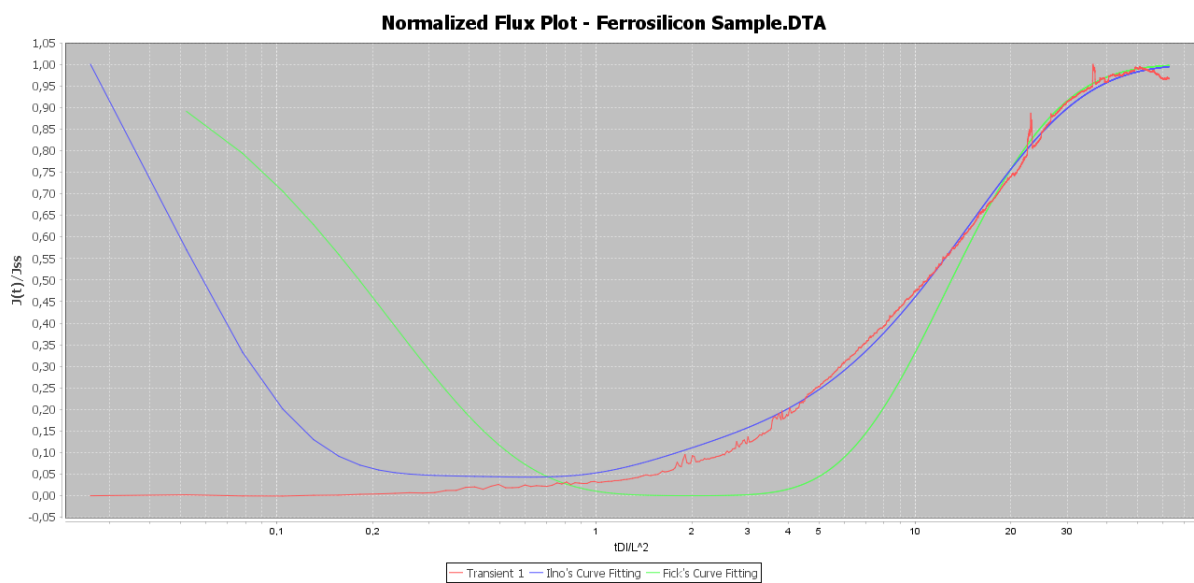


FIGURE 5-5: CHART DISPLAYING NORMALIZED FLUX AS A FUNCTION OF NORMALIZED TIME FOR A FERROSILICON SAMPLE, TESTED AT 50 DEGREES. IINO'S AND FICK'S CURVE FITTINGS ARE PLOTTED TOGETHER WITH THE EXPERIMENTAL DATA

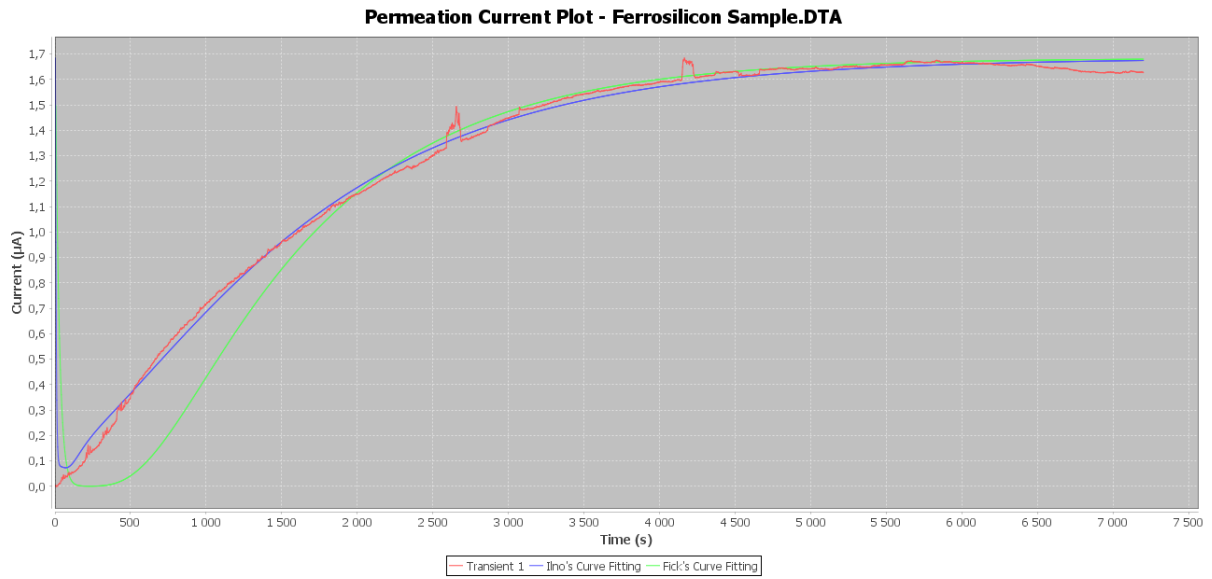


FIGURE 5-6: CHART DISPLAYING CATHODIC CURRENT AS A FUNCTION OF TIME FOR A FERROSILICON SAMPLE, TESTED AT 50 DEGREES. IINO'S AND FICK'S CURVE FITTINGS ARE PLOTTED TOGETHER WITH THE EXPERIMENTAL DATA

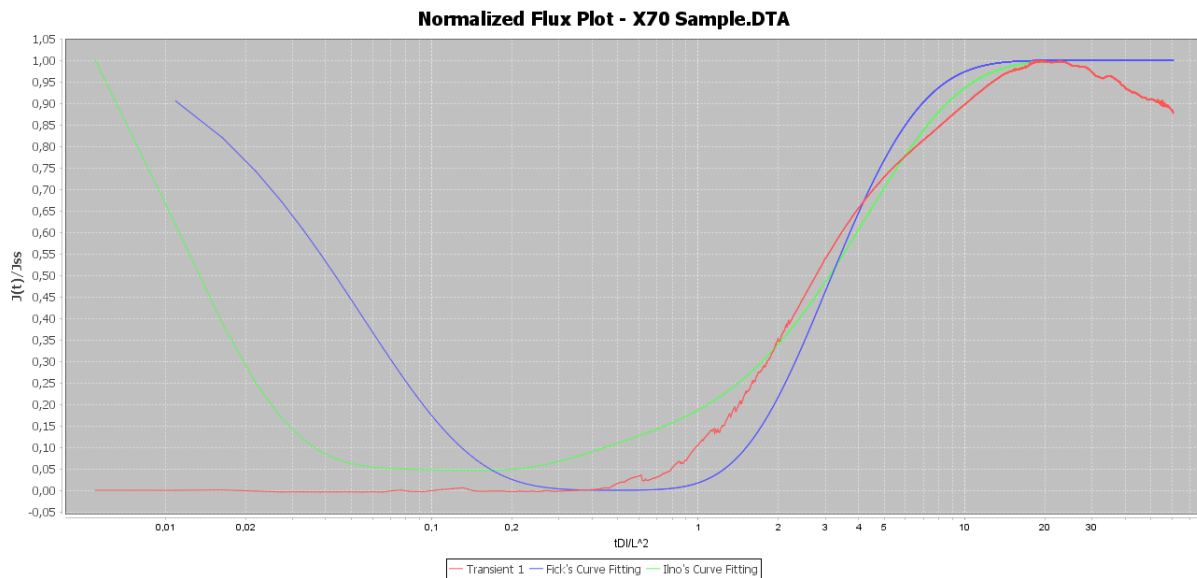


FIGURE 5-7 : CHART DISPLAYING NORMALIZED FLUX AS A FUNCTION OF NORMALIZED TIME FOR AN X70 SAMPLE, TESTED AT 30 DEGREES. IINO'S AND FICK'S CURVE FITTINGS ARE PLOTTED TOGETHER WITH THE EXPERIMENTAL DATA

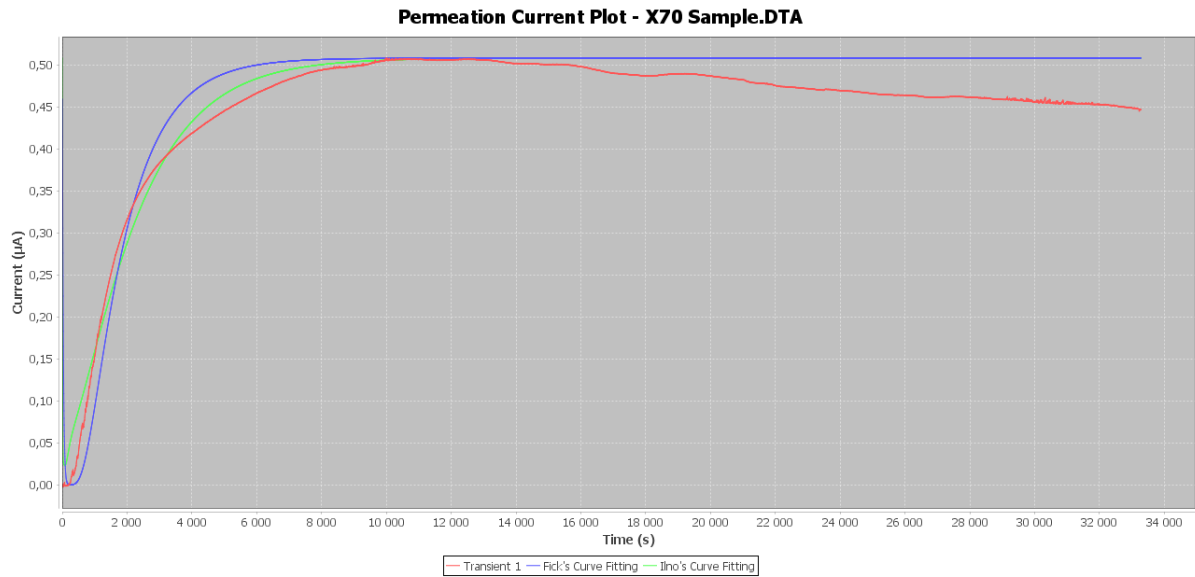


FIGURE 5-8: CHART DISPLAYING CATHODIC CURRENT AS A FUNCTION OF TIME FOR AN X70 SAMPLE, TESTED AT 30 DEGREES. IINO'S AND FICK'S CURVE FITTINGS ARE PLOTTED TOGETHER WITH THE EXPERIMENTAL DATA

Material	FeSi	X70
Elapsed Time D_{eff}	9.46E-7	3.37E-6
Fick's Fit D_{eff}	9.28E-7	3.36E-6
Iino's Fit D_{eff}	4.57E-6	1.62E-5
Iino's Kappa	1.0E-4	1.0E-4
Iino's Lambda	22.0	23.0
Iino's My	6.29	5.5

TABLE 5-1: TABLE DISPLAYING RESULTS FROM THE CURVE FITTINGS IN FIGURE 5-5 TO FIGURE 5-8

5.1.5 Noise Reduction

Figure 4-9 sketches a use case diagram covering the wanted functionalities related to curve fitting, which also includes the ability to manipulate the experimental data by using various filters, in order to reduce the effect of noise occurrence. The three implemented approaches, Iino's curve filter, custom low pass filter, and manually data remover, works differently and gives good representations on various datasets.

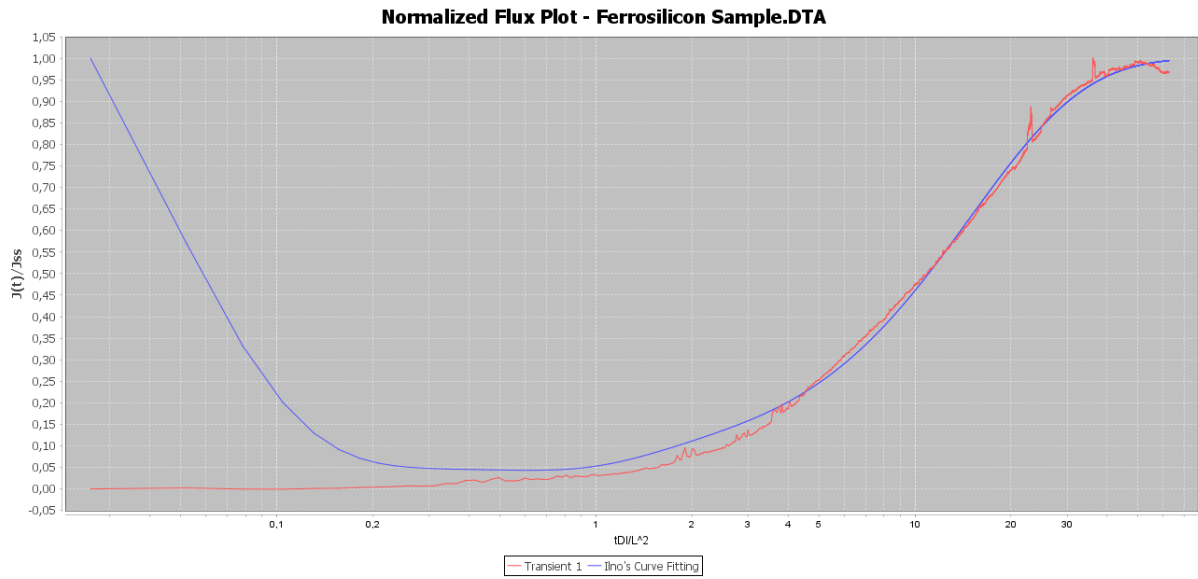


FIGURE 5-9: CHART DISPLAYING NORMALIZED FLUX AS A FUNCTION OF NORMALIZED TIME FOR A FERROSILICON SAMPLE, TESTED AT 50 DEGREES. THE IINO APPROXIMATION HAS LOW DEVIATION BEFORE NOISE REDUCTION, BUT THE HIGHEST POINT IS DETERMINED BY AN INTERFERENCE

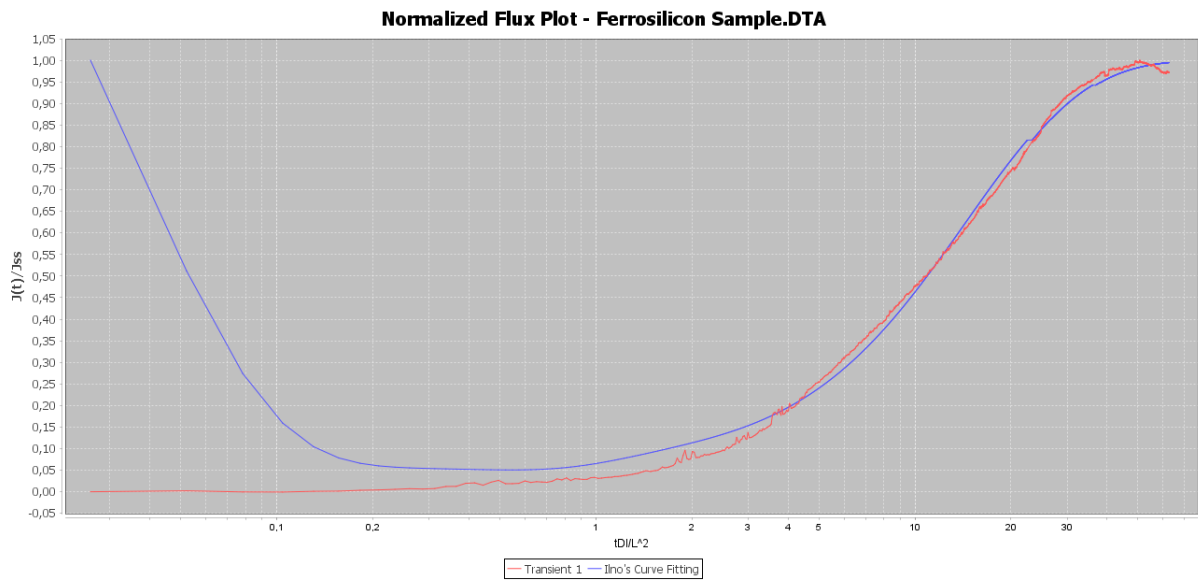


FIGURE 5-10: CHART DISPLAYING NORMALIZED FLUX AS A FUNCTION OF NORMALIZED TIME FOR A FERROSILICON SAMPLE, TESTED AT 50 DEGREES. THE NOISE HAVE BEEN REDUCED MANUALLY, WHICH GIVES A SLIGHTLY BETTER IINO APPROXIMATION

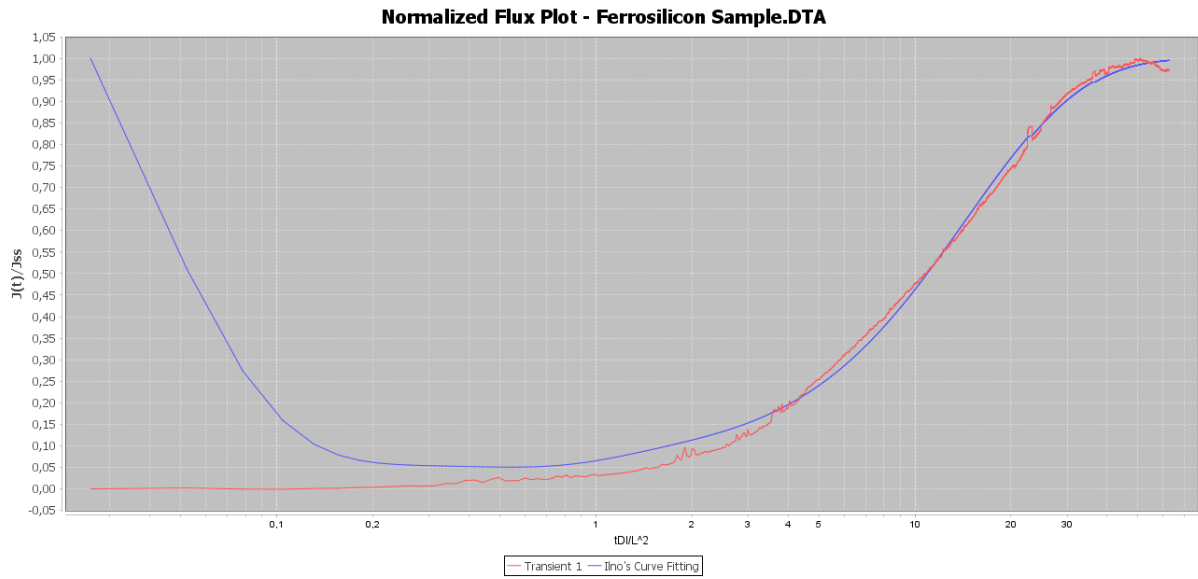


FIGURE 5-11: CHART DISPLAYING NORMALIZED FLUX AS A FUNCTION OF NORMALIZED TIME FOR A FERROSILICON SAMPLE, TESTED AT 50 DEGREES. THE NOISE HAVE BEEN REDUCED BY IINO'S FILTER, GIVING THE SAME APPROXIMATION AS IN FIGURE 5-10

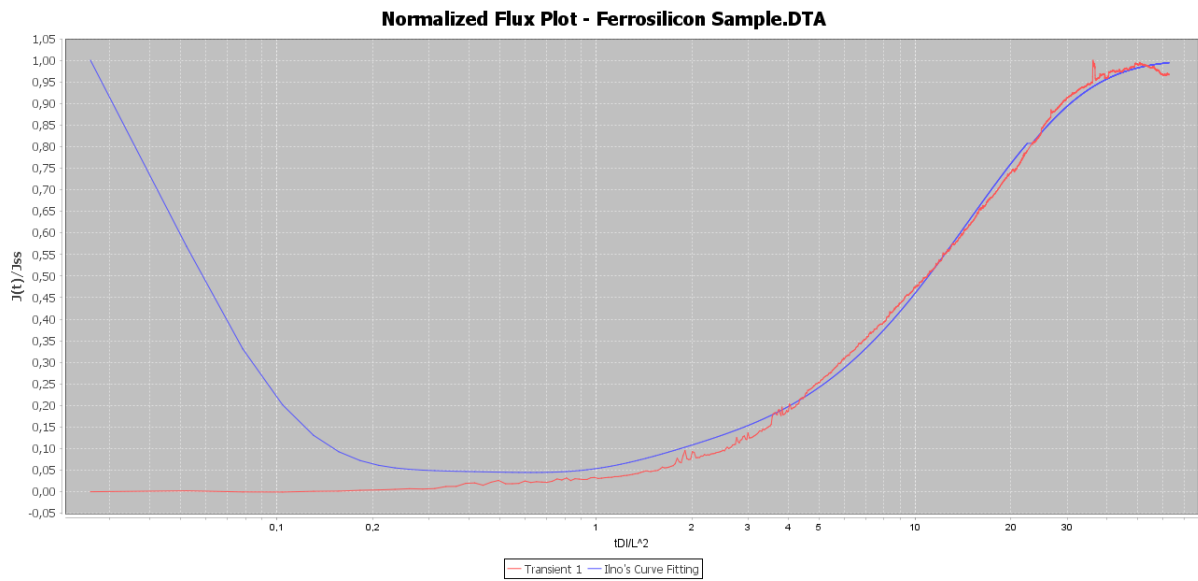


FIGURE 5-12: CHART DISPLAYING NORMALIZED FLUX AS A FUNCTION OF NORMALIZED TIME FOR A FERROSILICON SAMPLE, TESTED AT 50 DEGREES. THE NOISE HAVE BEEN REDUCED USING THE LOW PASS FILTER, GIVING A BIT BETTER APPROXIMATION, BUT FAILING AT REMOVING THE WORST NOISE

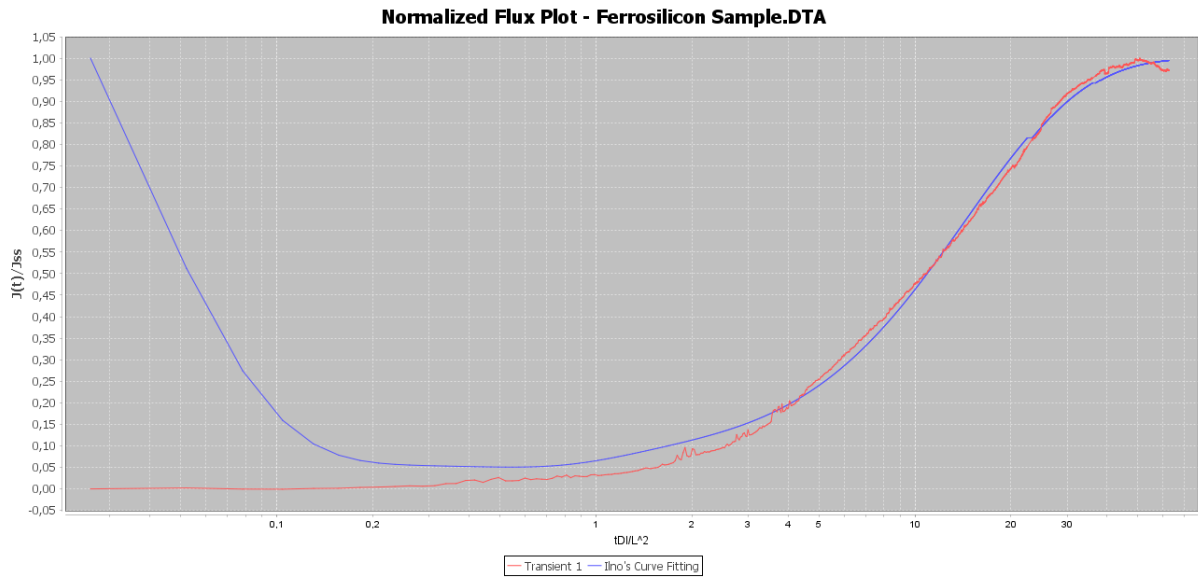


FIGURE 5-13: CHART DISPLAYING NORMALIZED FLUX AS A FUNCTION OF NORMALIZED TIME FOR A FERROSILICON SAMPLE, TESTED AT 50 DEGREES. NOISE REDUCED USING LOW PASS FILTER AND MANUAL DATA REMOVAL, RESULTING IN THE SAME APPROXIMATION AS FIGURE 5-10 AND FIGURE 5-11

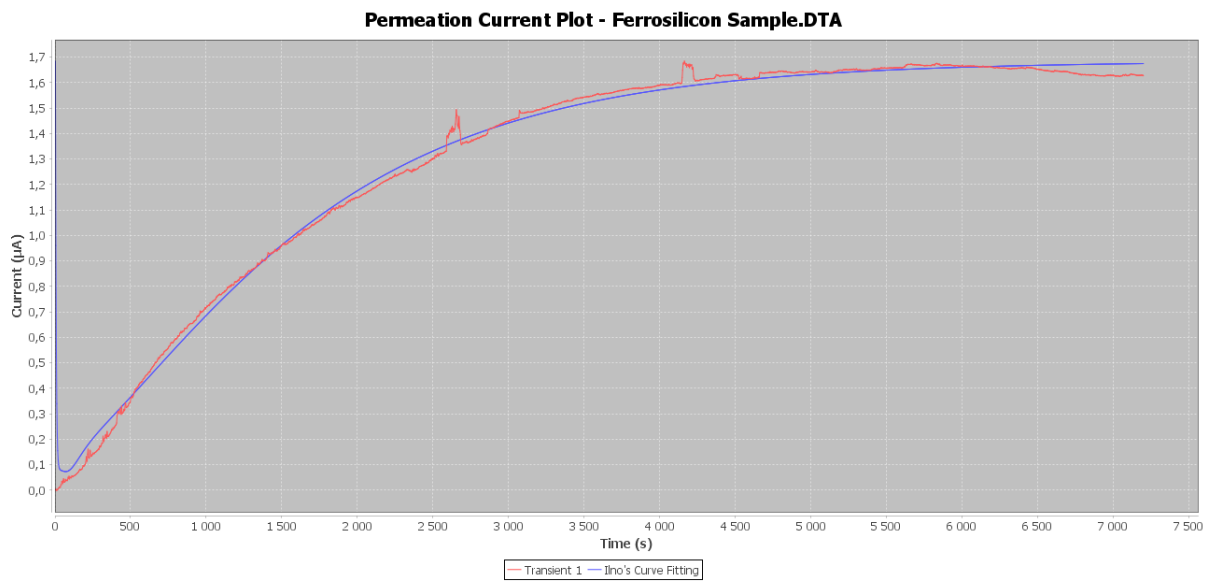


FIGURE 5-14: CHART DISPLAYING CATHODIC CURRENT AS A FUNCTION OF TIME FOR A FERROSILICON SAMPLE, TESTED AT 50 DEGREES. THE IINO APPROXIMATION HAS LOW DEVIATION BEFORE NOISE REDUCTION, BUT THE HIGHEST POINT IS DETERMINED BY AN INTERFERENCE

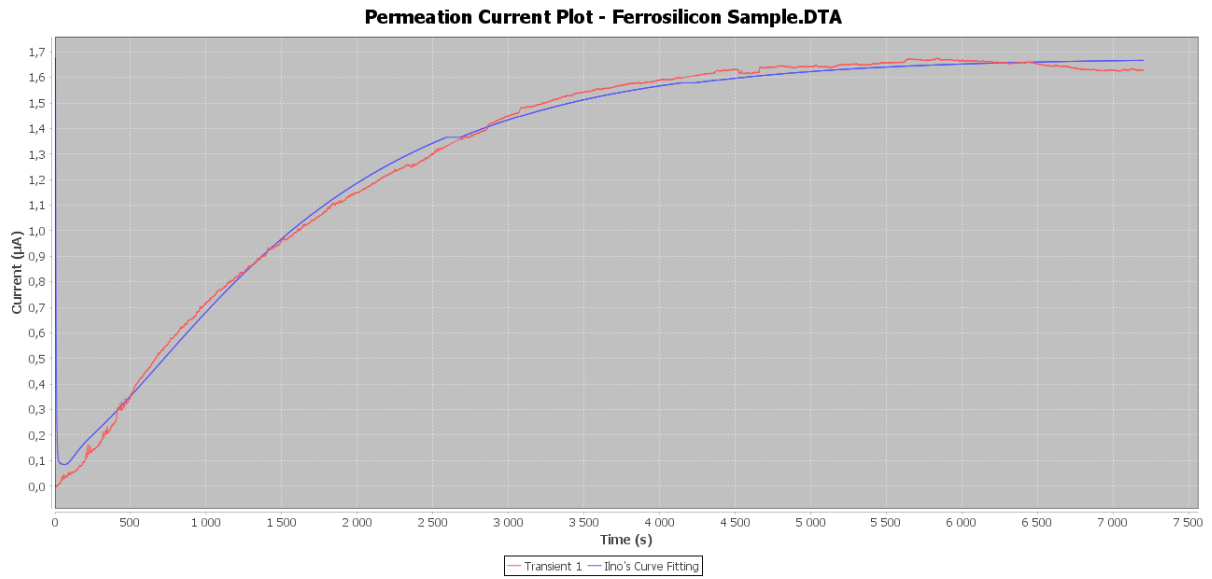


FIGURE 5-15: CHART DISPLAYING CATHODIC CURRENT AS A FUNCTION OF TIME FOR A FERROSILICON SAMPLE, TESTED AT 50 DEGREES. THE NOISE HAVE BEEN REDUCED MANUALLY, WHICH GIVES A BETTER IINO APPROXIMATION

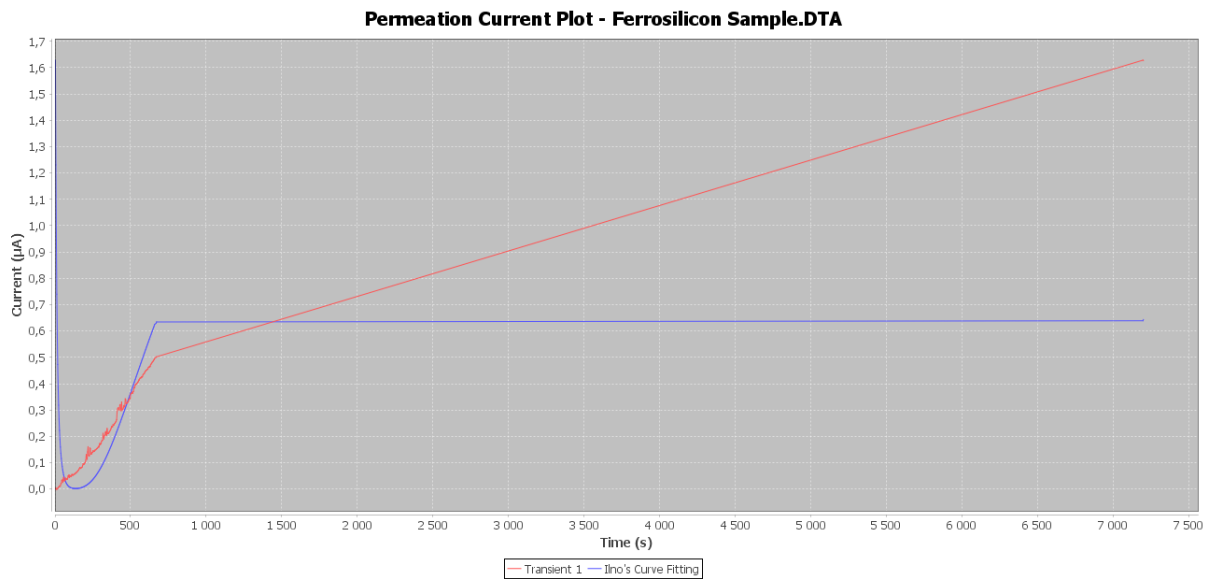


FIGURE 5-16: CHART DISPLAYING CATHODIC CURRENT AS A FUNCTION OF TIME FOR A FERROSILICON SAMPLE, TESTED AT 50 DEGREES. THE NOISE HAVE BEEN REDUCED USING THE IINO'S METHOD, WHICH REMOVES TO MUCH DATA, GIVING A WRONG APPROXIMATION BY IINO'S METHOD

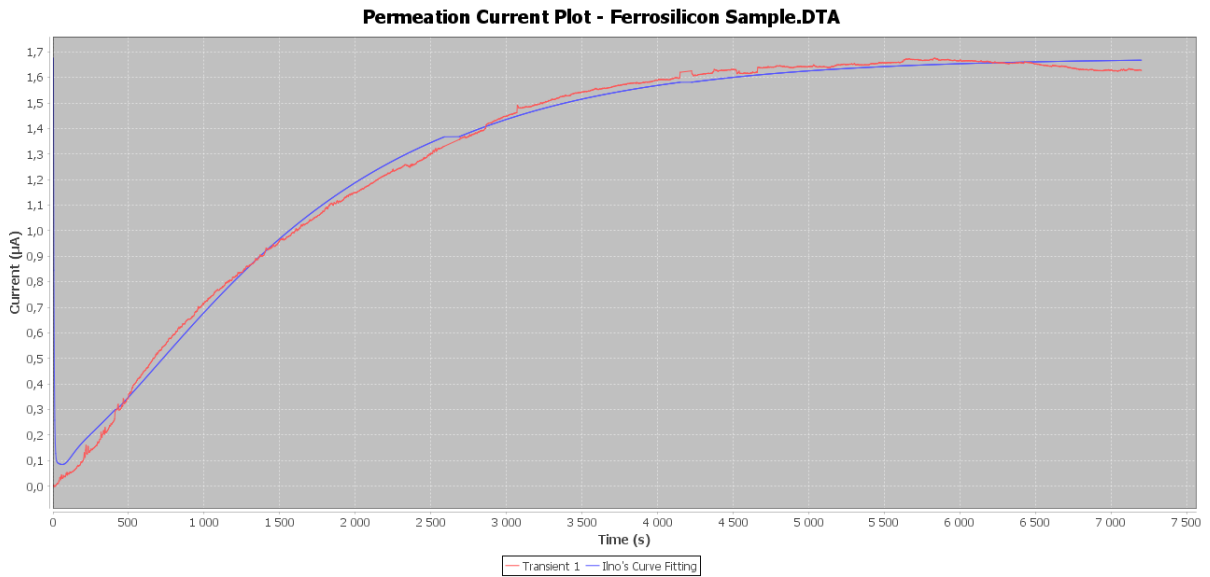


FIGURE 5-17: CHART DISPLAYING CATHODIC TIME AS A FUNCTION OF TIME FOR A FERROSILICON SAMPLE, TESTED AT 50 DEGREES. THE NOISE HAVE BEEN REDUCED USING THE LOW PASS FILTER, GIVING SLIGHTLY BETTER APPROXIMATION

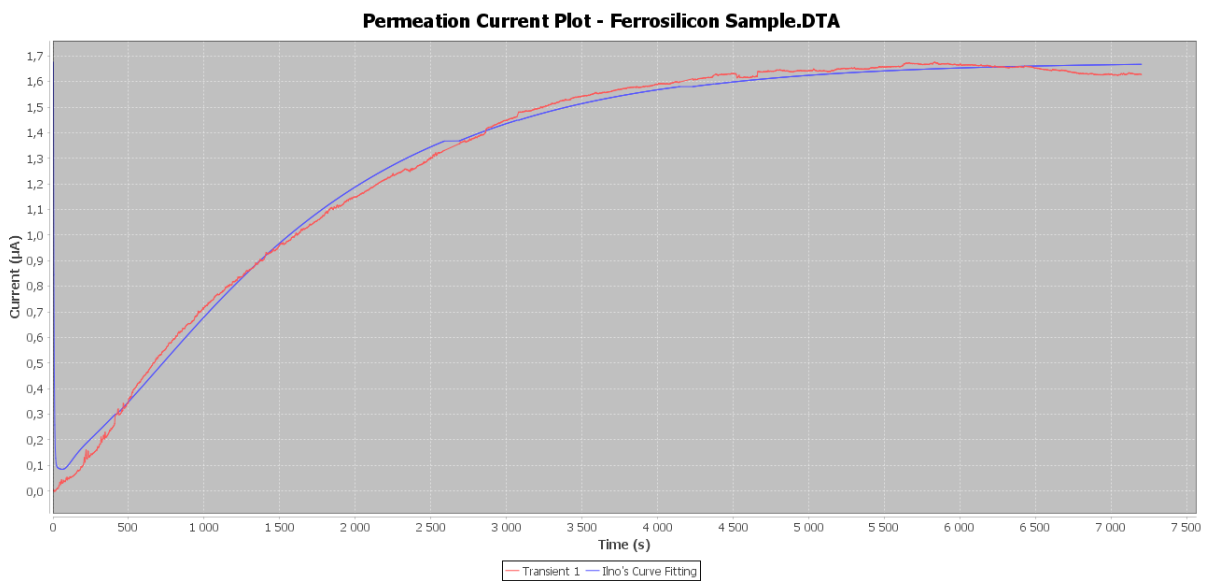


FIGURE 5-18: CHART DISPLAYING CATHODIC CURRENT AS A FUNCTION OF TIME FOR A FERROSILICON SAMPLE, TESTED AT 50 DEGREES. NOISE REDUCED BY APPLYING THE LOW PASS FILTER, AND USING THE DATA REMOVER FUNCTION, YIELDING THE SAME APPROXIMATION AS IN FIGURE 5-17

Noise Reduction for Flux	Ferrosilicon Noisy	Ferrosilicon Noise Reduced Manually	Ferrosilicon Noise Reduced Iino's Filter	Ferrosilicon Noise Reduced Low Pass Filter	Ferrosilicon Noise Reduced Low Pass Filter + Manually
Elapsed Time D_{eff}	9.46E-7	9.54E-7	9.54E-7	9.464322E-7	9.54E-7
Iino's Fit D_{eff}	4.57E-6	5.48E-6	5.48E-6	4.594643E-6	5.48E-6
Iino's Kappa	1.0E-4	1.0E-4	1.0E-4	1.0E-4	1.0E-4
Iino's Lambda	22.0	26.0	26.0	23.0	26.0
Iino's My	6.3	6.1	6.1	6.6	6.1

TABLE 5-2: RESULTS FROM NOISE REDUCTION PROCEDURES FOR NORMALIZED FLUX CHART DATA FROM FERROSILICON MATERIAL EXPERIMENTS DEPICTED IN FIGURE 5-9 TO FIGURE 5-13

Noise Reduction for Current	Ferrosilicon Noisy	Ferrosilicon Noise Reduced Manually	Ferrosilicon Noise Reduced Iino's Filter	Ferrosilicon Noise Reduced Low Pass Filter	Ferrosilicon Noise Reduced Low Pass Filter + Manually
Elapsed Time D_{eff}	9.46E-7	9.54E-7	2.4801593E-6	9.54E-7	9.54E-7
Iino's Fit D_{eff}	4.57E-6	5.48E-6	2.317016E-6	5.60E-6	5.60E-6
Iino's Kappa	1.0E-4	1.0E-4	1.0E-4	1.0E-4	1.0E-4
Iino's Lambda	22.0	26.0	93.0	26.0	26.0

Iino's My	6.3	6.1	295.0	6.0	6.0
-----------	-----	-----	-------	-----	-----

TABLE 5-3: RESULTS FROM NOISE REDUCTION PROCEDURES FOR CATHODIC CURRENT CHART DATA FROM FERROSILICON MATERIAL EXPERIMENTS DEPICTED IN FIGURE 5-14 TO FIGURE 5-18

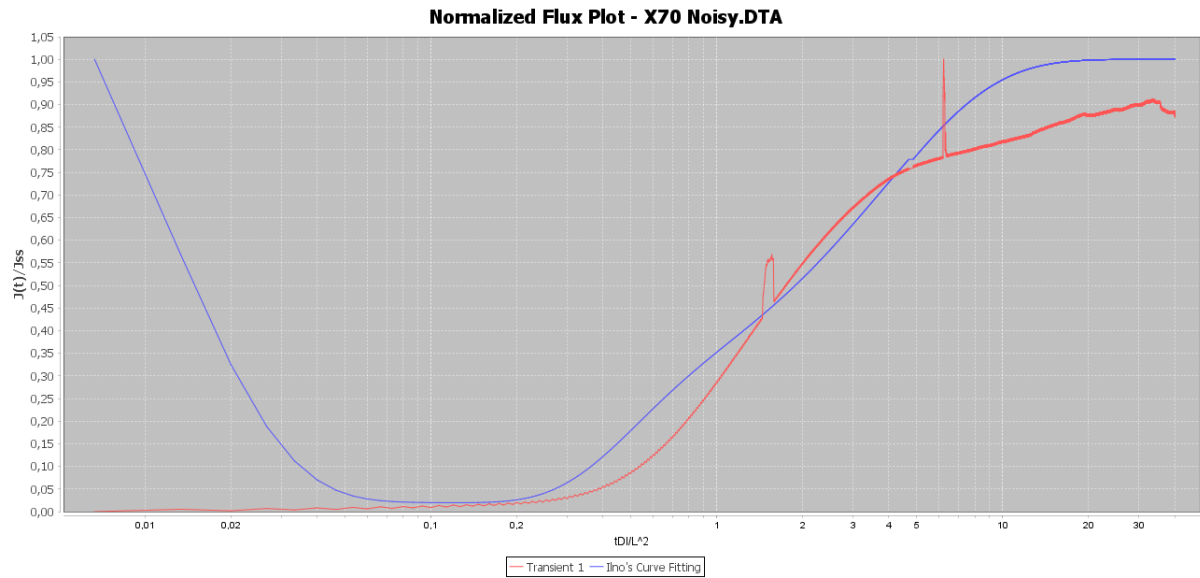


FIGURE 5-19: CHART DISPLAYING NORMALIZED FLUX AS A FUNCTION OF NORMALIZED TIME FOR AN X70 SAMPLE, TESTED AT 50 DEGREES. THE EXPERIMENTAL DATA IS VERY NOISY, AND THE IINO APPROXIMATION IS NOT ACCURATE

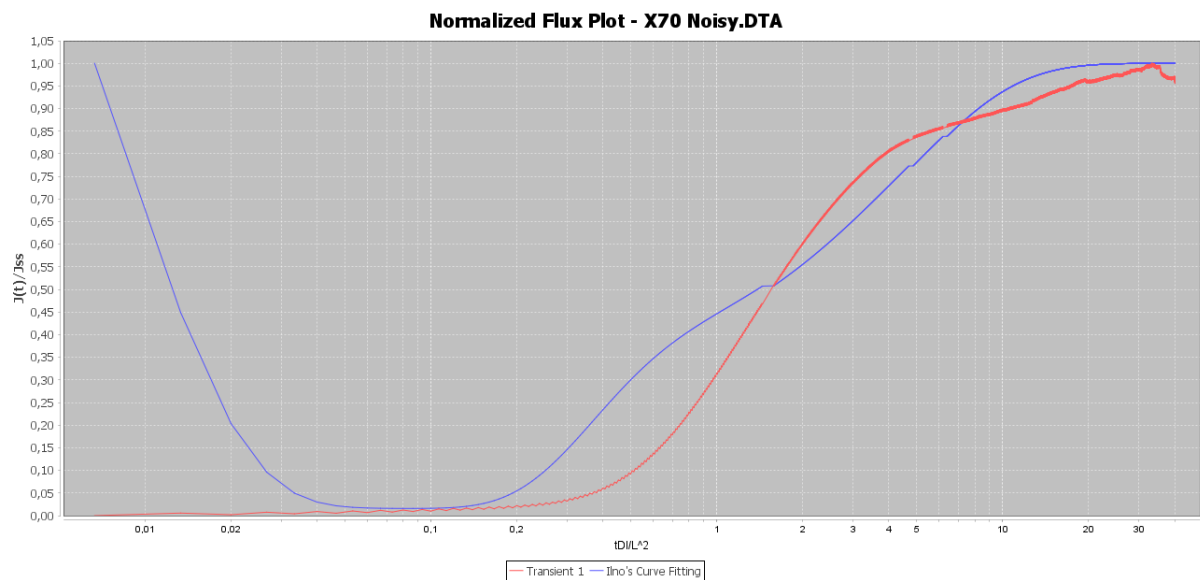


FIGURE 5-20: CHART DISPLAYING NORMALIZED FLUX AS A FUNCTION OF NORMALIZED TIME FOR AN X70 SAMPLE, TESTED AT 50 DEGREES. THE NOISE HAVE BEEN REDUCED MANUALLY, WHICH GIVES A BETTER IINO APPROXIMATION

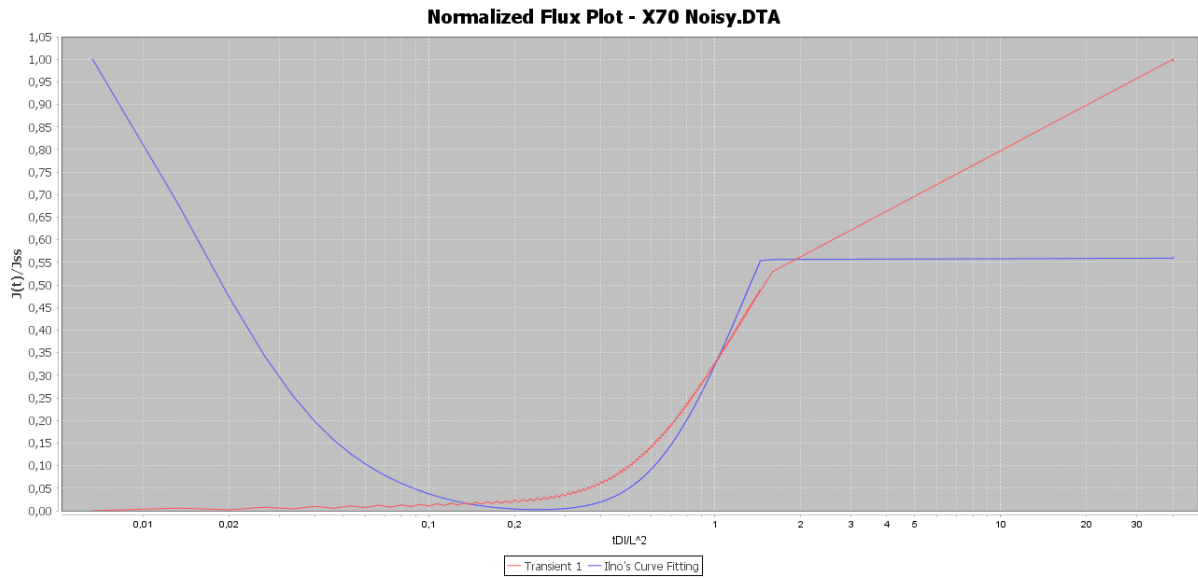


FIGURE 5-21: CHART DISPLAYING NORMALIZED FLUX AS A FUNCTION OF NORMALIZED TIME FOR AN X70 SAMPLE, TESTED AT 50 DEGREES. THE NOISE HAVE BEEN REDUCED USING IINO'S LOW PASS FILTER, REMOVING TOO MUCH EXPERIMENTAL DATA, GIVING AN WRONG APPROXIMATION BY IINO'S METHOD

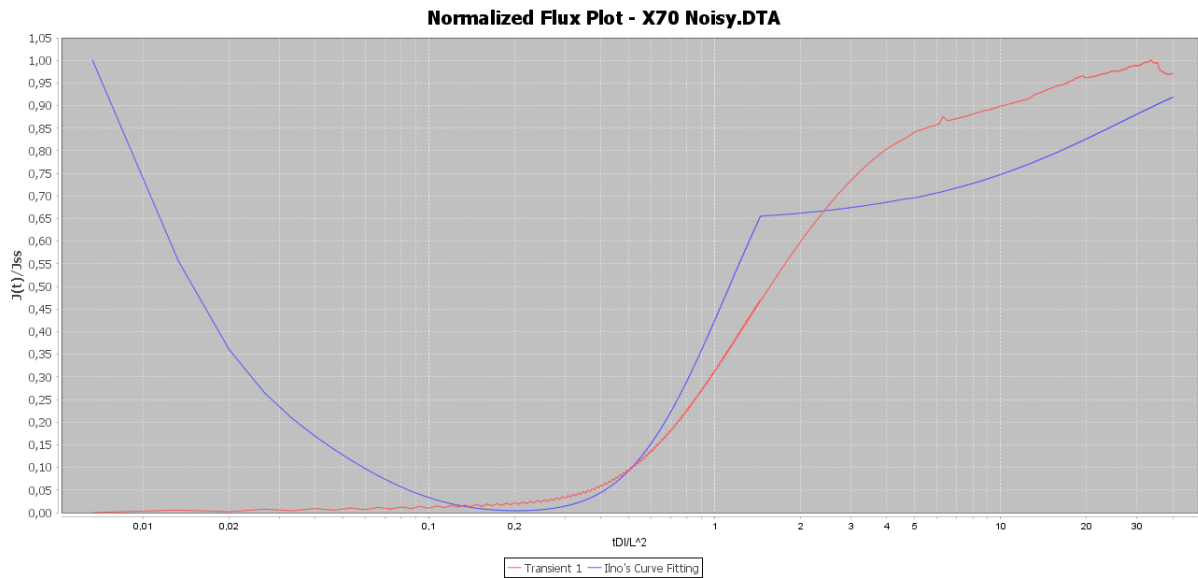


FIGURE 5-22: CHART DISPLAYING NORMALIZED FLUX AS A FUNCTION OF NORMALIZED TIME FOR AN X70 SAMPLE, TESTED AT 50 DEGREES. THE NOISE HAVE BEEN REDUCED USING THE LOW PASS FILTER MULTIPLE TIMES, GIVING A BETTER REPRESENTATION OF THE EXPERIMENTAL DATA, BUT STILL GIVING AN WRONG APPROXIMATION BY IINO'S METHOD

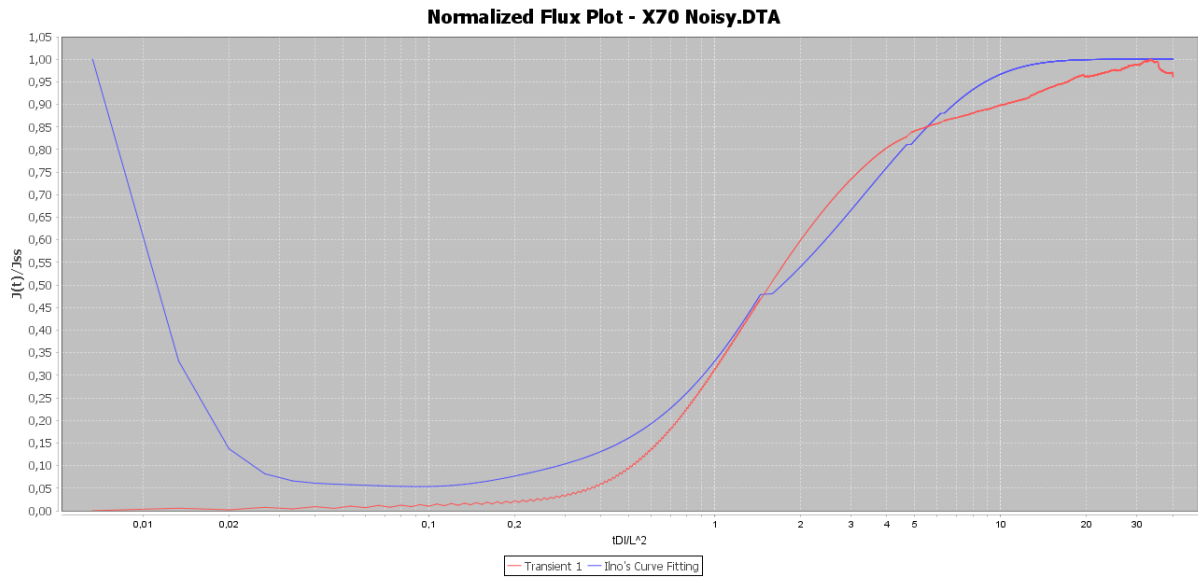


FIGURE 5-23: CHART DISPLAYING NORMALIZED FLUX AS A FUNCTION OF NORMALIZED TIME FOR AN X70 SAMPLE, TESTED AT 50 DEGREES. THE NOISE HAVE BEEN REDUCED USING THE LOW PASS FILTER ONE TIME TO REDUCE THE SMALL DIFFERENCES, AND THEN MANUALLY REMOVING THE BIGGEST DEVIATIONS. THIS GIVES THE BEST APPROXIMATION.

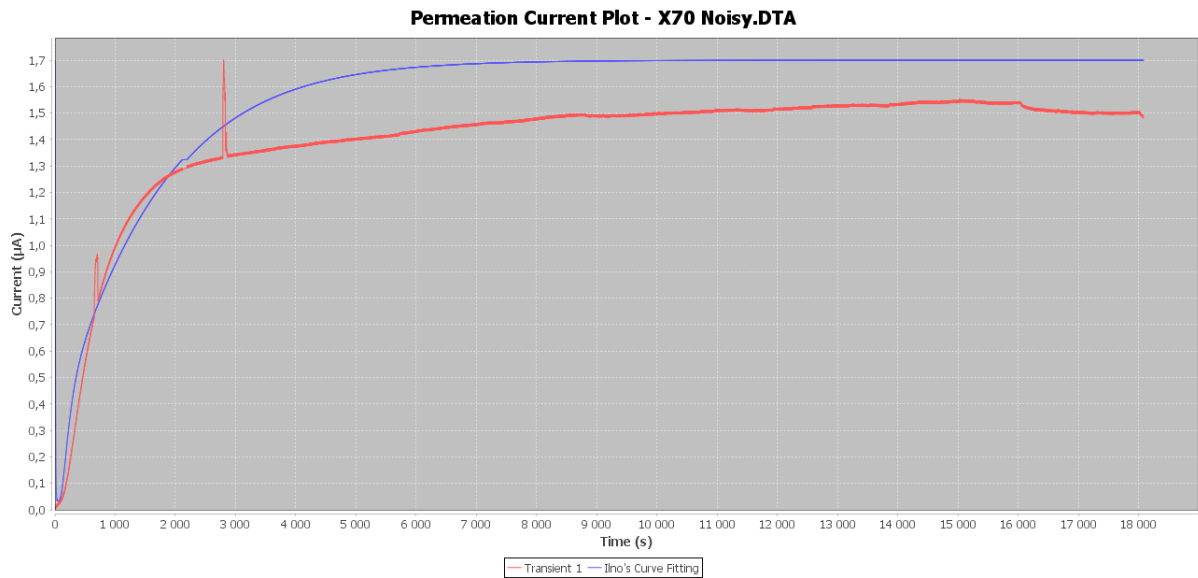


FIGURE 5-24: CHART DISPLAYING CATHODIC CURRENT AS A FUNCTION OF TIME FOR AN X70 SAMPLE, TESTED AT 50 DEGREES. THE EXPERIMENTAL DATA IS VERY NOISY, AND THE IINO APPROXIMATION IS NOT ACCURATE

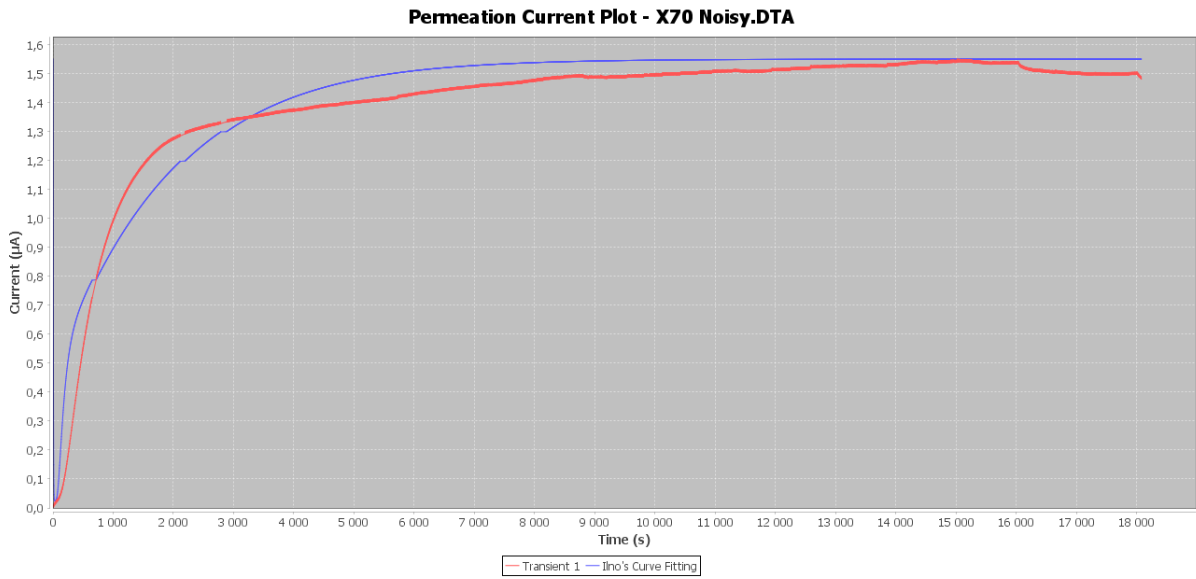


FIGURE 5-25: CHART DISPLAYING CATHODIC CURRENT AS A FUNCTION OF TIME FOR AN X70 SAMPLE, TESTED AT 50 DEGREES. THE NOISE HAVE BEEN REDUCED MANUALLY, WHICH GIVES A BETTER IINO APPROXIMATION

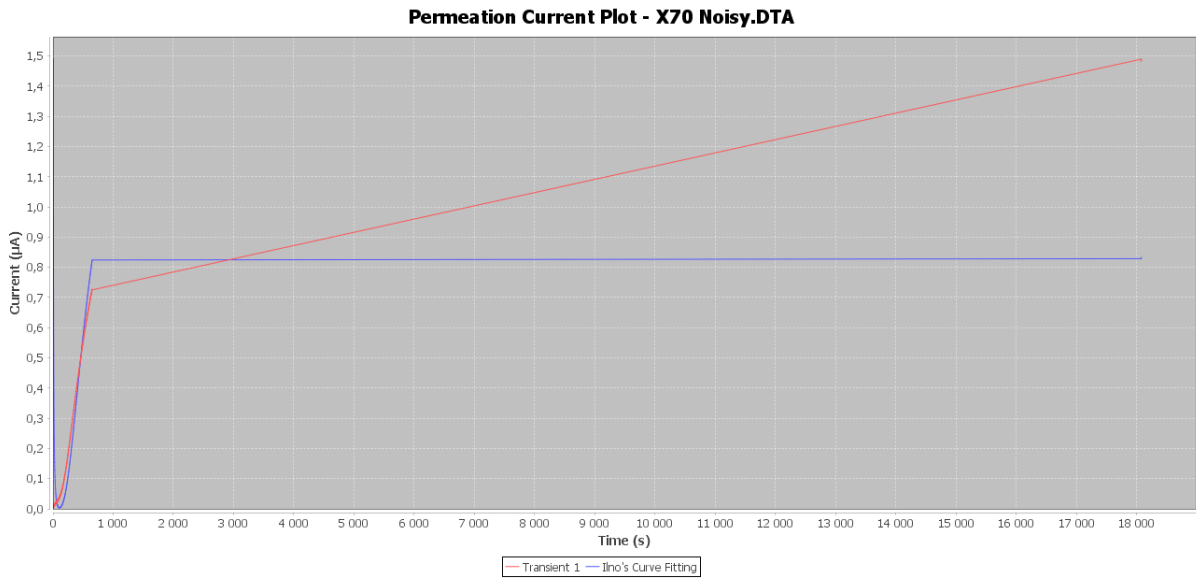


FIGURE 5-26: CHART DISPLAYING CATHODIC CURRENT AS A FUNCTION OF TIME FOR AN X70 SAMPLE, TESTED AT 50 DEGREES. THE NOISE HAVE BEEN REDUCED USING IINO'S LOW PASS FILTER, REMOVING TO MUCH EXPERIMENTAL DATA, GIVING AN WRONG APPROXIMATION

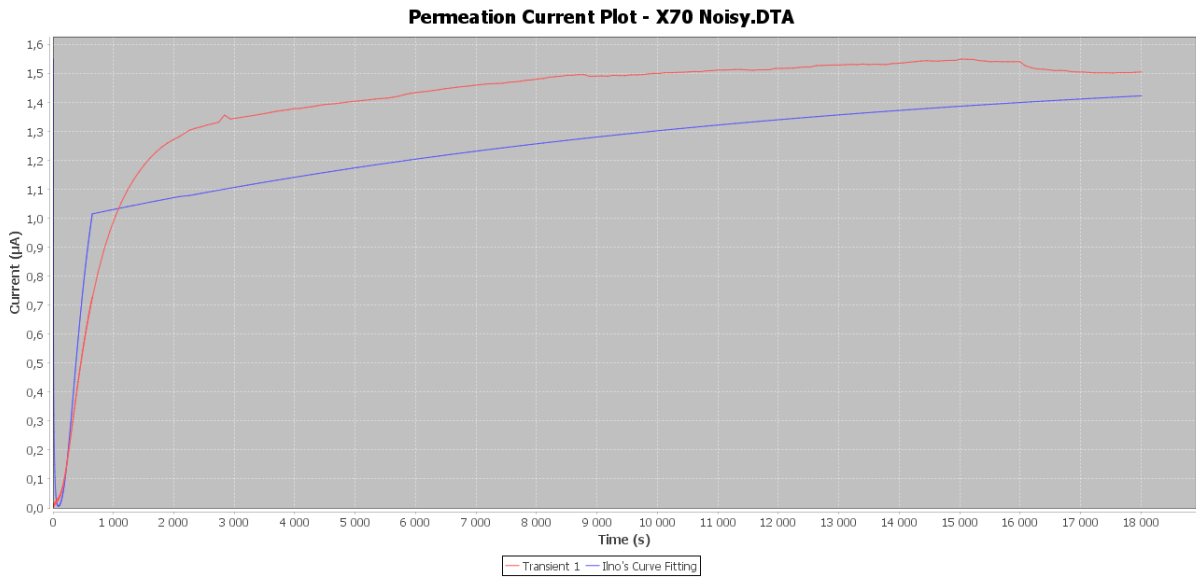


FIGURE 5-27: CHART DISPLAYING CATHODIC TIME AS A FUNCTION OF TIME FOR AN X70 SAMPLE, TESTED AT 50 DEGREES. THE NOISE HAVE BEEN REDUCED USING THE LOW PASS FILTER MULTIPLE TIMES, GIVING A BETTER REPRESENTATION OF THE EXPERIMENTAL DATA, BUT STILL GIVING AN WRONG APPROXIMATION BY IINO'S METHOD

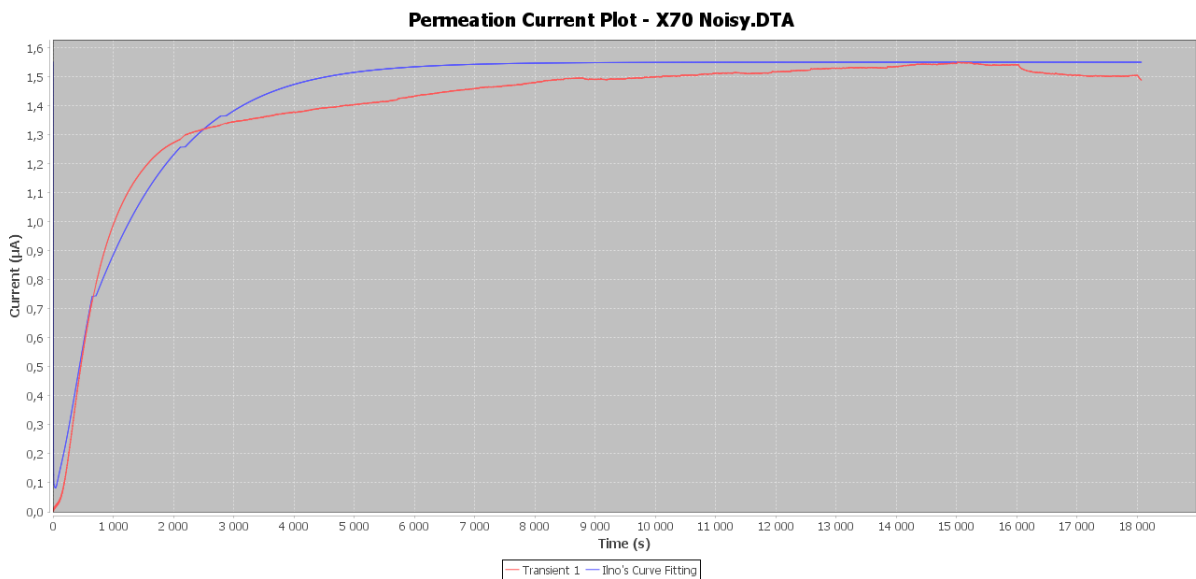


FIGURE 5-28: CHART DISPLAYING CATHODIC CURRENT AS A FUNCTION OF TIME FOR AN X70 SAMPLE, TESTED AT 50 DEGREES. THE NOISE HAVE BEEN REDUCED USING THE LOW PASS FILTER ONE TIME TO REDUCE THE SMALL DIFFERENCES, AND THEN MANUALLY REMOVING THE BIGGEST DEVIATIONS. THIS GIVES THE BEST APPROXIMATION.

Noise Reduction for Flux and Current	X70 Noisy	X70 Noise Reduced Manually	X70 Noise Reduced Iino's Filter	X70 Noise Reduced Low Pass Filter	X70 Noise Reduced Low Pass Filter + Manually
Elapsed Time D_{eff}	5.58E-6	6.75E-6	9.09E-6	6.94E-6	6.64E-6
Iino's Fit D_{eff}	1.77E-5	2.51E-5	1.2718457E-5	2.11E-5	3.63E-5
Iino's Kappa	1.0E-4	1.0E-4	1.0E-4	1.0E-4	1.0E-4
Iino's Lambda	9.0	7.0	81.0	156.0	29.0
Iino's My	3.3	1.7	205.0	163.0	7.69

TABLE 5-4: RESULTS FROM NOISE REDUCTION PROCEDURES FOR NORMALIZED FLUX CHART DATA FROM X70 MATERIAL EXPERIMENTS DEPICTED IN FIGURE 5-19 TO FIGURE 5-28

5.2 Iino's Method

Iino's method required extensive "training" in order to discover the initial and boundary conditions working for both the X70 (subsection 2.4.1) and the FeSi (subsection 2.4.2) steel specimens tested in the experiments. In order to make the method functional for both materials, the curve fitting is first given one set of initial and boundary conditions, traversing roughly through the method. Afterwards the best approximation alters the initial and boundary conditions, before the method is run again with smaller steps. This procedure is repeated one more time, with even smaller step sizes.

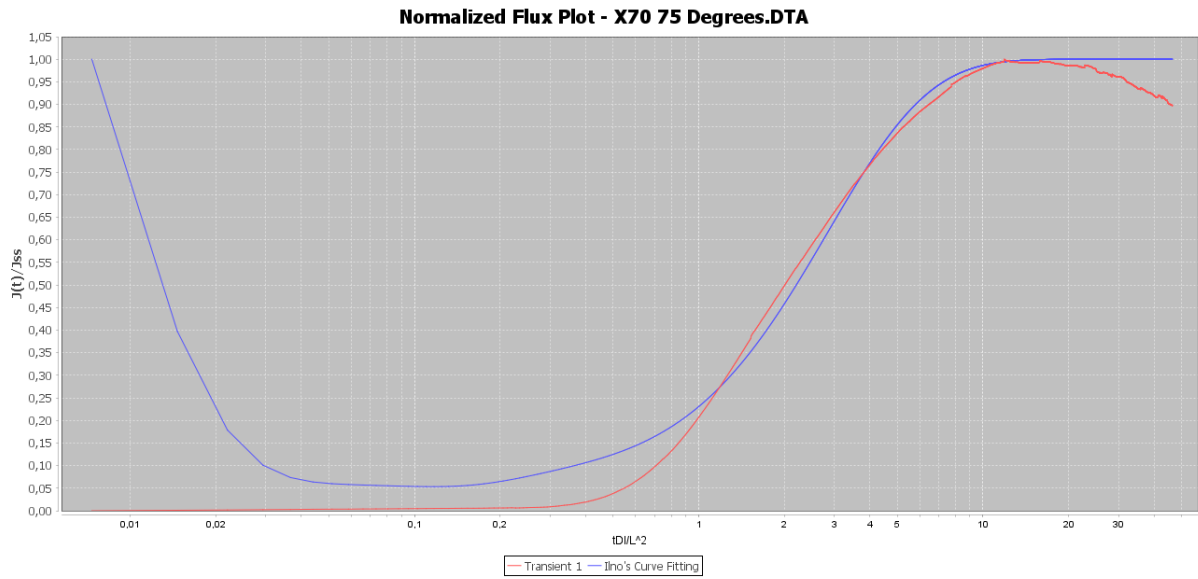


FIGURE 5-29: CHART DISPLAYING NORMALIZED FLUX AS A FUNCTION OF NORMALIZED TIME FOR AN X70 SAMPLE, TESTED AT 75 DEGREES. THE IINO NUMERICAL CURVE FITTING IS FAIRLY ACCURATE

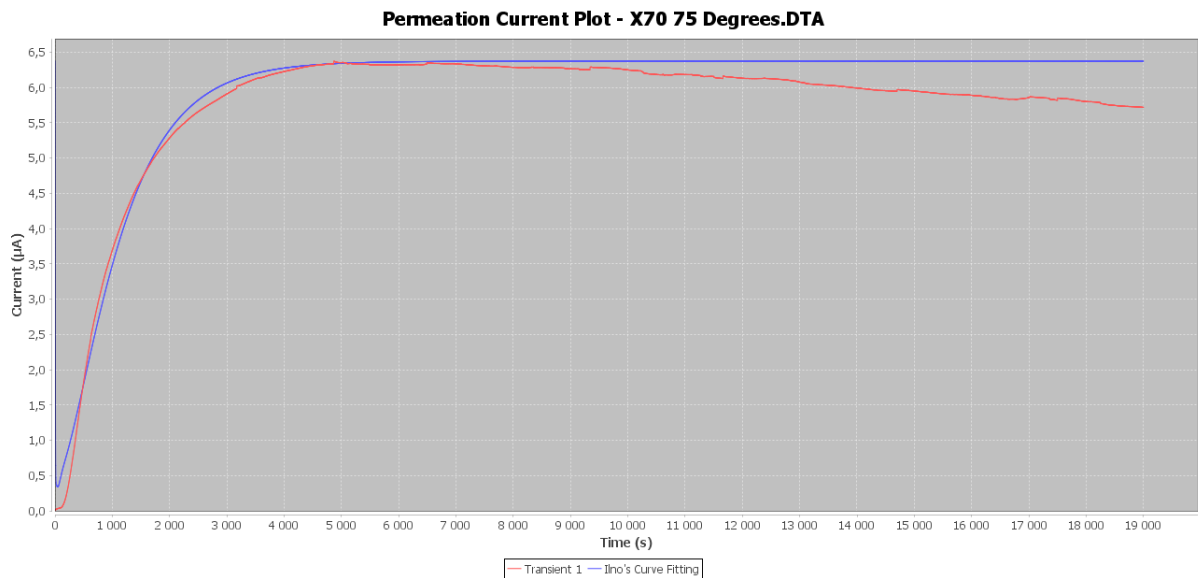


FIGURE 5-30: CHART DISPLAYING CATHODIC CURRENT AS A FUNCTION OF TIME FOR AN X70 SAMPLE, TESTED AT 75 DEGREES. THE IINO NUMERICAL CURVE FITTING IS FAIRLY ACCURATE

Elapsed Time D_{eff}	Iino's D_{eff}	Iino's Kappa	Iino's Lambda	Iino's My
6.08E-6	3.18E-5	1.0E-4	28.0	6.6

TABLE 5-5: RESULTS FROM THE CURVE FITTING OF AN X70 MATERIAL EXPERIMENTAL DATA SET, DEPICTED BY THE CHART IN FIGURE 5-29 AND FIGURE 5-30

The kappa value representing properties related to irreversible traps gave the best approximations if it is as close to zero as possible, thus rendering it constant through the analysis method.

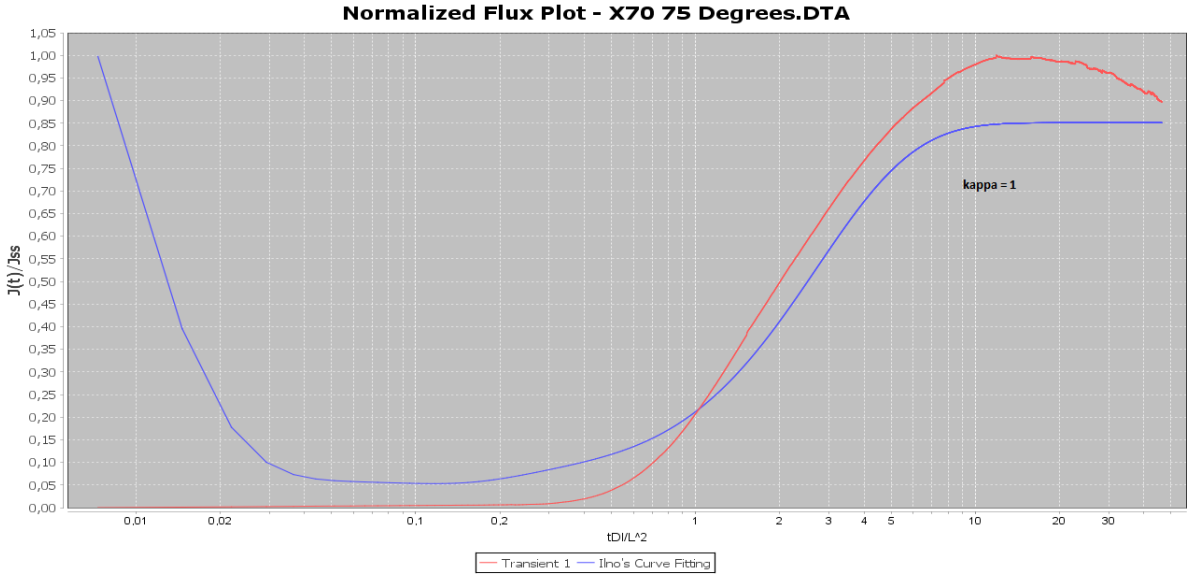


FIGURE 5-31: CHART DISPLAYING NORMALIZED FLUX AS A FUNCTION OF NORMALIZED TIME FOR AN X70 SAMPLE, TESTED AT 75 DEGREES. THE IINO NUMERICAL CURVE FITTING WITH KAPPA SET TO 1 IS ADDED

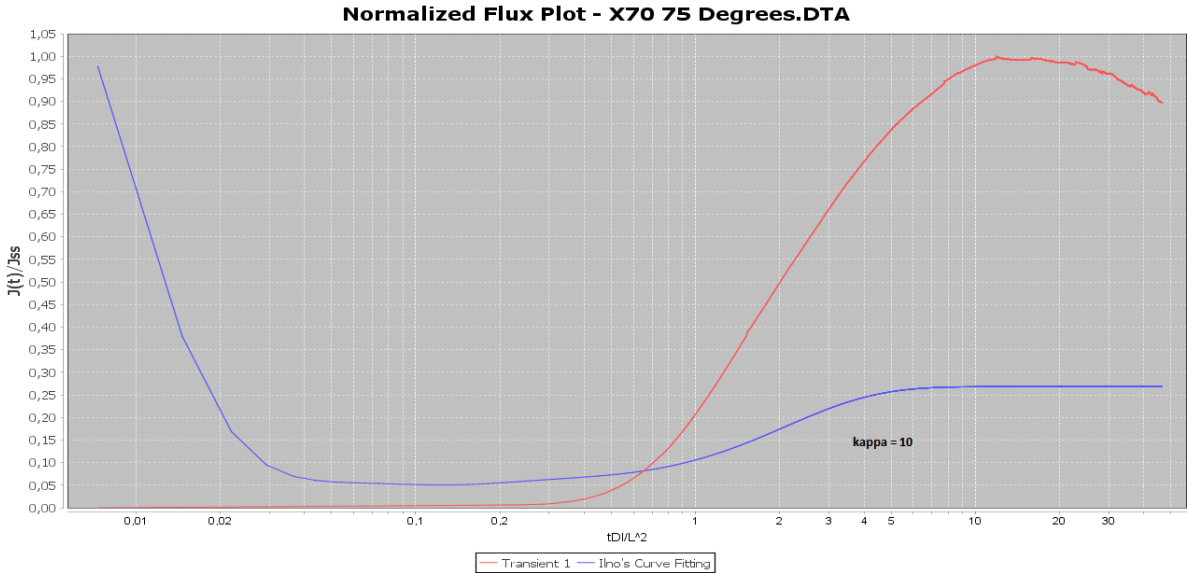


FIGURE 5-32: CHART DISPLAYING NORMALIZED FLUX AS A FUNCTION OF NORMALIZED TIME FOR AN X70 SAMPLE, TESTED AT 75 DEGREES. THE IINO NUMERICAL CURVE FITTING WITH KAPPA SET TO 10 IS ADDED

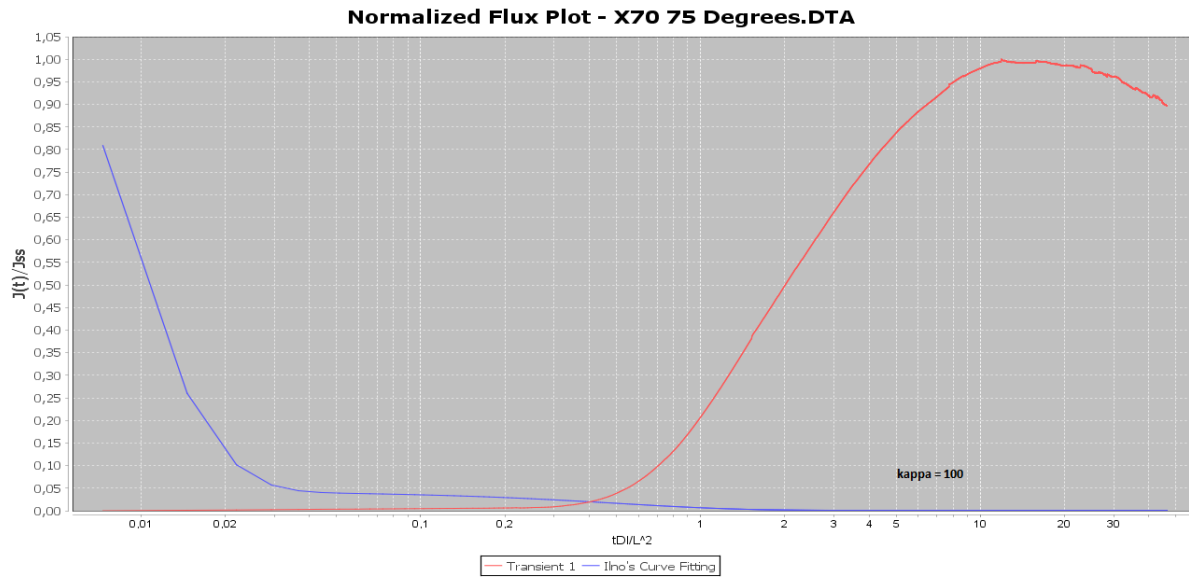


FIGURE 5-33: CHART DISPLAYING NORMALIZED FLUX AS A FUNCTION OF NORMALIZED TIME FOR AN X70 SAMPLE, TESTED AT 75 DEGREES. THE IINO NUMERICAL CURVE FITTING WITH KAPPA SET TO 100 IS ADDED

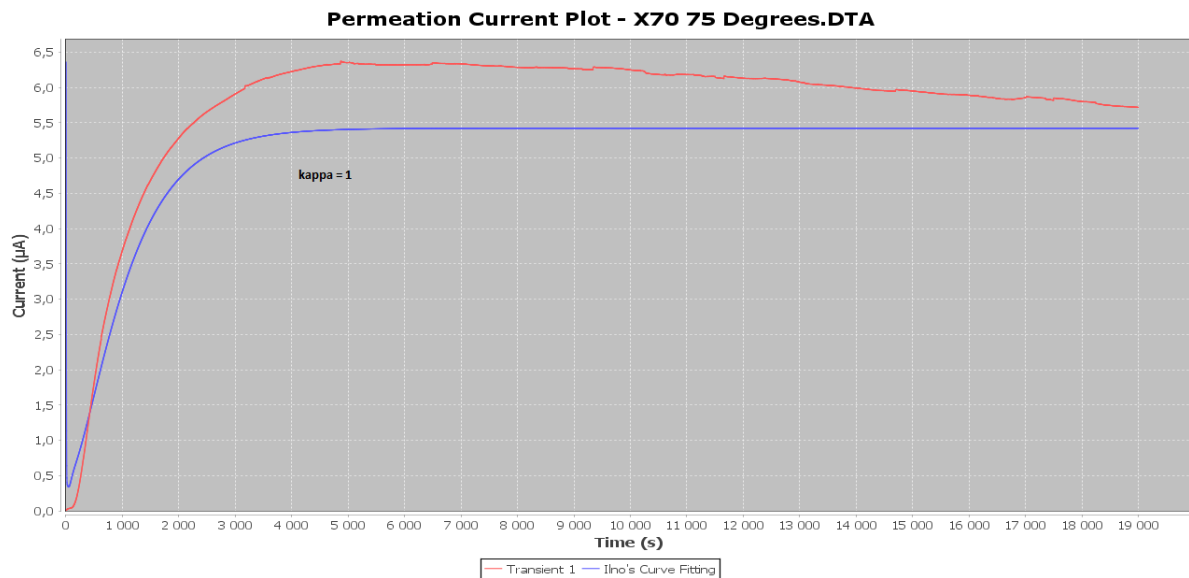


FIGURE 5-34: CHART DISPLAYING CATHODIC CURRENT AS A FUNCTION OF TIME FOR AN X70 SAMPLE, TESTED AT 75 DEGREES. THE IINO NUMERICAL CURVE FITTING WITH KAPPA SET TO 1 IS ADDED

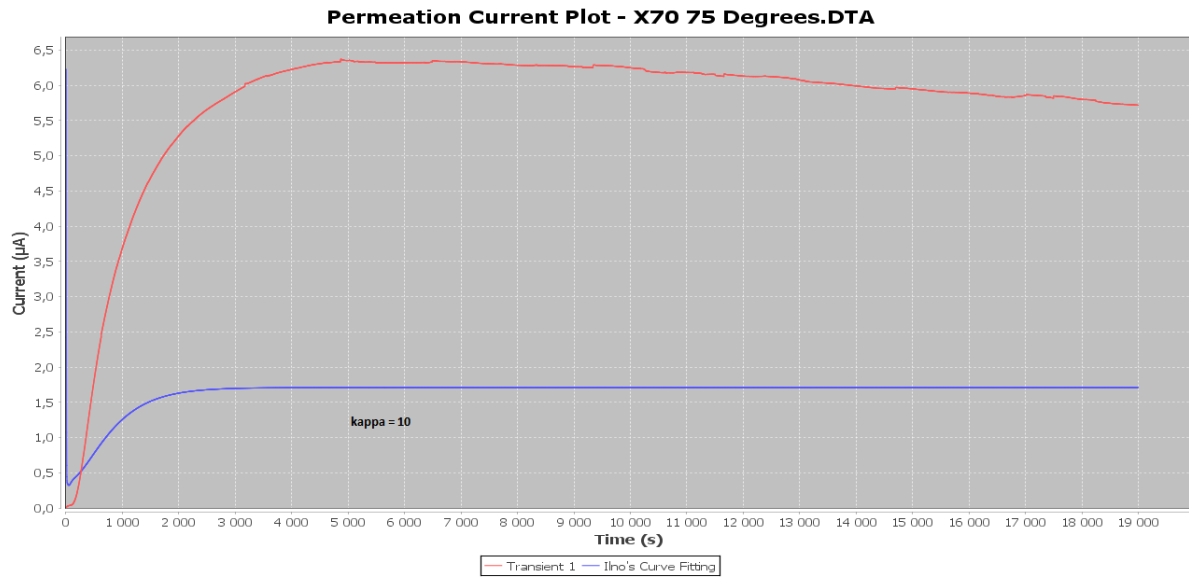


FIGURE 5-35: CHART DISPLAYING CATHODIC CURRENT AS A FUNCTION OF TIME FOR AN X70 SAMPLE, TESTED AT 75 DEGREES. THE IINO NUMERICAL CURVE FITTING WITH KAPPA SET TO 10 IS ADDED

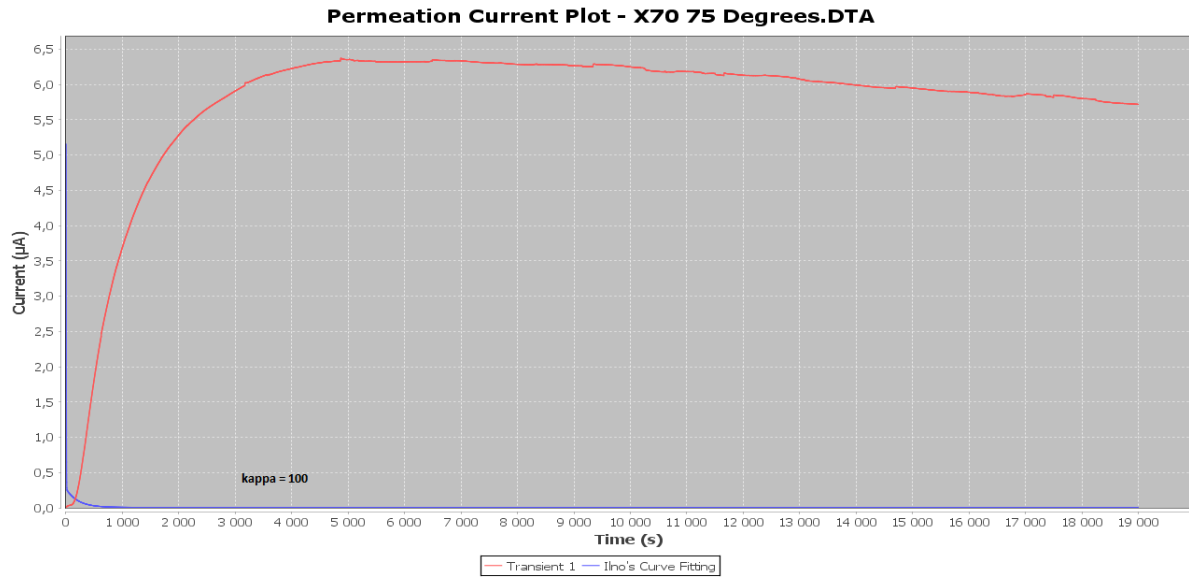


FIGURE 5-36: CHART DISPLAYING CATHODIC CURRENT AS A FUNCTION OF TIME FOR AN X70 SAMPLE, TESTED AT 75 DEGREES. THE IINO NUMERICAL CURVE FITTING WITH KAPPA SET TO 100 IS ADDED

The effective diffusion coefficient is the first field approximated in the fitting process, based on initial values and boundaries.

Iteration	Initial Value	Lower Boundary	High Boundary	Step Size
1.	Elapsed time D_{eff}	Initial Value/10	Initial Value*10	1E-7
2.	Best from last iteration	Initial Value-1E-7	Initial Value+1E-7	1E-8
3.	Best from last iteration	Initial Value-1E-8	Initial Value+1E-8	1E-9

TABLE 5-6: OVERVIEW OF THE INITIAL CONDITIONS AND BOUNDARY CONDITIONS FOR THE EFFECTIVE DIFFUSION COEFFICIENT

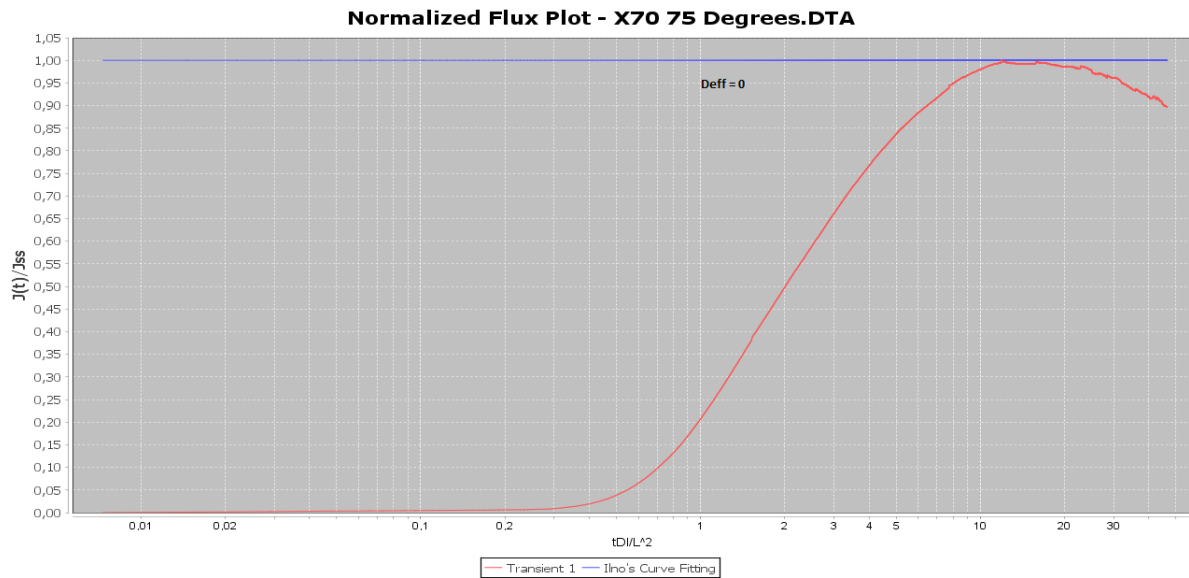


FIGURE 5-37: CHART DISPLAYING NORMALIZED TIME AS A FUNCTION OF NORMALIZED TIME FOR AN X70 SAMPLE, TESTED AT 75 DEGREES. THE IINO NUMERICAL CURVE FITTING WITH D_{EFF} SET TO 0 IS ADDED

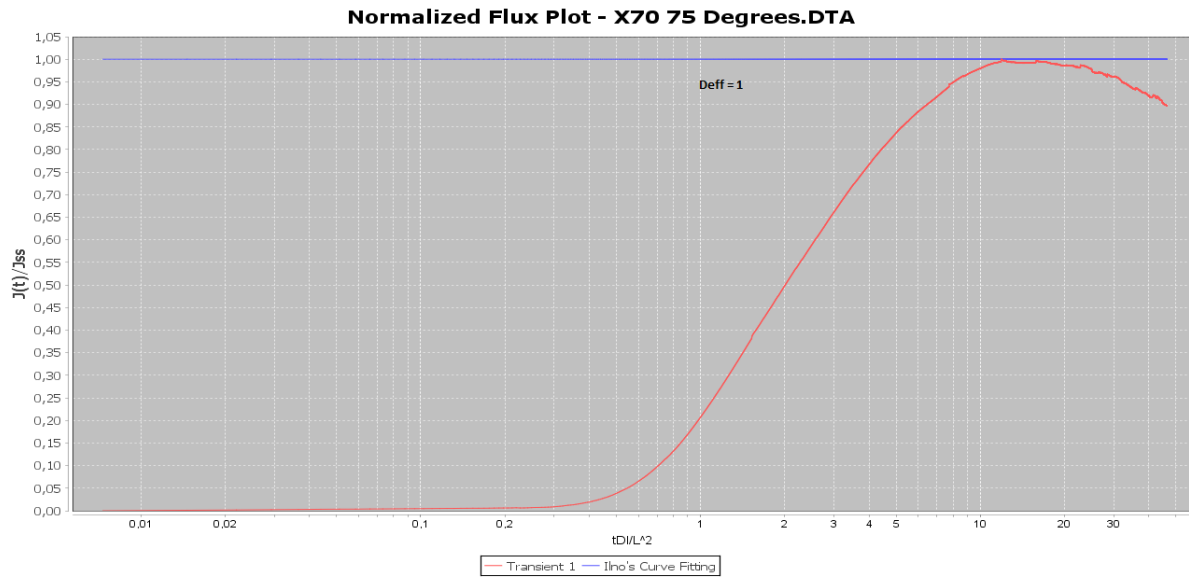


FIGURE 5-38: CHART DISPLAYING NORMALIZED TIME AS A FUNCTION OF NORMALIZED TIME FOR AN X70 SAMPLE, TESTED AT 75 DEGREES. THE IINO NUMERICAL CURVE FITTING WITH D_{EFF} SET TO 1 IS ADDED

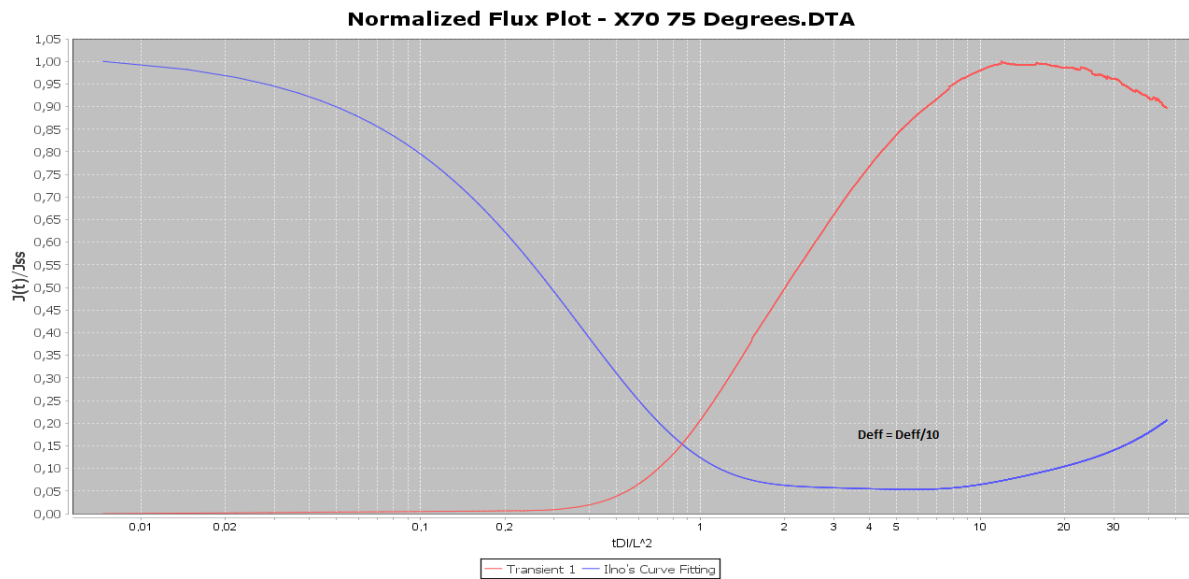


FIGURE 5-39: CHART DISPLAYING NORMALIZED TIME AS A FUNCTION OF NORMALIZED TIME FOR AN X70 SAMPLE, TESTED AT 75 DEGREES. THE IINO NUMERICAL CURVE FITTING WITH D_{EFF} SET TO THE ELAPSED TIME D_{EFF} DIVIDED BY 10 IS ADDED

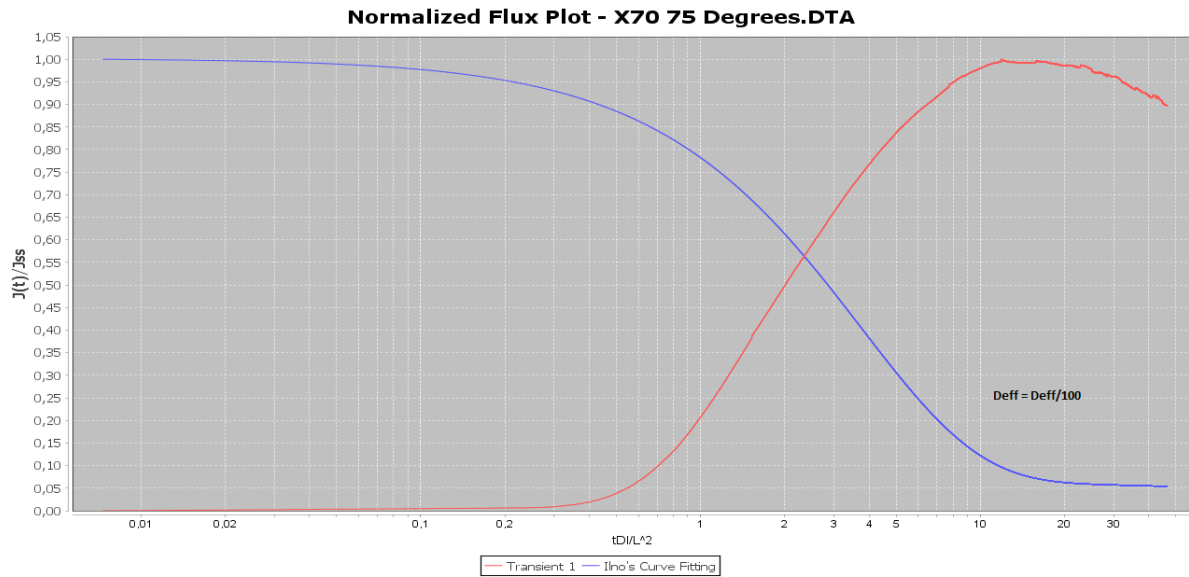


FIGURE 5-40: CHART DISPLAYING NORMALIZED TIME AS A FUNCTION OF NORMALIZED TIME FOR AN X70 SAMPLE, TESTED AT 75 DEGREES. THE IINO NUMERICAL CURVE FITTING WITH D_{EFF} SET TO THE ELAPSED TIME D_{EFF} DIVIDED BY 100 IS ADDED

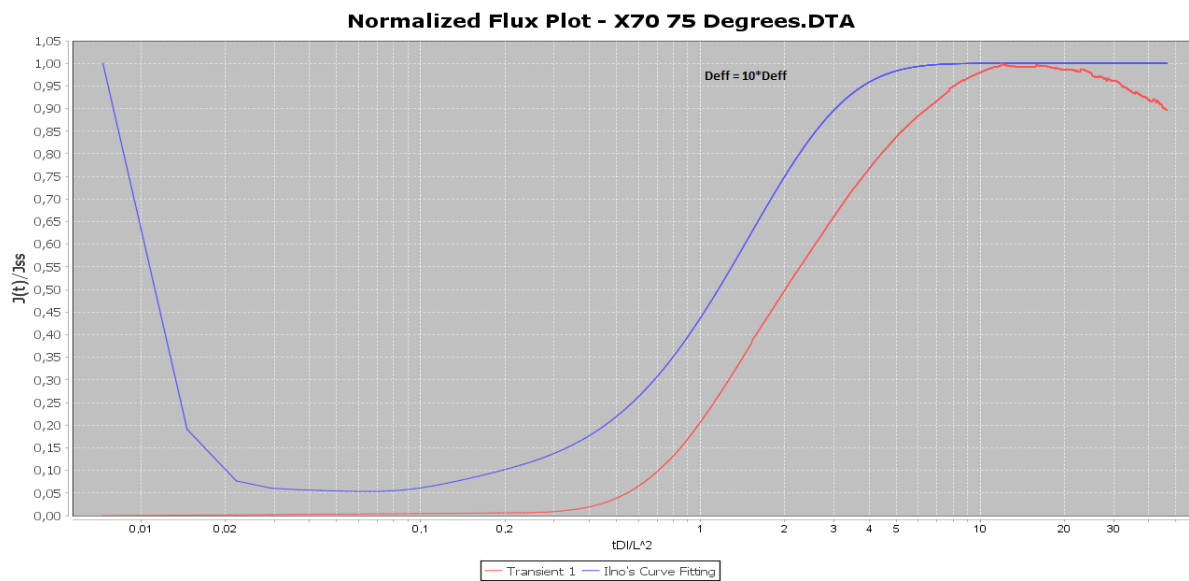


FIGURE 5-41: CHART DISPLAYING NORMALIZED TIME AS A FUNCTION OF NORMALIZED TIME FOR AN X70 SAMPLE, TESTED AT 75 DEGREES. THE IINO NUMERICAL CURVE FITTING WITH D_{EFF} SET TO THE ELAPSED TIME D_{EFF} MULTIPLIED BY 10 IS ADDED

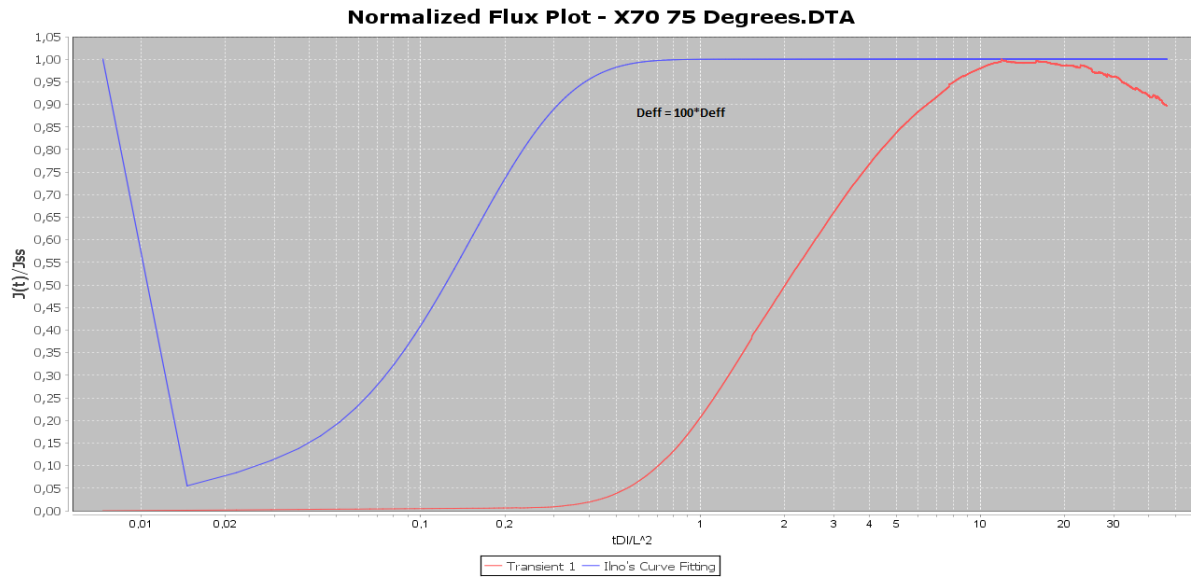


FIGURE 5-42: CHART DISPLAYING NORMALIZED TIME AS A FUNCTION OF NORMALIZED TIME FOR AN X70 SAMPLE, TESTED AT 75 DEGREES. THE IINO NUMERICAL CURVE FITTING WITH D_{EFF} SET TO THE ELAPSED TIME D_{EFF} MULTIPLIED BY 100 IS ADDED

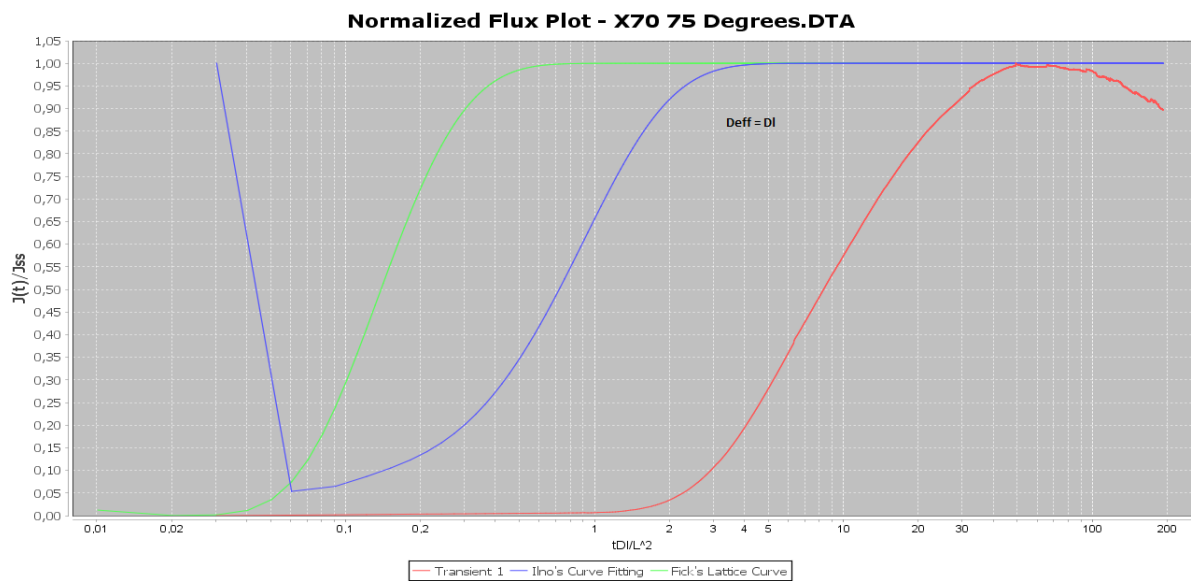


FIGURE 5-43: CHART DISPLAYING NORMALIZED TIME AS A FUNCTION OF NORMALIZED TIME FOR AN X70 SAMPLE, TESTED AT 75 DEGREES. THE IINO NUMERICAL CURVE FITTING WITH D_{EFF} SET TO THE LATTICE DIFFUSION COEFFICIENT D_L IS ADDED

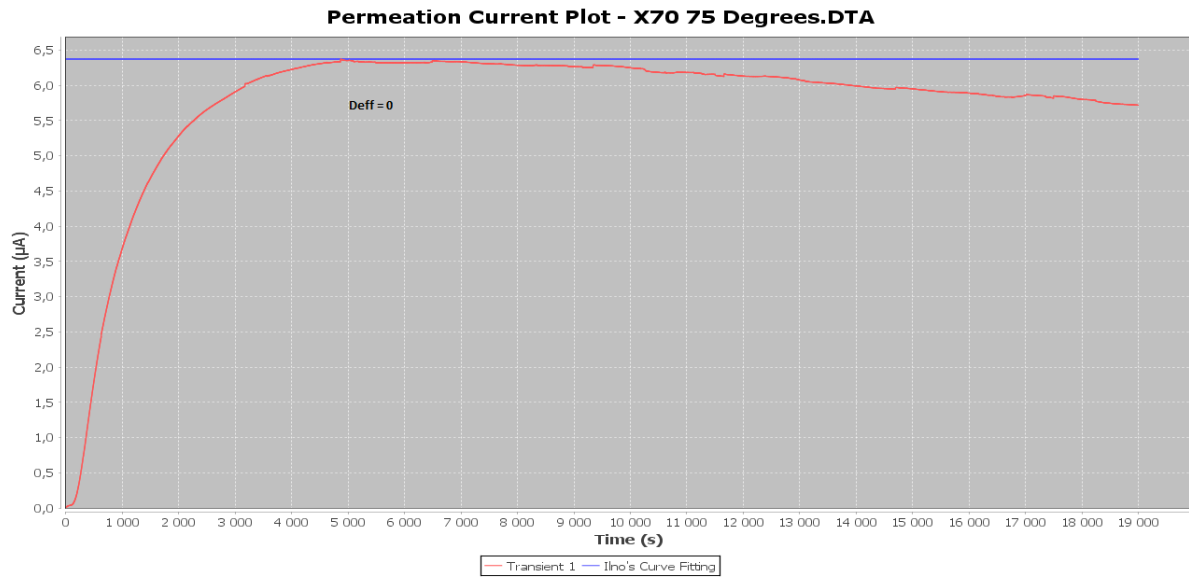


FIGURE 5-44: CHART DISPLAYING CATHODIC CURRENT AS A FUNCTION OF TIME FOR AN X70 SAMPLE, TESTED AT 75 DEGREES. THE IINO NUMERICAL CURVE FITTING WITH D_{EFF} SET TO 0 IS ADDED

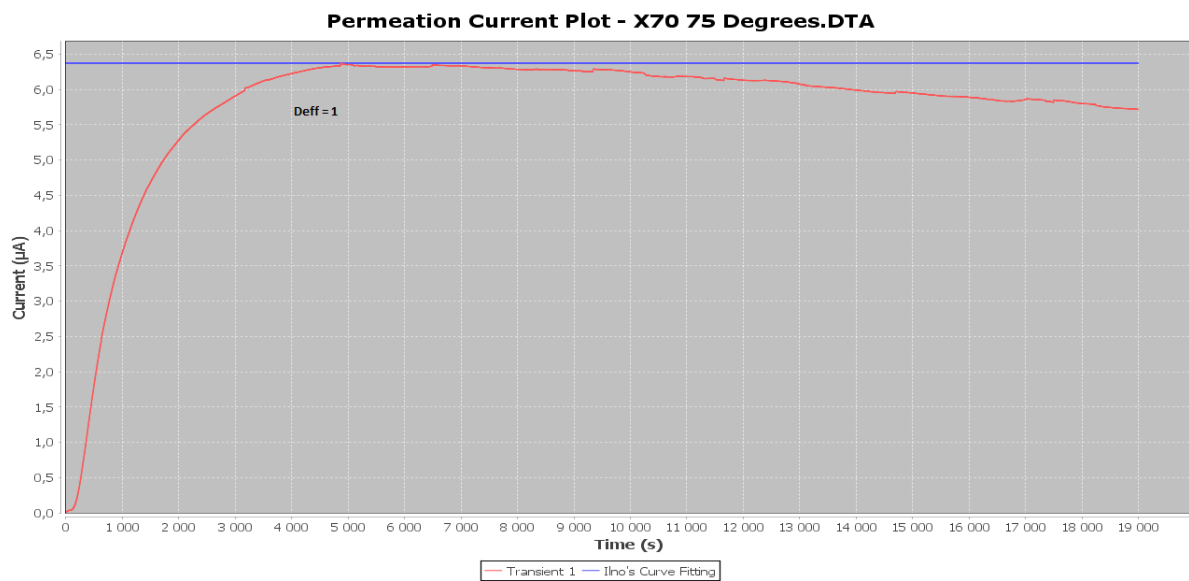


FIGURE 5-45: CHART DISPLAYING CATHODIC CURRENT AS A FUNCTION OF TIME FOR AN X70 SAMPLE, TESTED AT 75 DEGREES. THE IINO NUMERICAL CURVE FITTING WITH D_{EFF} SET TO 1 IS ADDED

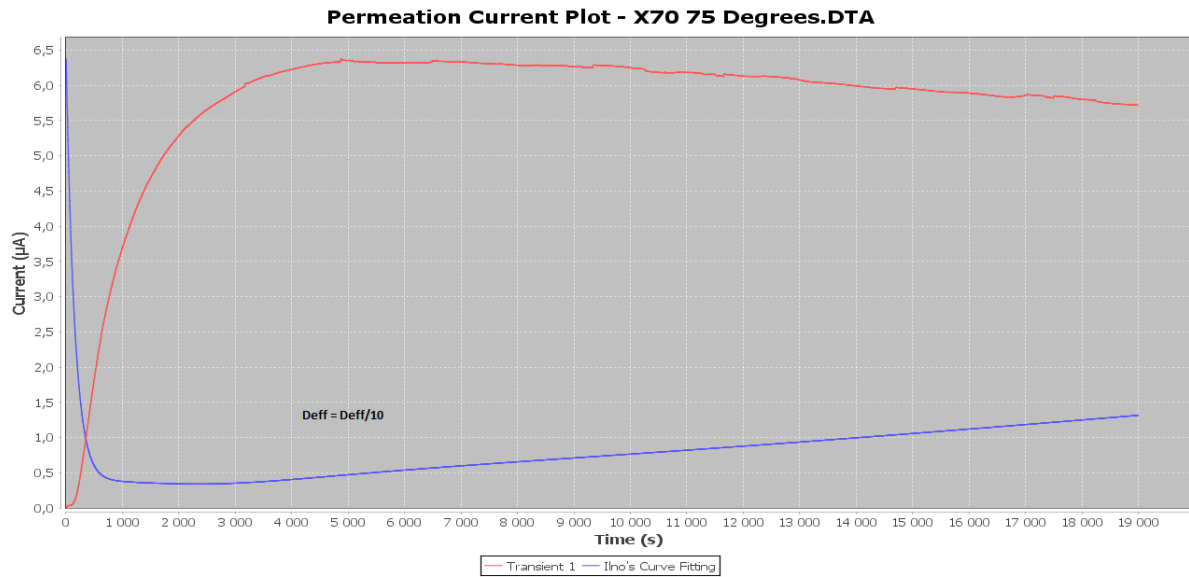


FIGURE 5-46: CHART DISPLAYING CATHODIC CURRENT AS A FUNCTION OF TIME FOR AN X70 SAMPLE, TESTED AT 75 DEGREES. THE IINO NUMERICAL CURVE FITTING WITH D_{EFF} SET TO THE ELAPSED TIME D_{EFF} DIVIDED BY 10 IS ADDED

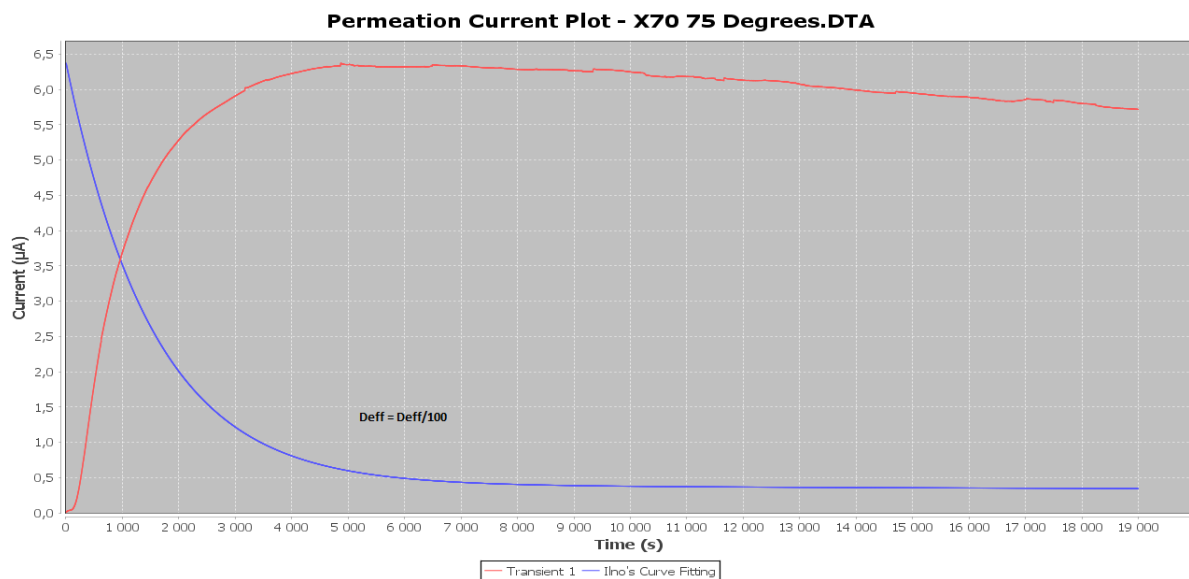


FIGURE 5-47: CHART DISPLAYING CATHODIC CURRENT AS A FUNCTION OF TIME FOR AN X70 SAMPLE, TESTED AT 75 DEGREES. THE IINO NUMERICAL CURVE FITTING WITH D_{EFF} SET TO THE ELAPSED TIME D_{EFF} DIVIDED BY 100 IS ADDED

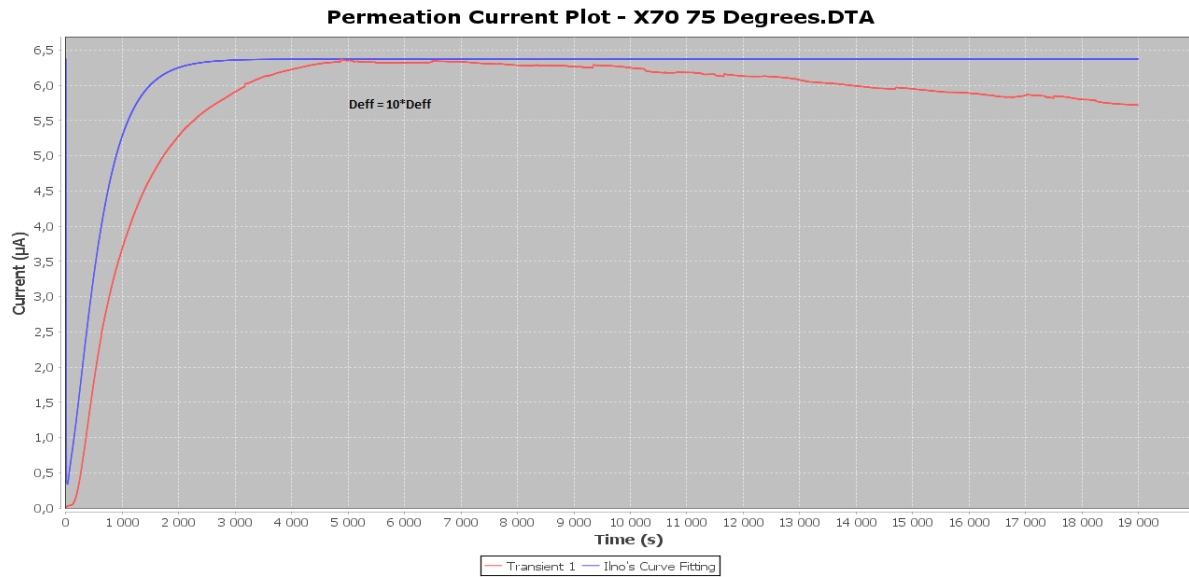


FIGURE 5-48: CHART DISPLAYING CATHODIC CURRENT AS A FUNCTION OF TIME FOR AN X70 SAMPLE, TESTED AT 75 DEGREES. THE IINO NUMERICAL CURVE FITTING WITH D_{EFF} SET TO THE ELAPSED TIME D_{EFF} MULTIPLIED BY 10 IS ADDED

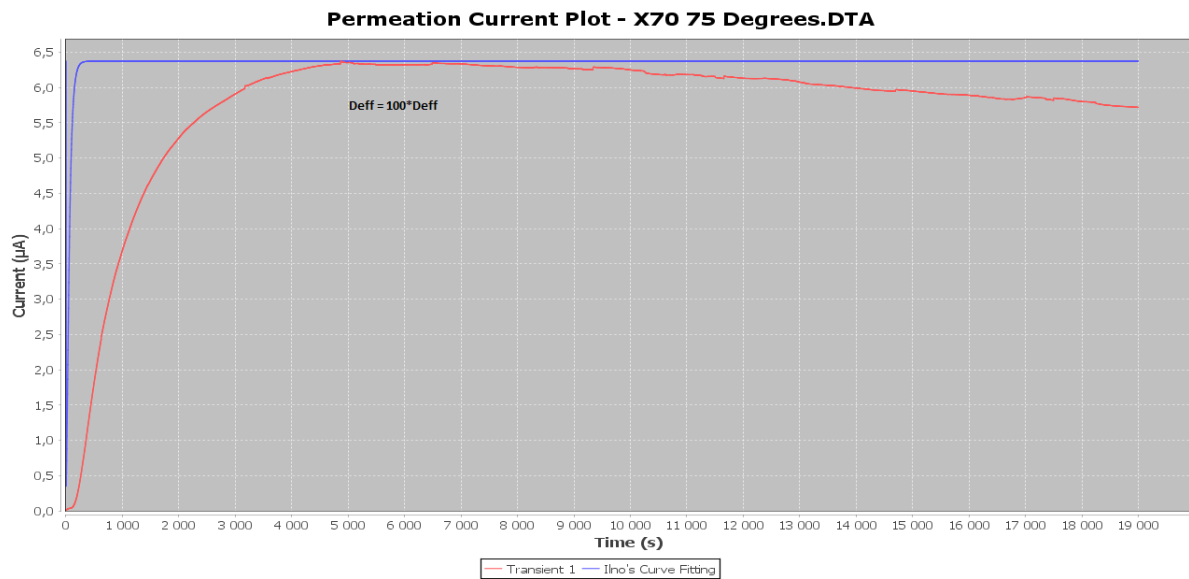


FIGURE 5-49: CHART DISPLAYING CATHODIC CURRENT AS A FUNCTION OF TIME FOR AN X70 SAMPLE, TESTED AT 75 DEGREES. THE IINO NUMERICAL CURVE FITTING WITH D_{EFF} SET TO THE ELAPSED TIME D_{EFF} MULTIPLIED BY 100 IS ADDED

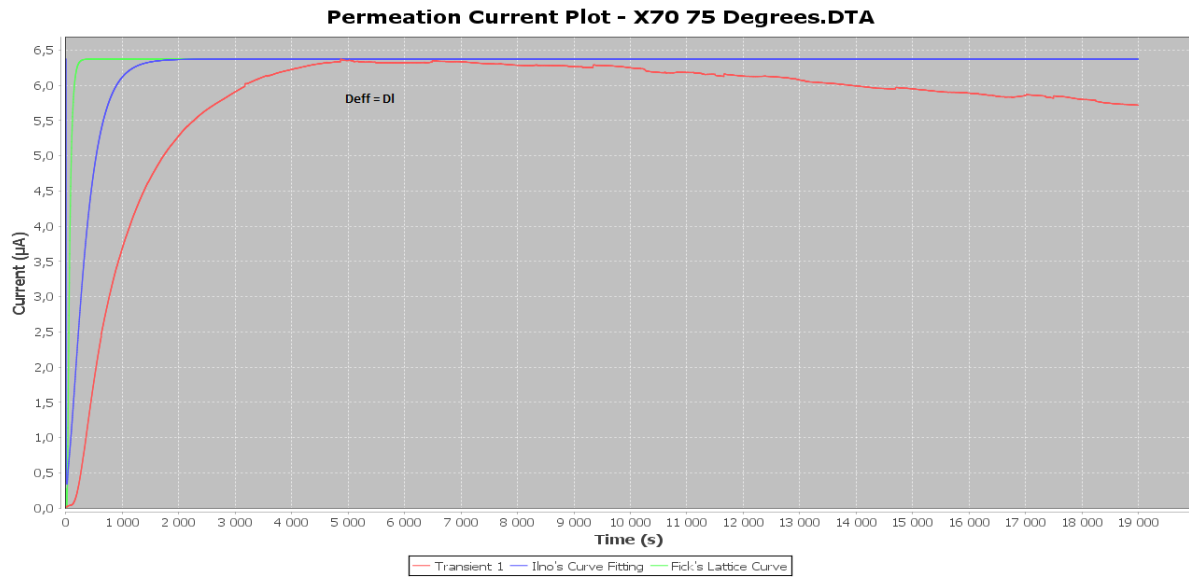


FIGURE 5-50: CHART DISPLAYING CATHODIC CURRENT AS A FUNCTION OF TIME FOR AN X70 SAMPLE, TESTED AT 75 DEGREES. THE IINO NUMERICAL CURVE FITTING WITH D_{EFF} SET TO THE LATTICE DIFFUSION COEFFICIENT D_L IS ADDED

After the effective diffusion coefficient is set, the lambda value is incremented in a loop.

Iteration	Initial Value	Lower Boundary	High Boundary	Step Size
1.	5	1	10000	100
2.	Best from last iteration	Initial Value-200	Initial Value+200	10
3.	Best from last iteration	Initial Value-10	Initial Value+10	1

TABLE 5-7: OVERVIEW OF THE INITIAL CONDITIONS AND BOUNDARY CONDITIONS FOR THE LAMBDA VARIABLE

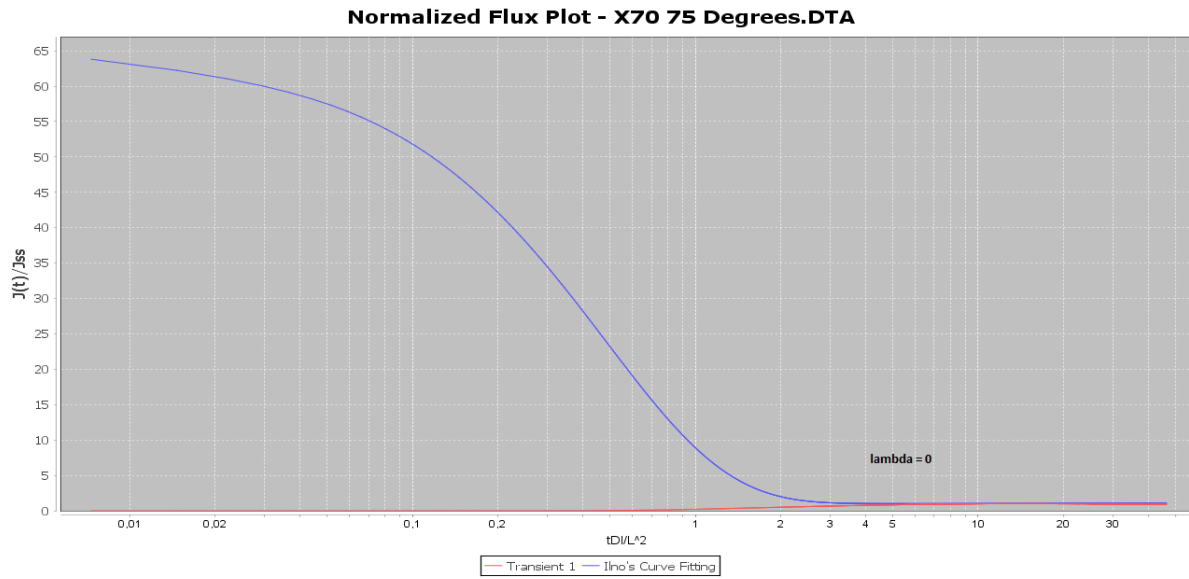


FIGURE 5-51: CHART DISPLAYING NORMALIZED TIME AS A FUNCTION OF NORMALIZED TIME FOR AN X70 SAMPLE, TESTED AT 75 DEGREES. THE IINO NUMERICAL CURVE FITTING WITH LAMBDA SET TO 0 IS ADDED

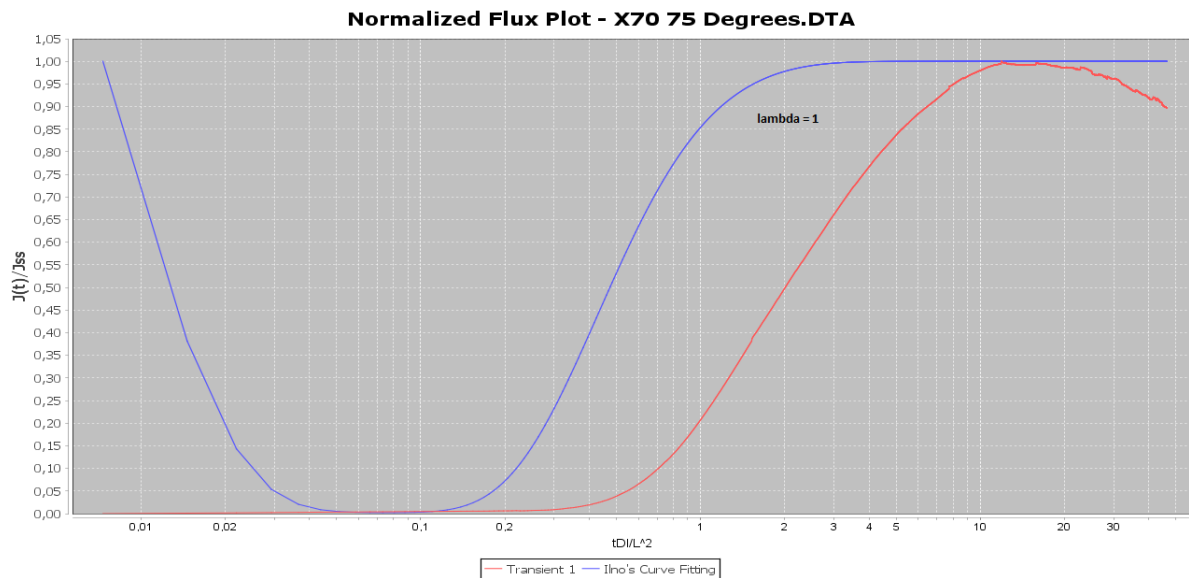


FIGURE 5-52: CHART DISPLAYING NORMALIZED TIME AS A FUNCTION OF NORMALIZED TIME FOR AN X70 SAMPLE, TESTED AT 75 DEGREES. THE IINO NUMERICAL CURVE FITTING WITH LAMBDA SET TO 1 IS ADDED

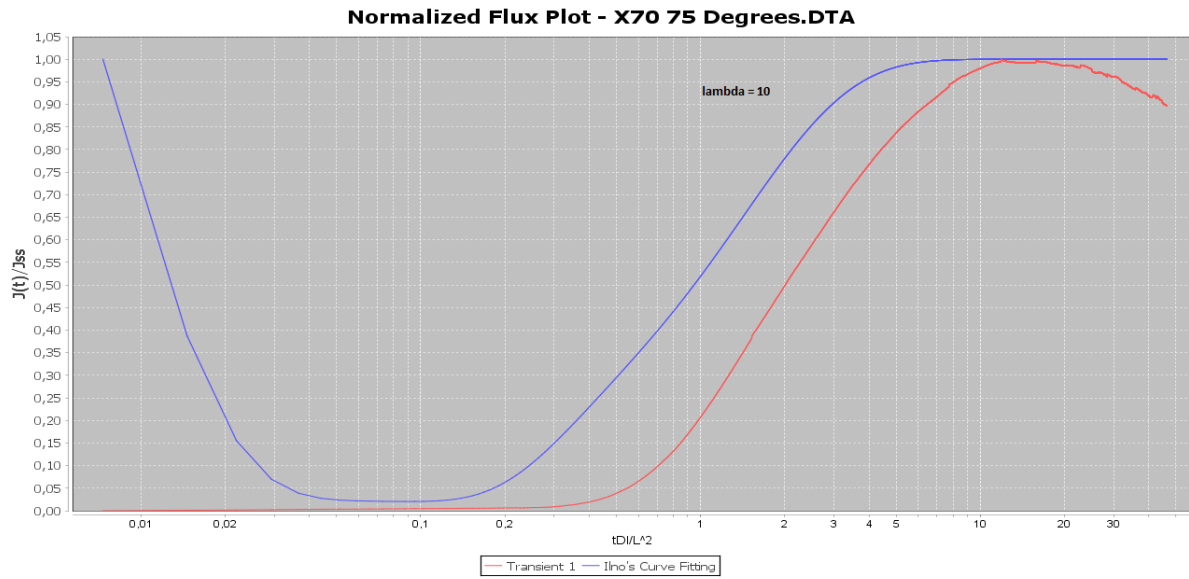


FIGURE 5-53: CHART DISPLAYING NORMALIZED TIME AS A FUNCTION OF NORMALIZED TIME FOR AN X70 SAMPLE, TESTED AT 75 DEGREES. THE IINO NUMERICAL CURVE FITTING WITH LAMBDA SET TO 10 IS ADDED

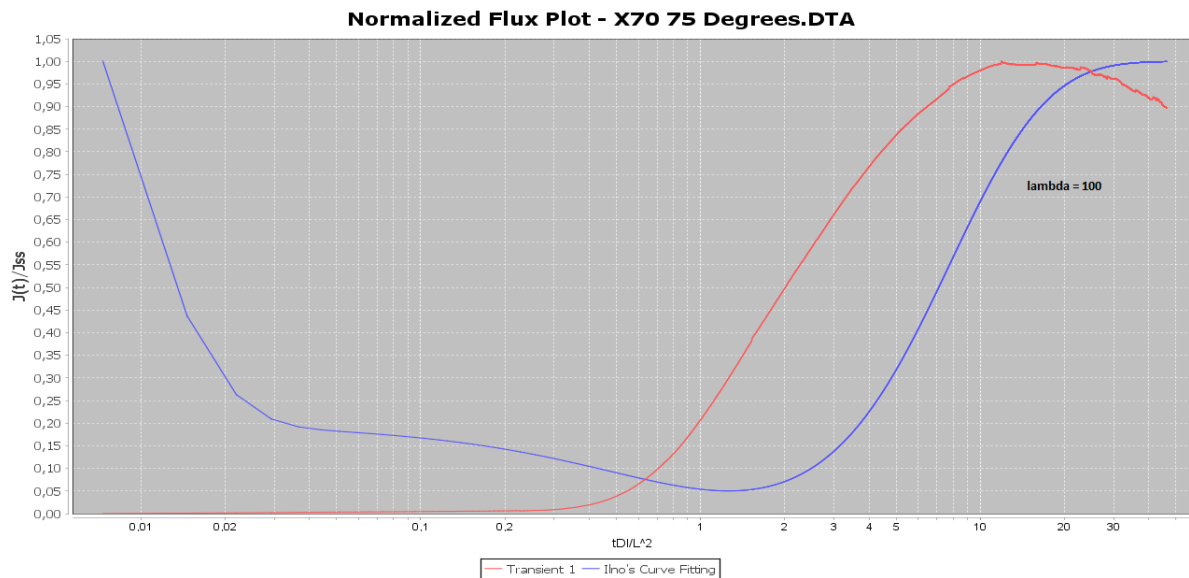


FIGURE 5-54: CHART DISPLAYING NORMALIZED TIME AS A FUNCTION OF NORMALIZED TIME FOR AN X70 SAMPLE, TESTED AT 75 DEGREES. THE IINO NUMERICAL CURVE FITTING WITH LAMBDA SET TO 100 IS ADDED

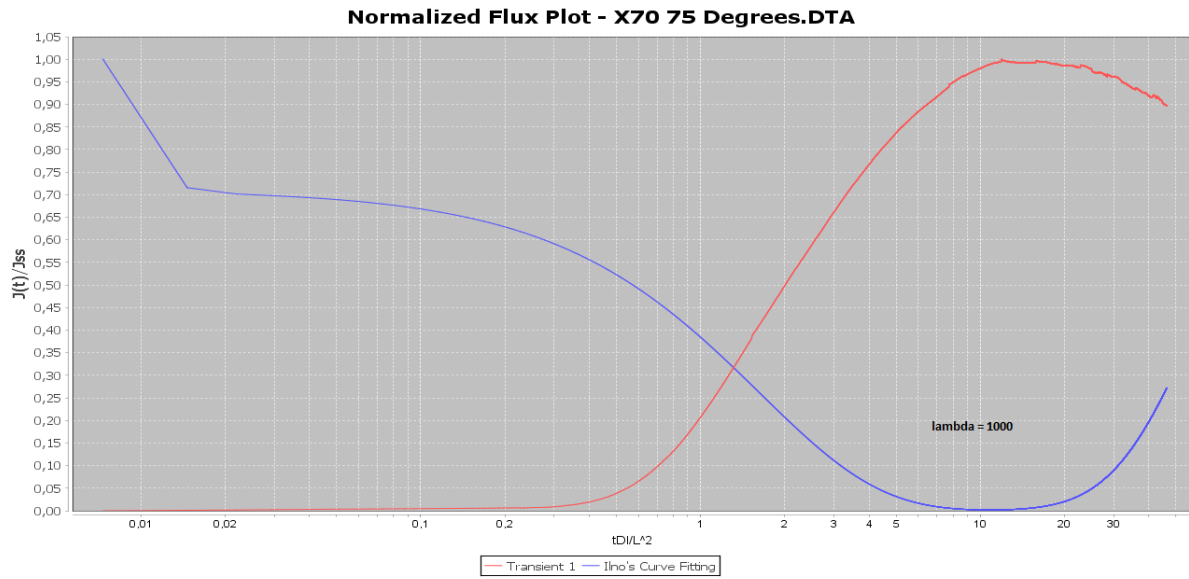


FIGURE 5-55: CHART DISPLAYING NORMALIZED TIME AS A FUNCTION OF NORMALIZED TIME FOR AN X70 SAMPLE, TESTED AT 75 DEGREES. THE IINO NUMERICAL CURVE FITTING WITH LAMBDA SET TO 1000 IS ADDED

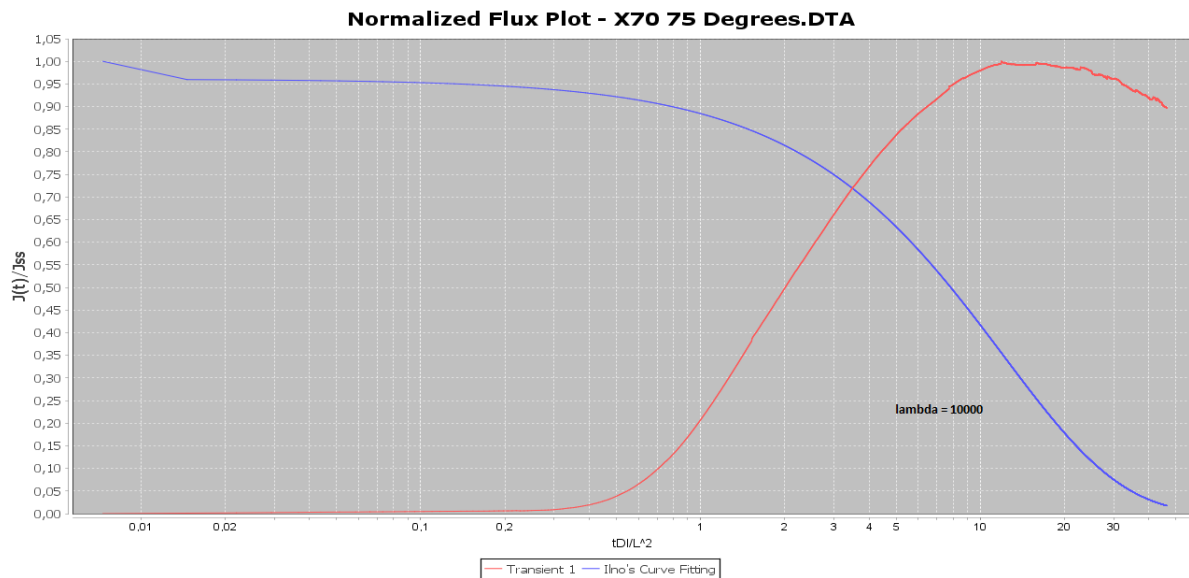


FIGURE 5-56: CHART DISPLAYING NORMALIZED TIME AS A FUNCTION OF NORMALIZED TIME FOR AN X70 SAMPLE, TESTED AT 75 DEGREES. THE IINO NUMERICAL CURVE FITTING WITH LAMBDA SET TO 10000 IS ADDED

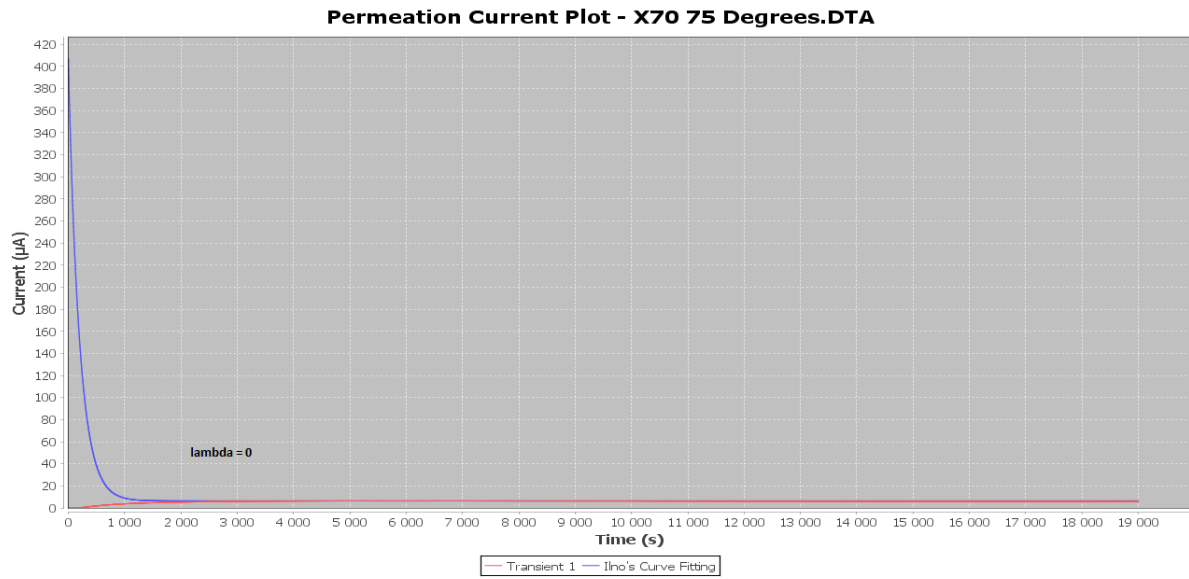


FIGURE 5-57: CHART DISPLAYING CATHODIC CURRENT AS A FUNCTION OF TIME FOR AN X70 SAMPLE, TESTED AT 75 DEGREES. THE IINO NUMERICAL CURVE FITTING WITH LAMBDA SET TO 0 IS ADDED

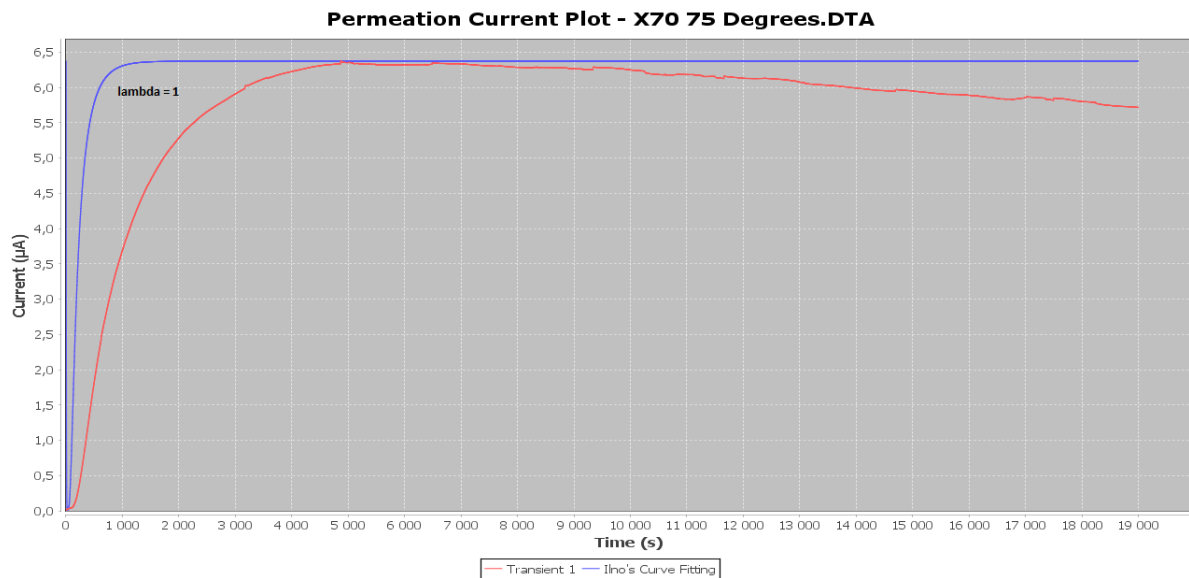


FIGURE 5-58: CHART DISPLAYING CATHODIC CURRENT AS A FUNCTION OF TIME FOR AN X70 SAMPLE, TESTED AT 75 DEGREES. THE IINO NUMERICAL CURVE FITTING WITH LAMBDA SET TO 1 IS ADDED

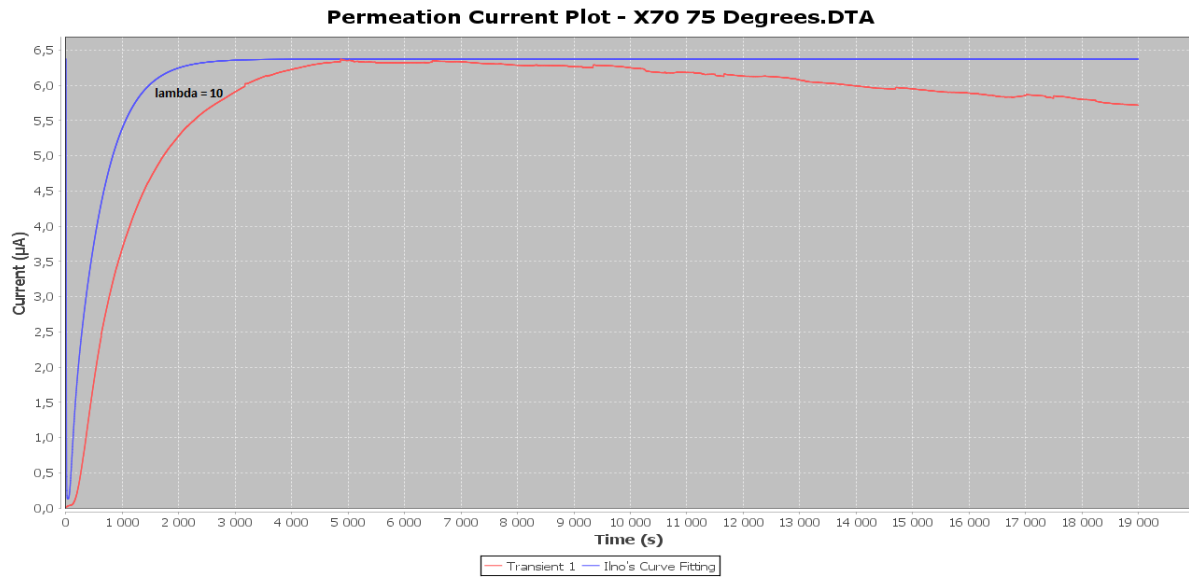


FIGURE 5-59: CHART DISPLAYING CATHODIC CURRENT AS A FUNCTION OF TIME FOR AN X70 SAMPLE, TESTED AT 75 DEGREES. THE IINO NUMERICAL CURVE FITTING WITH LAMBDA SET TO 10 IS ADDED

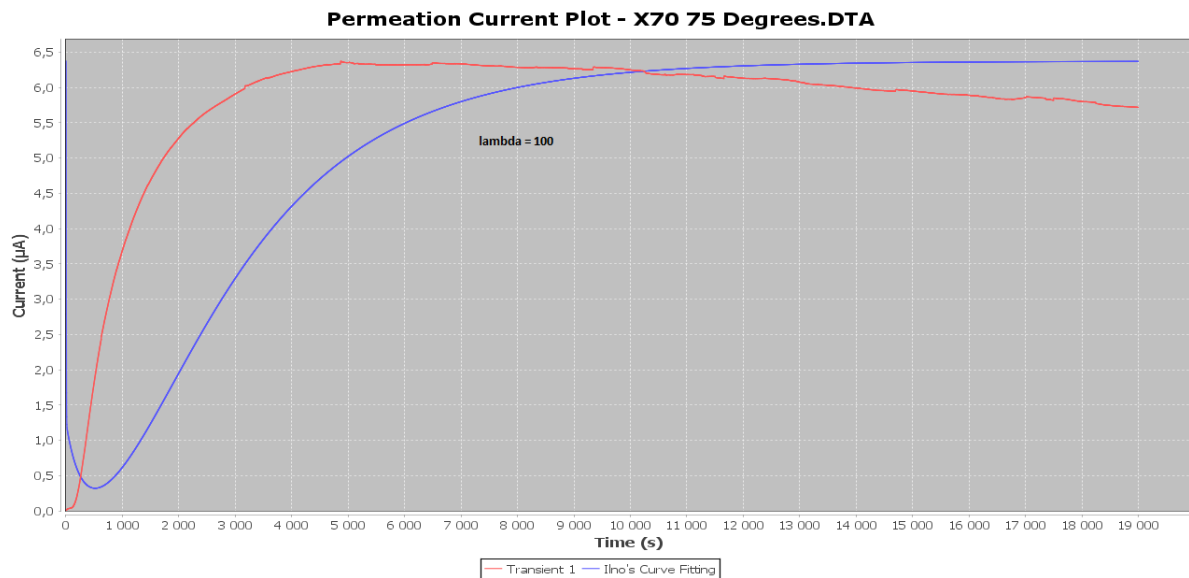


FIGURE 5-60: CHART DISPLAYING CATHODIC CURRENT AS A FUNCTION OF TIME FOR AN X70 SAMPLE, TESTED AT 75 DEGREES. THE IINO NUMERICAL CURVE FITTING WITH LAMBDA SET TO 100 IS ADDED

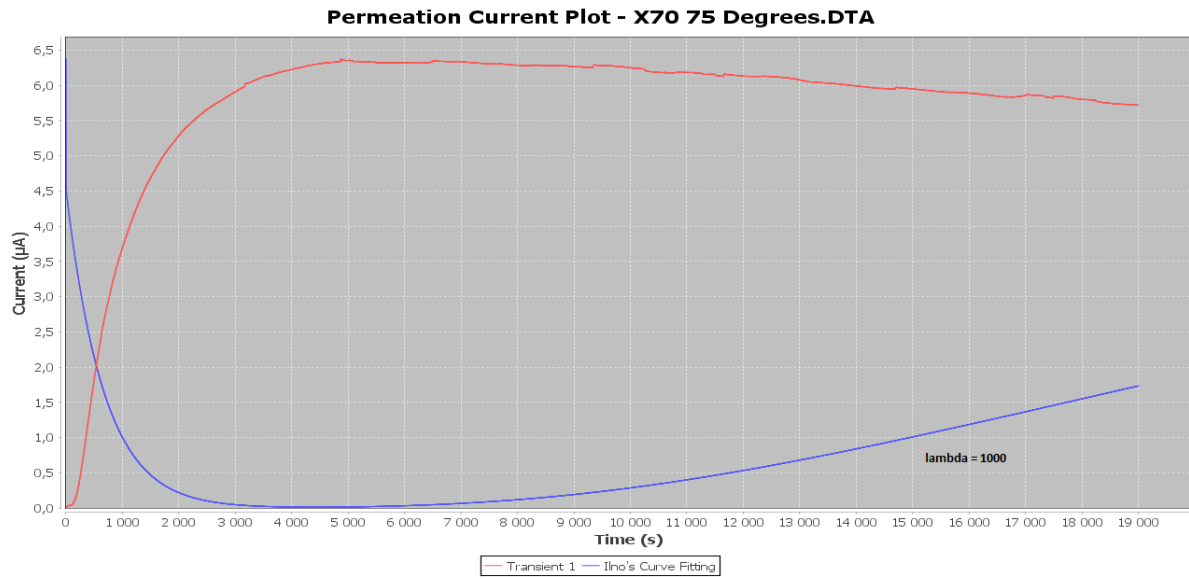


FIGURE 5-61: CHART DISPLAYING CATHODIC CURRENT AS A FUNCTION OF TIME FOR AN X70 SAMPLE, TESTED AT 75 DEGREES. THE IINO NUMERICAL CURVE FITTING WITH LAMBDA SET TO 1000 IS ADDED

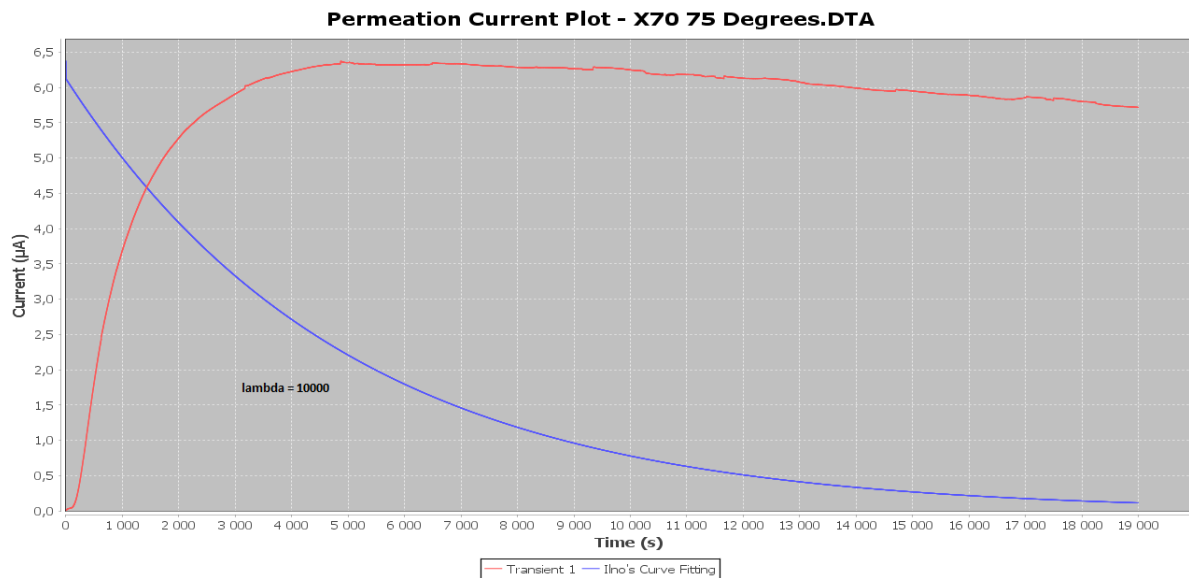


FIGURE 5-62: CHART DISPLAYING CATHODIC CURRENT AS A FUNCTION OF TIME FOR AN X70 SAMPLE, TESTED AT 75 DEGREES. THE IINO NUMERICAL CURVE FITTING WITH LAMBDA SET TO 10000 IS ADDED

The my value is approximated for every incrimination of the lambda value.

Iteration	Initial Value	Lower Boundary	High Boundary	Step Size
1.	1	0	2000	10
2.	Best from last iteration	Initial Value-50	Initial Value+50	1
3.	Best from last iteration	Initial Value-5	Initial Value+5	0.1

TABLE 5-8: OVERVIEW OF THE INITIAL CONDITIONS AND BOUNDARY CONDITIONS FOR THE MY VARIABLE

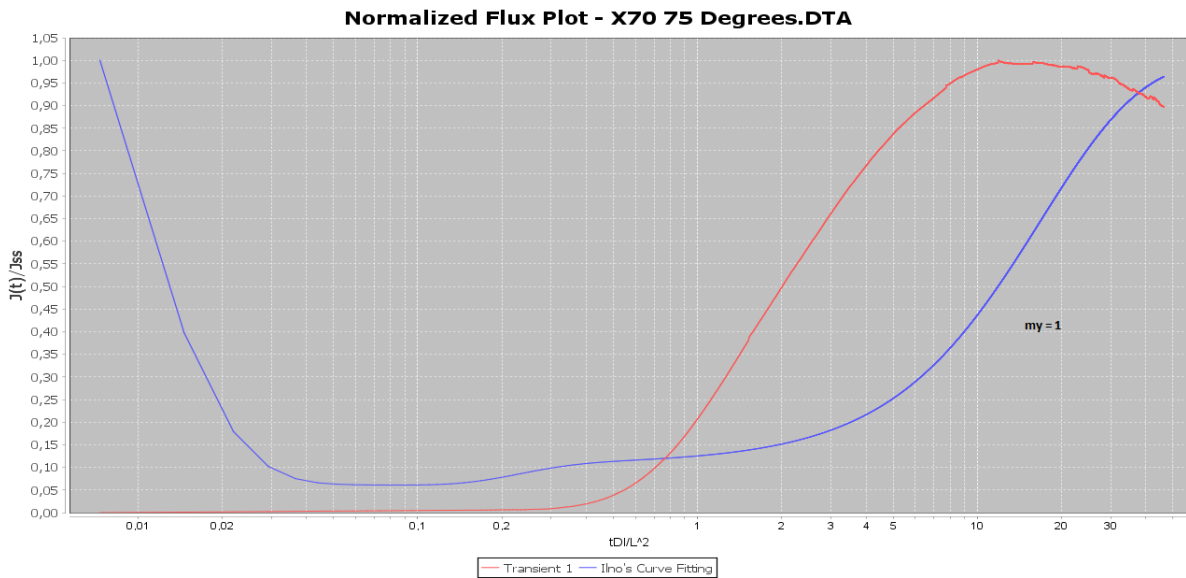


FIGURE 5-63: CHART DISPLAYING NORMALIZED TIME AS A FUNCTION OF NORMALIZED TIME FOR AN X70 SAMPLE, TESTED AT 75 DEGREES. THE IINO NUMERICAL CURVE FITTING WITH MY SET TO 1 IS ADDED

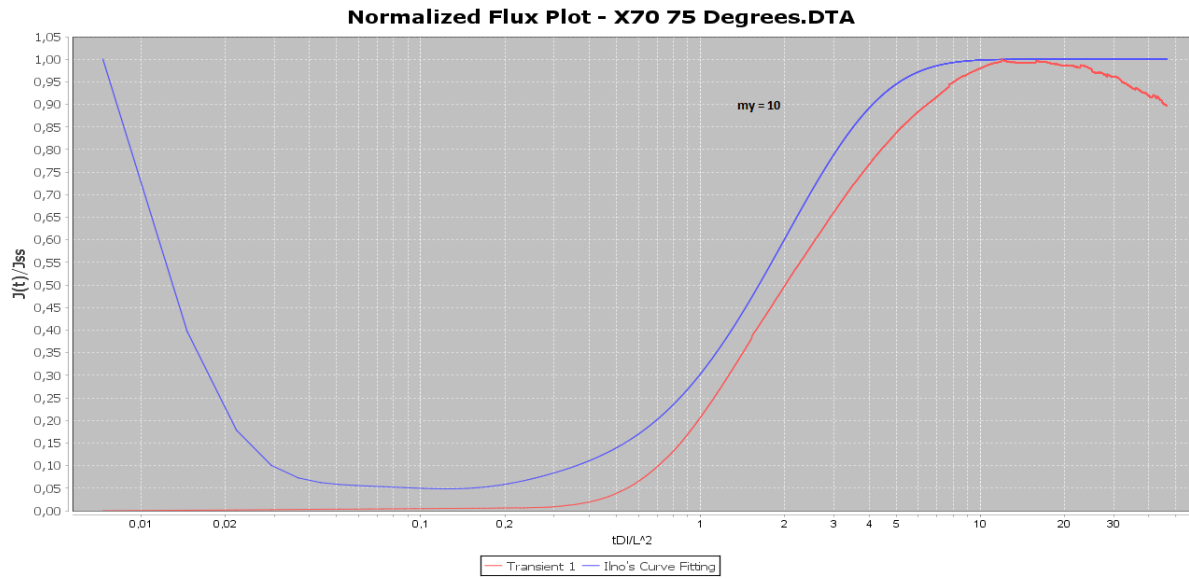


FIGURE 5-64: CHART DISPLAYING NORMALIZED TIME AS A FUNCTION OF NORMALIZED TIME FOR AN X70 SAMPLE, TESTED AT 75 DEGREES. THE IINO NUMERICAL CURVE FITTING WITH MY SET TO 10 IS ADDED

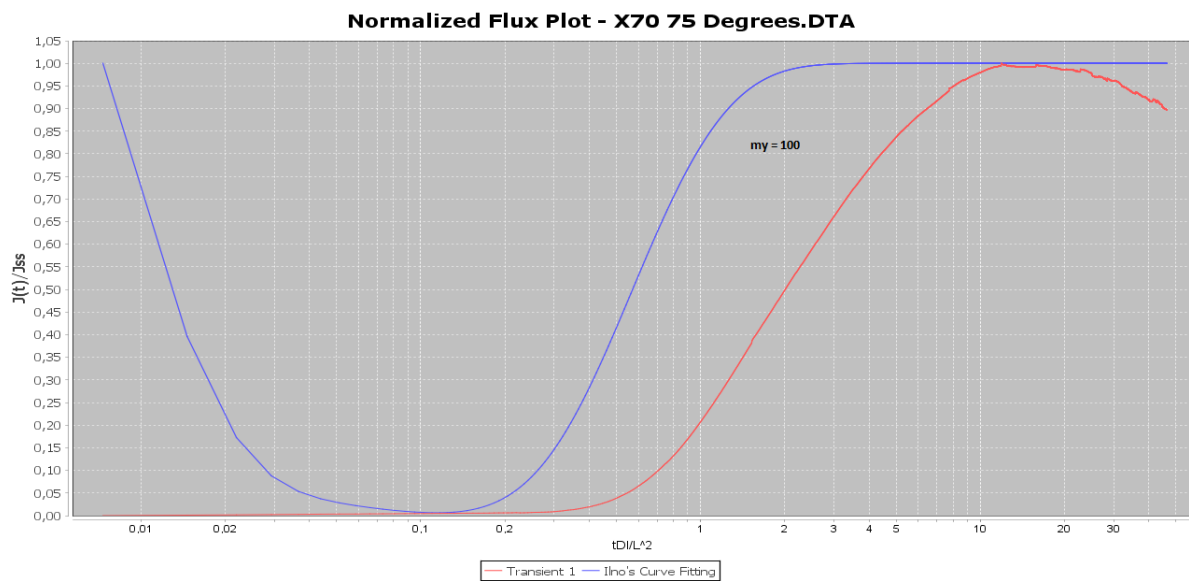


FIGURE 5-65: CHART DISPLAYING NORMALIZED TIME AS A FUNCTION OF NORMALIZED TIME FOR AN X70 SAMPLE, TESTED AT 75 DEGREES. THE IINO NUMERICAL CURVE FITTING WITH MY SET TO 100 IS ADDED

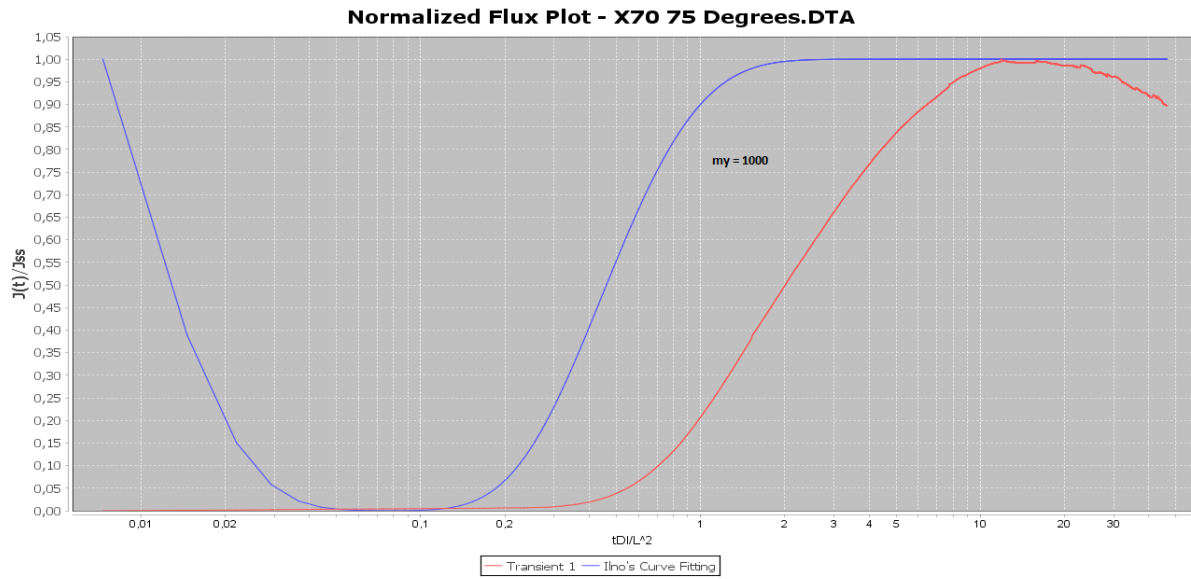


FIGURE 5-66: CHART DISPLAYING NORMALIZED TIME AS A FUNCTION OF NORMALIZED TIME FOR AN X70 SAMPLE, TESTED AT 75 DEGREES. THE IINO NUMERICAL CURVE FITTING WITH MY SET TO 1000 IS ADDED

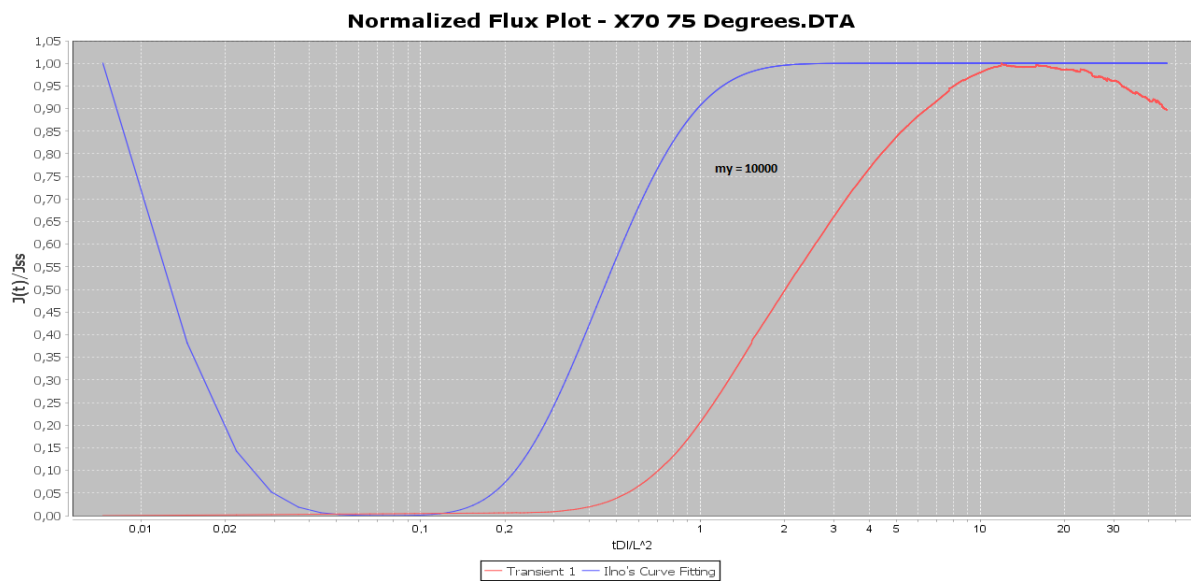


FIGURE 5-67: CHART DISPLAYING NORMALIZED TIME AS A FUNCTION OF NORMALIZED TIME FOR AN X70 SAMPLE, TESTED AT 75 DEGREES. THE IINO NUMERICAL CURVE FITTING WITH MY SET TO 10000 IS ADDED

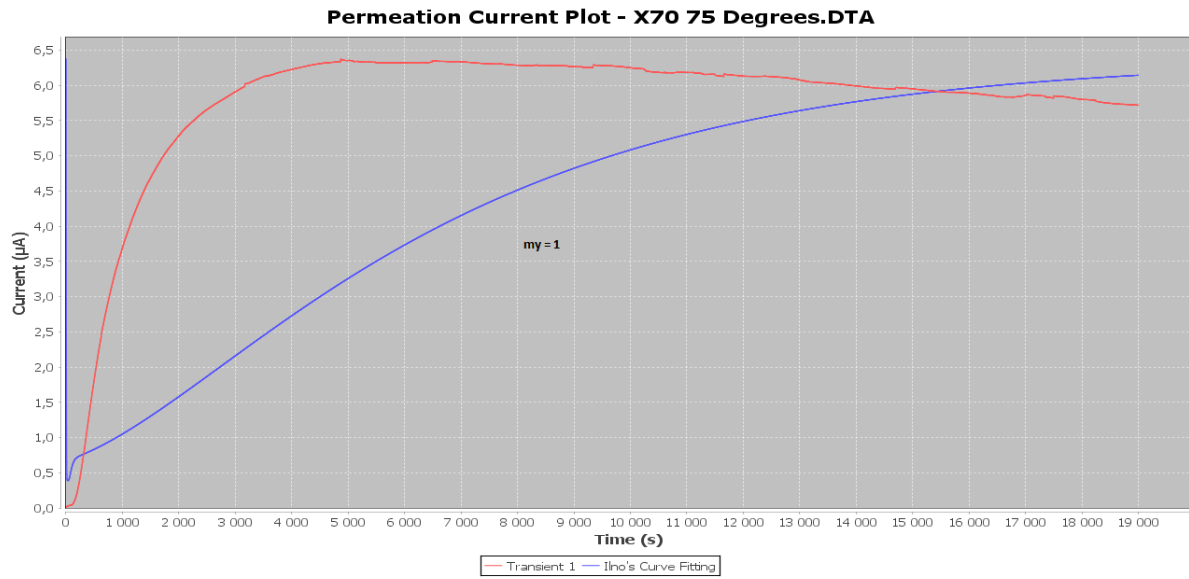


FIGURE 5-68: CHART DISPLAYING CATHODIC CURRENT AS A FUNCTION OF TIME FOR AN X70 SAMPLE, TESTED AT 75 DEGREES. THE IINO NUMERICAL CURVE FITTING WITH MY SET TO 1 IS ADDED

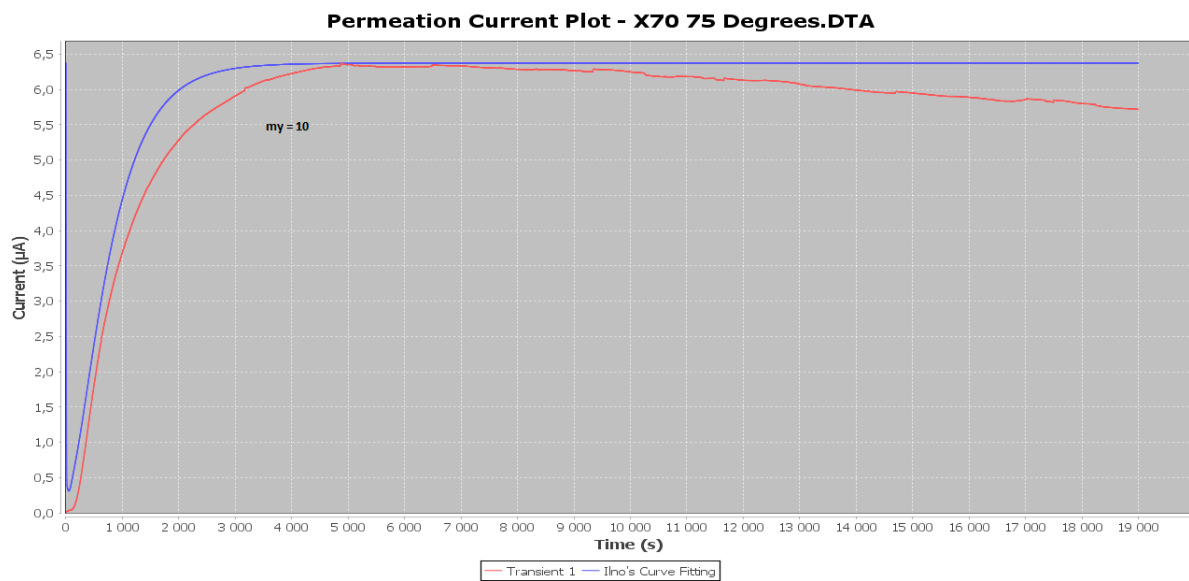


FIGURE 5-69: CHART DISPLAYING CATHODIC CURRENT AS A FUNCTION OF TIME FOR AN X70 SAMPLE, TESTED AT 75 DEGREES. THE IINO NUMERICAL CURVE FITTING WITH MY SET TO 10 IS ADDED

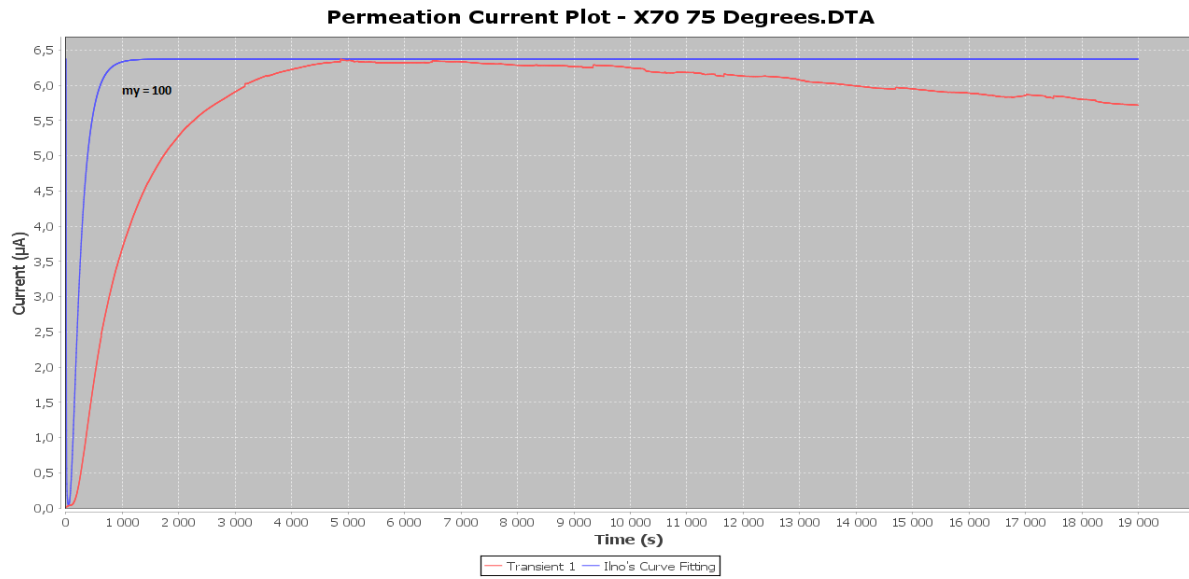


FIGURE 5-70: CHART DISPLAYING CATHODIC CURRENT AS A FUNCTION OF TIME FOR AN X70 SAMPLE, TESTED AT 75 DEGREES. THE IINO NUMERICAL CURVE FITTING WITH MY SET TO 100 IS ADDED

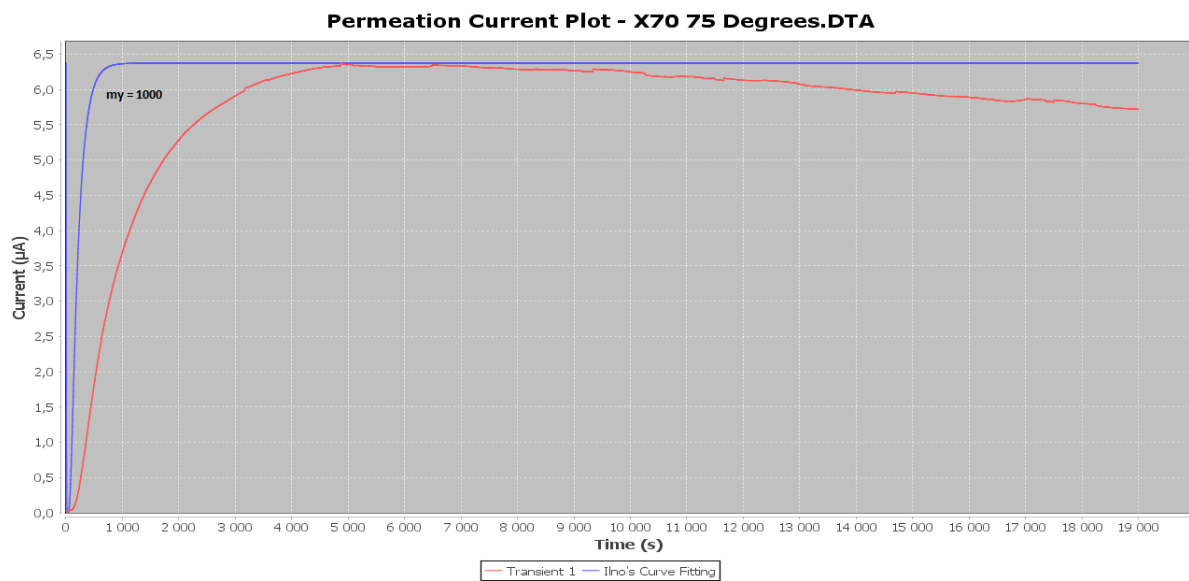


FIGURE 5-71: CHART DISPLAYING CATHODIC CURRENT AS A FUNCTION OF TIME FOR AN X70 SAMPLE, TESTED AT 75 DEGREES. THE IINO NUMERICAL CURVE FITTING WITH MY SET TO 1000 IS ADDED

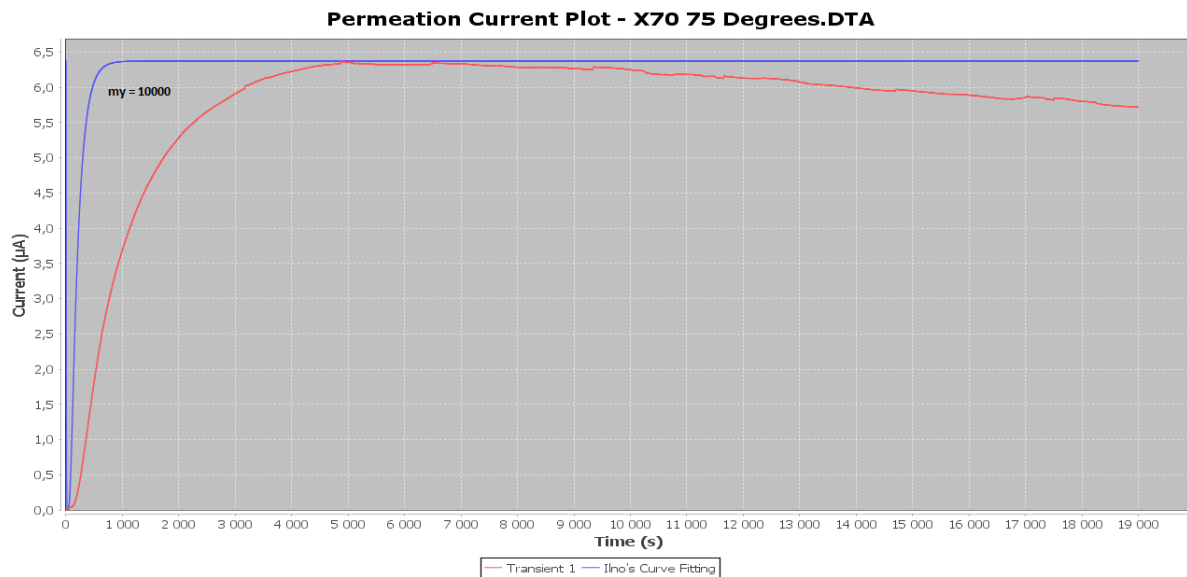


FIGURE 5-72: CHART DISPLAYING CATHODIC CURRENT AS A FUNCTION OF TIME FOR AN X70 SAMPLE, TESTED AT 75 DEGREES. THE IINO NUMERICAL CURVE FITTING WITH MY SET TO 10000 IS ADDED

5.3 Non-functional Properties

The non-functional functionalities were predefined in subsection 4.3.2, and in this section the usability, modifiability, and performance of the program will be determined.

5.3.1 Usability

The usability of the program is confirmed through use by Hope in her master thesis. The user guide to the software is attached in *Appendix B: Diffusion Calculator User Guide*, and explains all the functionalities available. In order to determine the usability more concretely, a more extensive user survey must be performed on both experienced and inexperienced users. As long as the data needed to generate a chart is provided, no former knowledge of hydrogen diffusion should be necessary in order to develop analysis data. The software provides more intuitive approaches to perform the analysis, and predefined models which only require parameters in order to perform computations. This makes it more usable than an excel approach, which was one of the user requirements. The JFreeChart, explained in subsection 4.2.3, offers great usability for the user, offering most of the actions wanted in a simple way.

5.3.2 Modifiability

The Model-View-Controller (MVC) pattern discussed in subsection 4.1.2 provides an intuitive structure of the code, which makes modifications easier to perform. A lot of

functionalities have been added throughout the development process, and no changes to former implementations were necessary. Additional buttons could be added to the main frame, connected to new views, without disrupting the old code. The author has not been able to run the application on a MacBook, possibly because of problems described in subsection 4.3.2. A list of all the modifications performed throughout the development process is attached in *Appendix C: Application Editions*.

5.3.3 Performance

Performance covers the storage, accuracy and runtime of the software. By using Model-View-Controller (MVC) presented in subsection 4.1.2, much of the lists containing the greatest amounts of data could be implemented locally. This frees a lot of storage when the data is not in use. Iino's curve fitting is the most time and storage consuming method among all the functionalities of the software. The accuracy and runtime of Iino's method is both improved by the initial conditions and boundary conditions, fully described in subsection 5.2. The smallest and the biggest datasets tested are represented by Table 5-9 and Table 5-10, giving accuracy and time improvements from an older version of the software. The noise reduction implemented is also contributing to better accuracy.

FeSi Material Tested at 50 Degrees. Duration 7200 secs	Old Software (12.05.2015)	New Software (31.05.2015)	Difference
Time	10 min	2 min	8 min
Least Squares Residual	2.09	0.38	1.71
Iino's D_{eff}	4.73E-6	4.57E-6	0.16
Iino's My	6.4	6.3	0.1
Iino's Lambda	23.0	22.0	1
Iino's Kappa	0.0001	0.0001	0

TABLE 5-9: OLD AND NEW SOFTWARE RUNNING IINO'S METHOD ON THE SAME EXPERIMENTAL DATA. RESULTS DISPLAYED FOR BOTH RUNS, AND THE DIFFERENCE IS COMPUTED. THE OLD SOFTWARE USE THE BRUTE FORCE TECHNIQUE, WITH UNTRAINED BOUNDARIES AND INITIAL CONDITIONS, RESULTING IN BAD RUNTIME AND ACCURACY. THE NEW SOFTWARE INCLUDES AN

INITIAL AND BOUNDARY CONDITION METHOD EVOLVING THROUGHOUT THE ANALYSIS, WHICH GIVES BETTER ACCURACY AND DECREASED RUNTIME. THE OLD SOFTWARE'S KAPPA VALUE WAS CHANGED IN ORDER TO MATCH THE NEW SOFTWARE

X65 Material Tested at 30 Degrees. Duration 45000 secs	Old Software (12.05.2015)	New Software (31.05.2015)	Difference
Time	105 min	23 min	82 min
Least Squares Residual	6.55	3.4	3.15
Iino's D_{eff}	5.64E-6	6.9E-6	1.26
Iino's My	6.3	5.5	0.8
Iino's Lambda	23.0	26.0	3
Iino's Kappa	1.0E-4	1.0E-4	0

TABLE 5-10 : OLD AND NEW SOFTWARE RUNNING IINO'S METHOD ON THE SAME EXPERIMENTAL DATA. RESULTS DISPLAYED FOR BOTH RUNS, AND THE DIFFERENCE IS COMPUTED. THE OLD SOFTWARE USES THE BRUTE FORCE TECHNIQUE, WITH UNTRAINED BOUNDARIES AND INITIAL CONDITIONS, RESULTING IN BAD RUNTIME AND ACCURACY. THE NEW SOFTWARE INCLUDES AN INITIAL AND BOUNDARY CONDITION METHOD EVOLVING THROUGHOUT THE ANALYSIS, WHICH GIVES BETTER ACCURACY AND DECREASED RUNTIME. THE OLD SOFTWARE'S KAPPA VALUE WAS CHANGED IN ORDER TO MATCH THE NEW SOFTWARE

6 Discussion

During the work with this master thesis, an application has been developed according to all predefined requirements given during the planning process. It has been utilized by Hope during her work [36], and has proven useful even before all planned functionalities were implemented. In this chapter the implemented file reading, data display, chart generator, curve fitter and noise reduction will be discussed, before the results from Iino's model will be analyzed. Lastly the attributes of the software will be reviewed.

6.1 System Functionalities

This section covers all results included in the functional properties section (5.1). Functionality bugs will be discussed, alongside potential improvements, but also advantages by implementing the methods the way they have been.

The file reader is currently only able to read files from a Gamry potentiostat, and is implemented in a primitive way, by skipping lines. The advantage of this approach is the simplicity regarding skipping lines and determining the duration of the dataset. Not all files reveals the same structure, and sometimes the data columns starts later in the file than the ordinary ones, due to error messages from the procedure or other extra information. This gives errors later in the program, and should be identified by the reader. Different files generated from other potentiostats should also be identified by the software, and give correct readings. A custom file opener has been mentioned to be the solution of this problem, letting the user see a display of the data before reading it, thus letting the user select which columns to read and from where.

The data display works as a main menu for the software, and gives the user all connections to other functionalities of the program. The table representation of the readings from the data file works well with excel if the user wants to paste in the results for comparing, and offers a well arranged display of the data. Further input from the user in order to perform computations could be a bit tricky, since the input fields requires the enter button to be pressed after typing, which is less intuitive for most users. The representation of the calculated results should get a neater output layout. By offering a browse file button in this window, the user could reload new files to be analyzed, without exiting the program and launching it again in order to retrieve new data.

The chart generators created with JFreeChart (4.2.3) offers great usability for the user, making the charts manageable and accessible for other programs. Fick's lattice diffusion and elapsed time diffusion curve gives good representations of data, and is generated in almost no runtime. The adding of two more transients let the user compare his/hers results, together with the curves already generated from Fick's methods. The save method should give a custom naming convention, and a default destination folder. It should also save the file in a way that is readable when the program is launched from the start, but the comments regarding the file reader could potentially solve this problem as well. Fick's elapsed time curve is plotted as a function of normalized time based on the effective diffusion coefficient and not the lattice diffusion coefficient as the experimental data, which gives deviations.

The curve fitter options are the most central in the software, and Iino's model is discussed in depth in the next section. Fick's curve fitter computes a curve, which is similar to Fick's curve based on the elapsed time diffusion coefficient, and is therefore neglectable. Iino's curve gives a much better representation of data since it takes trapping into account, but has a heavier computation time due to many unknowns. Adjusting the methods to work with both material types, have been especially tricky, since boundary conditions and initial conditions vary greatly between all specimens. To make the performance good enough regarding runtime, some experimental data sets with different tendencies than the ones in focus, reveals faulty approximations. This is because the curve fitters utilize parts of the experimental data when performing the predictions, instead of the entire data set. Both curve fittings suffers from the deviation problem regarding normalized time computation as mentioned for Fick's elapsed time curve. There should be a save and load button for the curve fittings, which would be handy when comparing different approaches to the fittings, as discussed in the next section. If the user could manually input the variables for the two models, it could reveal a better method to approach a fitting, than doing it automatically, but the heavy computing time when generating charts obstructs continuous updating of curves.

The noise reduction functionalities have various success rates regarding execution. The manual removing of data points by double clicking renders the best results, but is equally time consuming. The Iino filter gives wrong approximation in Figure 5-16, where too much data is removed, due to too low thresholds for removal. The same data, but in a normalized flux plot (Figure 5-11) gives a good noise reduction using the same filter, since the y-axis have bigger deviations for the current chart. Different thresholds should be implemented for the two charts in order to solve this. The noisy X70 sample presented in subsection 5.1.5 includes abnormal

tendencies, thus revealing bad approximations and wrong noise reductions. Either the custom filter and manual filter, or only manual filter gives equally good reductions, but the approximation deviates from the experimental data. Other approaches suffer from low threshold values, and remove too much data. A better trained Iino method could solve this problem, alongside different thresholds.

6.2 Iino's Results

This section will go through the results from section 5.2, and describe the effect of the unknowns related to Iino's model (subsection 3.4.4). Arguments for the initial and boundary conditions utilized for the different parameters during fitting will be made, as well as comparing it with other papers discoveries.

Kappa is the parameter describing irreversible trapping in Iino's model (equation (3.67)), which is the main modification of Iino's approach from McNabb and Foster's model described by equation (3.12) and (3.13). The results in Figure 5-31 to Figure 5-36 illustrates what has been earlier discussed in this paper, that the kappa value decides the altitude of the curve, which decreases when the kappa value increases. The value has therefore been set to 0.0001 as a constant, since higher values results in deviations. As Fallahmohammadi discusses in his paper [23], the irreversible traps have bigger influence for the first transient, where they are filled, thus not affecting later transients. Most of the first transients looked at through the work with this paper has been too noisy to analyze.

The effective diffusion coefficient affects the horizontal position of the graph as shown in Figure 5-37 to Figure 5-50. By utilizing good initial values from the other unknowns, the effective diffusion coefficient could be approximated fairly accurate. The boundaries discovered to work well is the elapsed time diffusion coefficient divided by 10 as lower boundary, and multiplied with 10 as an upper boundary. When the value is set to equal the lattice diffusion coefficient, the curve is shown to lie to the right of Fick's lattice curve (Figure 5-43 and Figure 5-50). This could be due to the different computation of normalized time, discussed earlier.

The lambda parameter is one of the unknowns describing reversible trapping in Iino's model. As shown in Figure 5-51 to Figure 5-62, it influences the steepness of the curve, decreasing the slope as its value increases. It is shown to lie between 1 and 10000 in value, but is very dependent on my's value.

The my parameter is approximated by every iteration of the lambda value, since they both describe reversible trapping in Iino's model and are highly dependent of each other. As displayed in Figure 5-63 to Figure 5-72 my's value influences the slope of the curve as well, but in an opposite way of the lambda value. It gives good approximations for most datasets, with boundaries between 0 and 2000.

The results obtained from Hope's work [36], attached in *Appendix D: Hope Data*, gives a wider understanding of the materials as she have been testing more samples, than what is done during this work. Her effective diffusion coefficient have been found to range from 2.25E-8 to 5.12E-6 for the ferrosilicon and from 1.09E-6 to 9.9E-6 for the X70 steel, when computed by the elapsed time method. The effective diffusion coefficient ranges from 9.74E-7 to 2.13E-5 for the ferrosilicon and from 5E-6 to 5.22E-5 for the X70 steel, when computed by the Iino's curve fitting method. For both methods and materials the effective diffusion coefficient is generally smaller for low temperatures than for high temperatures.

The elapsed time effective diffusion coefficient is in agreement with boundaries presented in the conclusion of Hauge's master thesis [37] for X70 steel. When the Iino method approximates the value, the result is at least 2 times as big as the result from the elapsed time method. If these computations are correct, it displays the importance of including traps in the computations.

The lambda value lies between the boundaries 4 to 100 for both materials, except a few samples, which required values closer to 10000. The my value ranges from 0 to 115 for both materials, but some samples requires values around 2000. The my and lambda value is independent of material type and temperature.

Tendencies of the two materials tested deviates greatly, and should ideally be approached in different ways. Different values of the parameters could yield equally good curve predictions, leaving an uncertainty regarding actual accuracy of the fittings.

6.3 Software Attributes

This section will discuss the results from section 5.3, and decide the fulfillment of the non-functional requirements (4.3.2). The usability and modifiability of the program is ensured by the use of Model-View-Controller and the different frameworks, but need to be tested by more users and programmers, in order to obtain any concrete results.

The performance of the program is measured by runtime and accuracy of Iino's method, which is covered by Table 5-9 and Table 5-10. The least squares residual value is the sum illustrated by equation (3.68), and the fitting is found to give acceptable accuracy if this value is beneath 5, but it is varying between the permeation current chart and the normalized flux chart, as the y-axis values is scaled down for the flux. The improvement from the older versions gives an indication of the advantages of the trained conditions. Initially the brute force method was used, by doing a curve fit for every increment on every parameter, which is very time consuming. By realizing the accuracy of the approximation of the effective diffusion coefficient if good initial conditions was used, made it possible to outsource it from the main loop, saving valuable time. The decision to run through the entire procedure three times with different step sizes narrowed down the sum of steps needed, and made it possible to perform more precise adjustment during the last iteration. It exist better algorithms to locate the best predictions, which could be approached if it is desired to improve the runtime even more. By doing more extensive testing, better initial and boundary conditions could be retrieved, resulting in less search time for each parameter.

7 Conclusion

During this master thesis a software product has been developed with indisputable advantages of approximations to experimental hydrogen diffusion data, by using known mathematical models. The software still needs some modifications discussed in the next chapter, but the basis for a powerful tool have been produced. The study of Iino's method and its use in the software has resulted in a better understanding of the properties of X70 and FeSi steel. Additional data have been received from Hope [36], attached in *Appendix D: Hope Data*, in order to specify tendencies from use of the software.

- Different values of parameters could provide equally good curve fittings because of all the unknowns, making the results more uncertain regarding actual accuracy.
- The significance of irreversible traps have been debated, and found neglectable during analysis of other transients than the first. The irreversible traps have then already been filled, and contribute in little or no degree as sinks or sources of hydrogen. Therefore the altering of the kappa value has not been in focus during the work with this application.
- The effective diffusion coefficient have been found to range from $2.25\text{E-}8$ to $5.12\text{E-}6$ for the ferrosilicon and from $1.09\text{E-}6$ to $9.9\text{E-}6$ for the X70 steel, when computed by the elapsed time method.
- The effective diffusion coefficient have been found to range from $9.74\text{E-}7$ to $2.13\text{E-}5$ for the ferrosilicon and from $5\text{E-}6$ to $5.22\text{E-}5$ for the X70 steel, when computed by the Iino's curve fitting method.
- The lambda value is dependent of the my value, and lies between the boundaries 4 to 100 for both materials, except a few samples, which required values closer to 10000.
- The my value is dependent of the lambda value, and ranges from 0 to 115 for both materials, but some samples requires values around 2000.

8 Future work

The application developed in this work is a prototype, and in this chapter the author will present his recommendations towards further developing and modification.

- The reader needs to be able to read different files with data, easiest solved by implementing a custom file reader giving more freedom to the user by giving a display of the file, and give the opportunity to decide which data to be handled.
- The file browsing should be accessible from the main menu of the program, so the user does not have to exit and launch the program in order to read data from a new file.
- Easier input interface, in order to enter specimen thickness, temperature, and background current should be implemented.
- Results from the first calculations should be displayed in a neater way, and explained more extensively.
- Name of curves removed with restore buttons remains in the view, should be removed as well.
- The Fick's curve fitting method in the chart views should be modified or removed completely, as the present state gives the user no analytical value.
- The problem regarding computation of normalized time for Fick's elapsed time curve, Fick's fit curve, and Iino's fit curve should be reviewed, in order to display them in the same way as the experimental curve.
- The user should be able to save which curve he would like, and a more intuitive default name setting should be provided.
- The user should be asked to load any curve he would like, generating a more fitting name related to the curve loaded.
- Noise reduction by the custom filter and Iino's filter needs modifications, with higher threshold values so they do not remove too much data.
- The removal of noise points should be reviewed, as a replacement would give a better representation of the data.
- Iino's fit curve should be reviewed and worked more on, in order to train it into a better state. It is currently not working as good for all transients, so the boundary and initial conditions needs to be improved.

- There should be implemented a functionality where the user gets to input the different parameters for Iino's curve, displaying the results for every change. This could reveal to be the best approach in order to make the curve fit perfect.
- There should be a timer display for Iino's method, informing the user how much time is left of the procedure.
- The display of data from curve fittings needs to be outputted more neatly, and explained better.
- Further study of Iino's parameters is needed, in order to fully understand their properties, and enabling more usable computations from the application.
- Error messages should warn the user if wrong inputs have been performed.
- There should be made an abstract class representing charts, ensuring correspondence and making it easier to modify the two similar classes.
- General GUI improvements are needed to make the application design better, and controls more intuitive.

Bibliography

- [1] ASTM International , "Standard Practice for Evaluation of Hydrogen Uptake, Permeation and Transport in Metals by an Electrochemical Technique," 2003.
- [2] M. A. V Devanathan and Z Stachurski, "The adsorption and diffusion of electrolytic hydrogen in palladium," *Proceedings of the Royal Society of London. Series A, Mathematical and Physical*, vol. 270, pp. 90-102, October 1962.
- [3] R. A. Oriani, "Diffusion and Trapping of Hydrogen in Steel," *Acta Metallurgica*, vol. 18, no. 1, pp. 147-157, January 1970.
- [4] Ejim Francis Okwudiri, "Hydrogen Diffusion in Pipeline Steel," Politecnico di Milano, Master thesis 2012.
- [5] Afrooz Barnoush, "Hydrogen Embrittlement," Saarland University, Saarbrücken, Thesis 2011.
- [6] William H. Johnson, "On some Remarkable Changes Produced in Iron and Steel by the Action of Hydrogen and Acids," *Proceedings of the Royal Society of London*, vol. 23, pp. 168-179, 1874.
- [7] V Olden, C Thaulow, and R Johnson, "Modelling of Hydrogen Diffusion and Hydrogen Induced Cracking in Supermartensitic and Duplex Stainless Steels," *Materials & Design*, vol. 29, no. 10, pp. 1934-1948, December 2008.
- [8] A. Smirnova, "Hydrogen Permeation in 13% Cr Super Martensitic Stainless Steel and API X70 Pipeline Steel," Norwegian University of Science and Technology, PhD thesis 2010.
- [9] T Okstad, Ø Rannestad, R Johnson, and K Nisancioglu, "Significance of Hydrogen Evolution During Cathodic Protection of Carbon Steel in Seawater," *Corrosion*, vol. 63, no. 9, pp. 857-865, 2007.
- [10] R Kumar and D Gaur, "Overview of Hydrogen Embrittlement in Fasteners," *Impact*, vol. 2, no. 4, pp. 239-244, April 2014.
- [11] E.M.K Hillier and M.J Robinson, "Hydrogen Embrittlement of High Strength Steel Electroplated with Zinc-Cobalt Alloys," *Corrosion Science*, vol. 46, no. 3, pp. 715-727, March 2004.
- [12] M. R. Louthan, "Hydrogen Embrittlement of Metals: A Primer for the Failure Analyst," Savannah River National Laboratory, 2008.
- [13] SJ Kim and KY Kim, "A Review of Corrosion and Hydrogen Diffusion Behaviors of

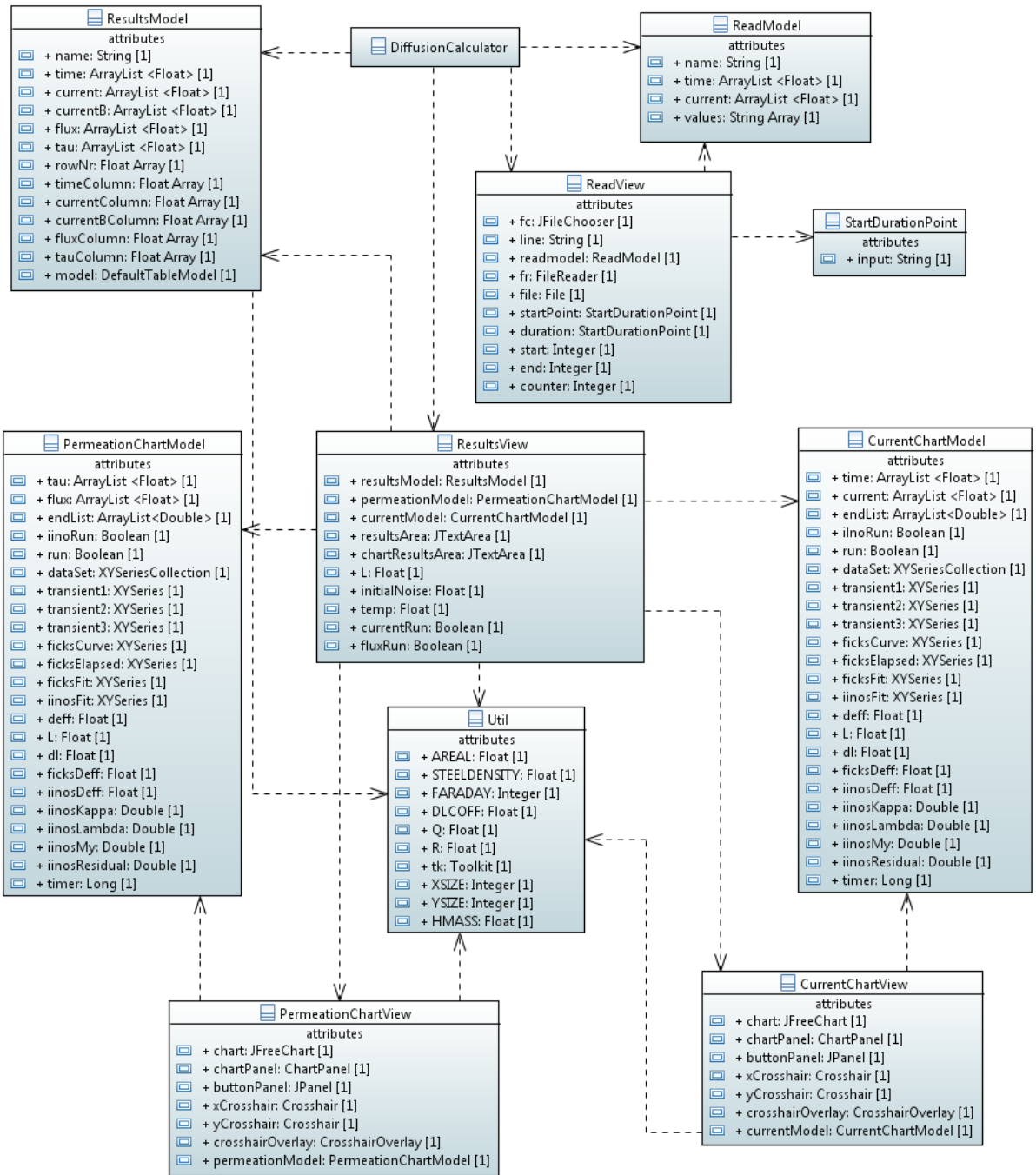
- High Strength Pipe," *Journal of Welding and Joining*, vol. 32, no. 5, 2014.
- [14] C. D. Beachem, "New Model for Hydrogen-assisted Cracking (Hydrogen Embrittlement)," *Metallurgical Transactions*, vol. 3, no. 2, pp. 441-455, 1972.
- [15] H.K Birnbaum and P Sofronis, "Hydrogen-enhanced localized plasticity - A mechanism for Hydrogen-related Fracture.," *Materials Science and Engineering A-structural Materials Properties Microstructure and Processing*, vol. 176, no. 1-2, pp. 191-202, 1994.
- [16] Lynch SP, "Progress Towards Understanding Mechanisms of Hydrogen Embrittlement and Stress Corrosion Cracking," NACE: NACE International, NACE-07493 2007.
- [17] E.A Steigerwald, F.W Schaller, and A.R Troiano, "The Role of Stress in Hydrogen Induced Delayed Failure.," *Trans. Met. Soc. AIME*, vol. 218, pp. 832-841, October 1960.
- [18] Thomas Graham, "Diffusion Processes," in *Diffusion Processes: Proceedings of the Thomas Graham Memorial Symposium, University of Strathclyde.*: Gordon and Breach, 1971, vol. 1, pp. 6-7.
- [19] Malin Berglund Hope, "Hydrogen Uptake in Steel," Norwegian University of Science and Technology, Trondheim, Master Project 2014.
- [20] Christian Thaulow and Henry Valberg, *TMM4140 Plastisk deformasjon og brudd*. Trondheim: Norwegian University of Science and Technology, 2012.
- [21] GT Park, SU Koh, HG Jung, and KY Kim, "Effect of Microstructure on the Hydrogen Trapping Efficiency and Hydrogen Induced Cracking of Linepipe Steel," *Corrosion Science*, vol. 50, pp. 1865-1871, 2008.
- [22] William D. Callister and David G. Rethwisch, *Materials Science and Engineering*, 8th ed.: John Wiley & Sons, 2011.
- [23] Ehsan Fallahmohammadi, "Diffusion and Trapping of Hydrogen in Pipeline Steels," Politecnico Di Milano, Milano, PhD Thesis 2014.
- [24] A Turnbull, M. W Carroll, and D. H Ferriss, "Analysis of Hydrogen Diffusion and Trapping in a 13% Chromium Martensitic Stainless Steel," *Acta Metallurgica*, vol. 37, no. 7, pp. 2039-2046, 1989.
- [25] A. Fick, "On Liquid Diffusion," *Journal of Membrane Science*, vol. 100, pp. 33-38, 1995.
- [26] E Fallahmohammadi, F Bolzoni, and L Lazzari, "Measurement of Lattice and Apparent Diffusion Coefficient of Hydrogen in X65 and F22 Pipeline steels," *International*

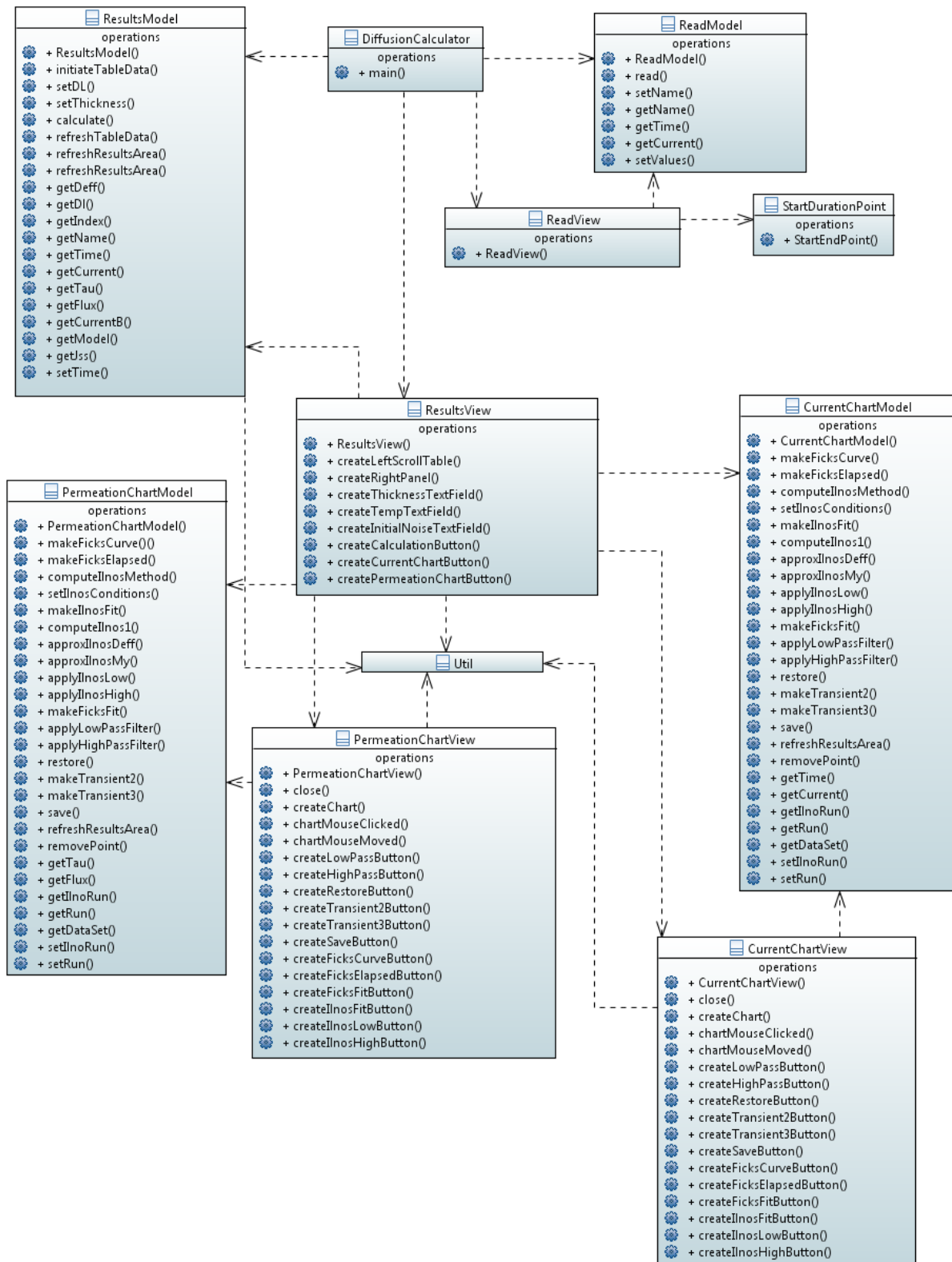
Journal of Hydrogen Energy, vol. 38, pp. 2531-2543, 2013.

- [27] K. Kiuchi and R.B McLellan, "The Solubility and Diffusivity of Hydrogen in Well annealed and Deformed Iron," *Acta Metallurgica*, vol. 31, no. 7, pp. 961-984, 1983.
- [28] A McNabb and P. K Foster, "A New Analysis of the Diffusion of Hydrogen in Iron and Ferritic Steels," *Transactions of the Metallurgical Society of AIME*, vol. 227, no. 6, pp. 618-627, 1963.
- [29] George R.,JR Caskey and William L. Pillinger, "Effect of Trapping on Hydrogen Permeation," *Metallurgical Transactions A*, vol. 6, no. 3, pp. 467-476, March 1975.
- [30] Peter G. Thomas and Ellen J. Stern, "Efficient Numerical Modelling of Hydrogen Diffusion with Trapping," *Journal of Materials Science*, vol. 16, pp. 3122-3130, 1981.
- [31] M Iino, "A More Generalized Analysis of Hydrogen Trapping," *Acta Metallurgica*, vol. 30, pp. 367-375, 1982.
- [32] Frank Buschmann, Regine Meunier, Hans Rohnert, Peter Sommerlad, and Michael Stal, *PATTERN-ORIENTED SOFTWARE ARCHITECTURE. Volume I: A System of Patterns*. Germany: John Wiley & Sons, Inc., 2001.
- [33] Partha Kuchana, *Software Architecture Design Patterns in Java*. USA: Auerbach Publications, 2004.
- [34] Kishori Sharan, *Beginning Java 8 APIs, Extensions and Libraries Swing, JavaFX, JavaScript, JDBC and Network Programming APIs.:* Apress, 2014.
- [35] David Gilbert, "The JFreeChart Class Library Version 0.9.1," Reference Documentation 2002.
- [36] Malin Berglund Hope, "Effect of Plastic Deformation and Microstructure on Hydrogen Diffusion in Steel," Norwegian University of Science and Technology, Trondheim, Master Thesis 2015.
- [37] Anders Senumstad Hauge, "Hydrogen Embrittlement in Subsea Pipelines Made from X70 - Effect of Plastic Deformation on Hydrogen Diffusion," Norwegian University of Science and Technology, Trondheim, Master Thesis 2011.

Appendix A: Class Diagram

Two class diagrams, one showing classes with their fields, and the other showing their methods.



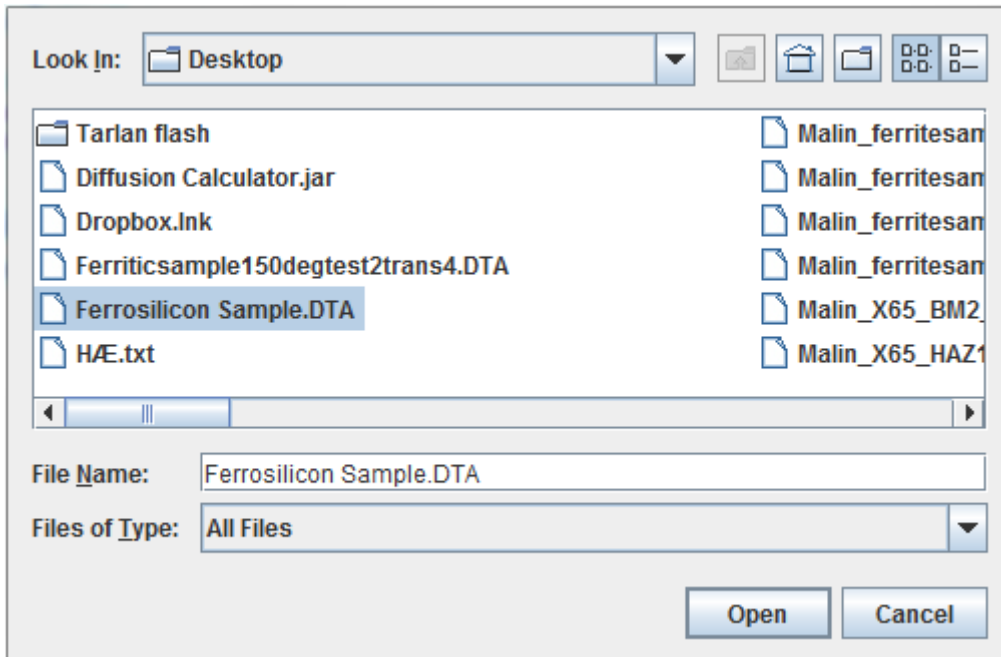


Appendix B: Diffusion Calculator User Guide

This appendix walks the user through every aspect and functionality of the program step by step.

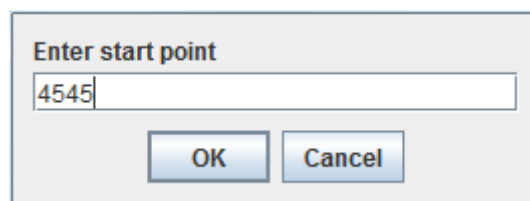
Step 1: Choosing a File

The file chooser should automatically pop up, when you open it from the desktop. Choose a .dta file and press open.



Step 2: Input a Starting Point

An option pane should pop up; prompting the user to enter a start value. The start value represents the experiment start time. Press ok.



Step 3: Input the Duration

See step 2. Input a value for the duration and press ok.

Enter duration

7200

OK Cancel

Step 4: Input Correct Parameters

A scrollable table halfway filled should pop up, with some text fields and buttons. The user needs to input values IN CORRECT ORDER, starting with the thickness of sample, temperature of the environment and then the background current. The background current could be copied and pasted from the top current value if this is the correct value. Remember to press enter after EACH of the three inputs. When the background current is correctly entered, the rest of the columns should be filled with data.

Nr.	Time	Current	Current - Backgro...	J(t)/Jss	tDI/L^2
0.0	3.0	5.06294E-6			
1.0	6.0	5.0666E-6			
2.0	9.0	5.06228E-6			
3.0	12.0	5.06184E-6			
4.0	15.0	5.06462E-6			
5.0	18.0	5.06539E-6			
6.0	21.0	5.06865E-6			
7.0	24.0	5.07009E-6			
8.0	27.0	5.07232E-6			
9.0	30.0	5.07481E-6			
10.0	33.0	5.07358E-6			
11.0	36.0	5.0754E-6			
12.0	39.0	5.08343E-6			
13.0	42.0	5.08391E-6			
14.0	45.0	5.09577E-6			
15.0	48.0	5.09741E-6			
16.0	51.0	5.08848E-6			
17.0	54.0	5.10006E-6			
18.0	57.0	5.10711E-6			
19.0	60.0	5.09419E-6			
20.0	63.0	5.09433E-6			
21.0	66.0	5.09563E-6			
22.0	69.0	5.10488E-6			
23.0	72.0	5.09907E-6			
24.0	75.0	5.10214E-6			
25.0	78.0	5.10066E-6			
26.0	81.0	5.09983E-6			
27.0	84.0	5.10394E-6			
28.0	87.0	5.11297E-6			
29.0	90.0	5.10885E-6			
30.0	93.0	5.11686E-6			
31.0	96.0	5.1067E-6			
32.0	99.0	5.11378E-6			
33.0	102.0	5.11235E-6			
34.0	105.0	5.11078E-6			
35.0	108.0	5.11112E-6			
36.0	111.0	5.11758E-6			
37.0	114.0	5.11862E-6			
38.0	117.0	5.11481E-6			
39.0	120.0	5.11597E-6			
40.0	123.0	5.11785E-6			

0.1

50

5.06294E-6

RESULTS

index

DI

imax

tDI/L^2

tIag

Deff

Co(mol/cm^3)

Co(g/cm^3)

Co(ppm)

Calculate

Permeation Current Chart

Normalized Flux Chart

CHART RESULTS

Fick's Fit Deff

IIno's Fit Deff

IIno's Kappa

IIno's Lambda

IIno's My

IIno's Residual

IIno's Runtime

Update

Step 5: Calculating Values and Plotting

The three values that are marked should be filled with data before this step. If the "Calculate" button is pressed, the "Results" text area will be filled with values. The two chart buttons can now be clicked, in whatever order the user wants, creating different charts.

Nr.	Time	Current	Current - Backgro...	Normalized Flux	Normalized Time
0.0	3.0	5.06294E-6	0.0	0.0	0.026064876
1.0	6.0	5.0666E-6	3.6598067E-9	0.002173243	0.052129753
2.0	9.0	5.06228E-6	-6.6029315E-10	-3.920911E-4	0.07819463
3.0	12.0	5.06184E-6	-1.1000338E-9	-6.5321516E-4	0.104259506
4.0	15.0	5.06462E-6	1.6798367E-9	9.9751E-4	0.13032438
5.0	18.0	5.06539E-6	2.449724E-9	0.0014546795	0.15638927
6.0	21.0	5.06865E-6	5.7098077E-9	0.0033905618	0.18245414
7.0	24.0	5.07009E-6	7.1499926E-9	0.004245763	0.20851901
8.0	27.0	5.07232E-6	9.380074E-9	0.0055700163	0.23458388
9.0	30.0	5.07481E-6	1.1869815E-8	0.0070484583	0.26064876
10.0	33.0	5.07358E-6	1.0639724E-8	0.0063180136	0.28671363
11.0	36.0	5.0754E-6	1.2460077E-8	0.0073989644	0.31277853
12.0	39.0	5.08343E-6	2.0490006E-8	0.012167245	0.3388434
13.0	42.0	5.08391E-6	2.0969765E-8	0.012452133	0.36490828
14.0	45.0	5.09577E-6	3.283003E-8	0.019494921	0.39097315
15.0	48.0	5.09741E-6	3.446985E-8	0.020468667	0.41703802
16.0	51.0	5.08848E-6	2.5539975E-8	0.015165988	0.4431029
17.0	54.0	5.10006E-6	3.7120117E-8	0.022042435	0.46916777
18.0	57.0	5.10711E-6	4.4170065E-8	0.026228787	0.49523264
19.0	60.0	5.09419E-6	3.1249783E-8	0.018556548	0.5212975
20.0	63.0	5.09433E-6	3.1389845E-8	0.018639721	0.5473624
21.0	66.0	5.09563E-6	3.2689968E-8	0.01941175	0.57342726
22.0	69.0	5.10488E-6	4.1939984E-8	0.024904538	0.59949213
23.0	72.0	5.09907E-6	3.613013E-8	0.021454565	0.62555707
24.0	75.0	5.10214E-6	3.920013E-8	0.023277573	0.65162194
25.0	78.0	5.10066E-6	3.771993E-8	0.02239861	0.6776868
26.0	81.0	5.09983E-6	3.6890015E-8	0.021905797	0.7037517
27.0	84.0	5.10394E-6	4.100002E-8	0.024346374	0.72981656
28.0	87.0	5.11297E-6	5.002994E-8	0.029708464	0.7558814
29.0	90.0	5.10885E-6	4.590993E-8	0.027261943	0.7819463
30.0	93.0	5.11686E-6	5.3919848E-8	0.03201834	0.80801123
31.0	96.0	5.1067E-6	4.3759883E-8	0.025985217	0.83407605
32.0	99.0	5.11378E-6	5.0839844E-8	0.030189395	0.860141
33.0	102.0	5.11235E-6	4.941012E-8	0.029340405	0.8862058
34.0	105.0	5.11078E-6	4.7839876E-8	0.028407974	0.9122707
35.0	108.0	5.11112E-6	4.8180027E-8	0.02860996	0.93833554
36.0	111.0	5.11758E-6	5.4639713E-8	0.03244581	0.9644005
37.0	114.0	5.11862E-6	5.567972E-8	0.033063382	0.9904653
38.0	117.0	5.11481E-6	5.1869847E-8	0.030801026	1.0165303
39.0	120.0	5.11597E-6	5.3029908E-8	0.031489886	1.042595
40.0	123.0	5.11785E-6	5.4909833E-8	0.03260621	1.06866

0.1

50

5.06294E-6

RESULTS

index 586

DI 8.688293E-5

imax 1.6840299E-6

ID/L^2 15.300083

ltag 1760.9999

Deff 9.464321E-7

Co(mol/cm^3) 4.1912915E-7

Co(g/cm^3) 4.2244028E-7

Co(ppm) 0.053473454

Calculate

Permeation Current Chart

Normalized Flux Chart

CHART RESULTS

Fick's Fit Deff

lino's Fit Deff

lino's Kappa

lino's Lambda

lino's My

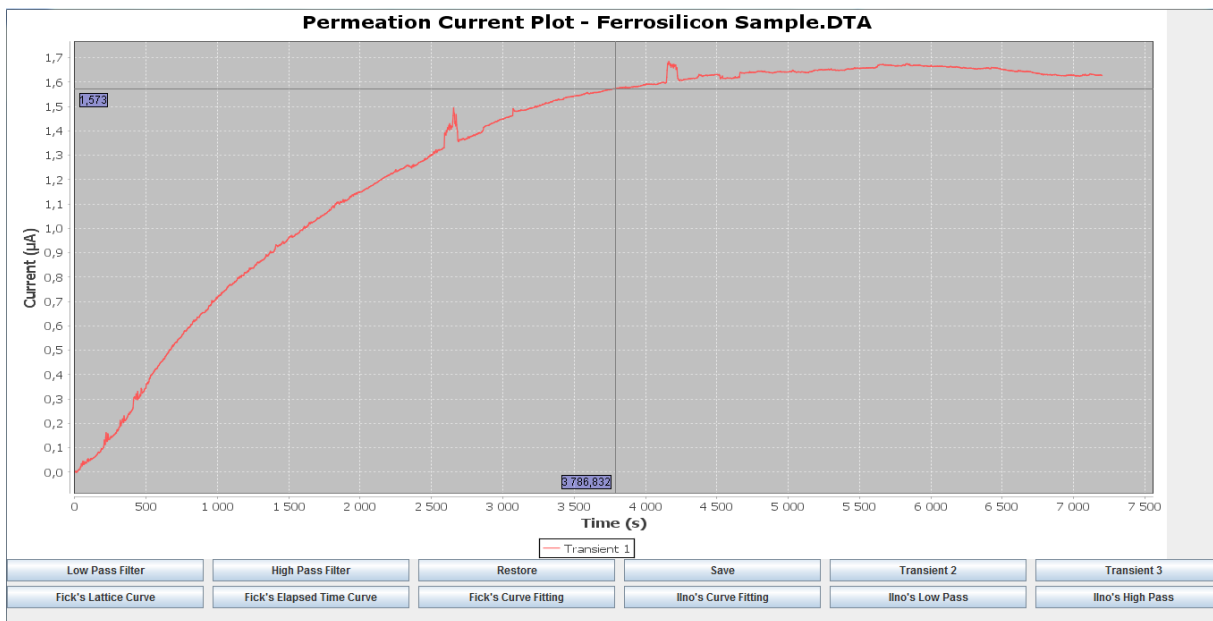
lino's Residual

lino's Runtime

Update

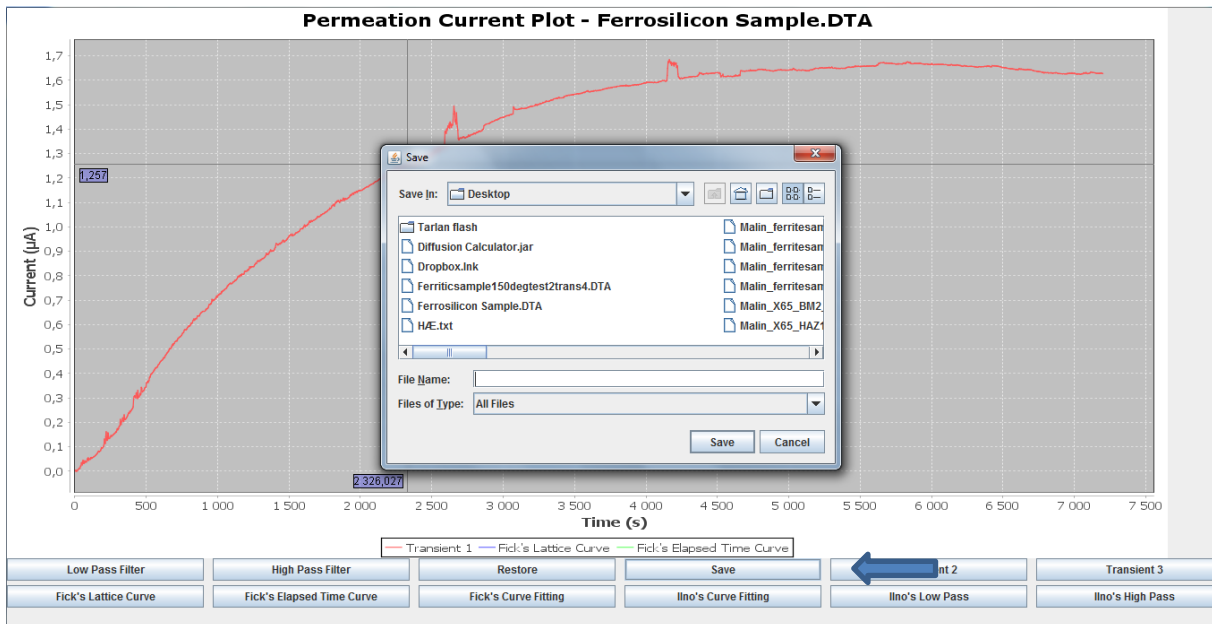
Step 6: Current/Time Chart

After pressing the “Permeation Current Chart” button in the last frame, the chart below will pop up. Crosshairs are following mouse movements over the chart, but are bound to the data. Y and X values can be read from the labels.



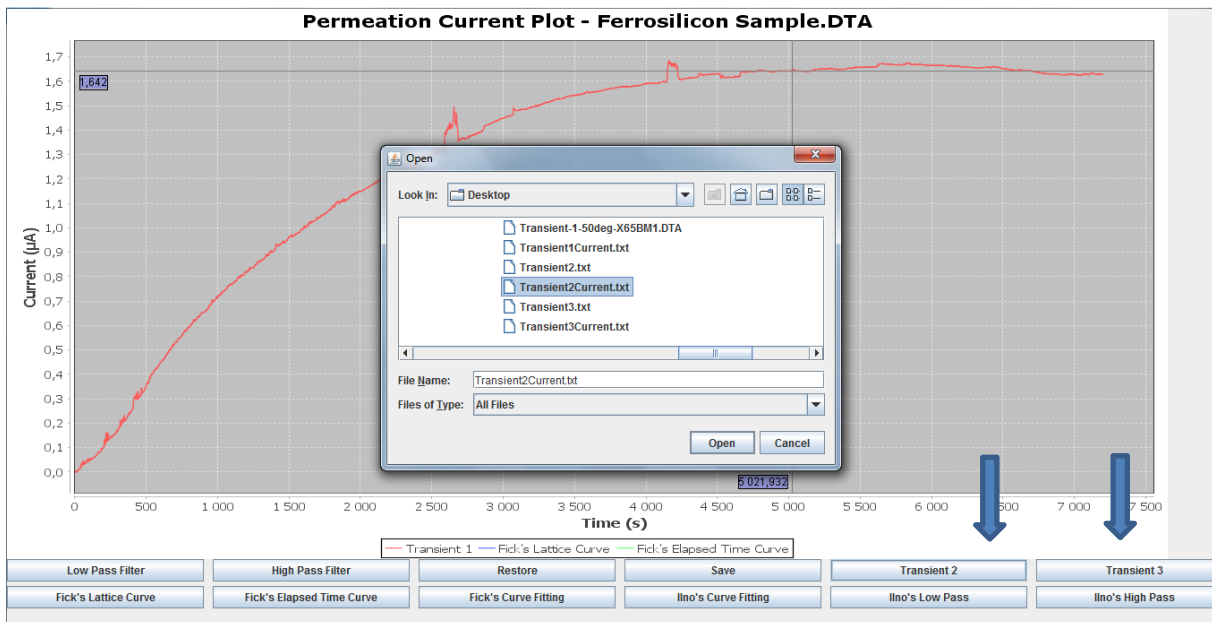
Step 7: Save

Button used to save the current experimental data, to a .txt file.

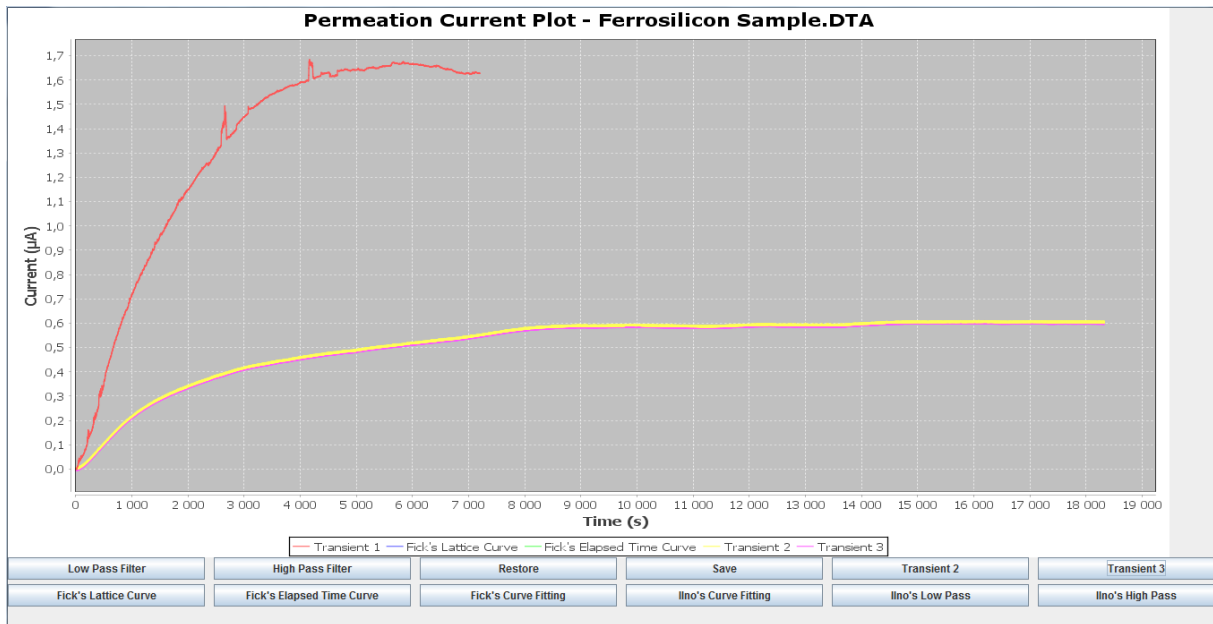


Step 8: Add Transient

Buttons to load former saved experiment data .txt file.

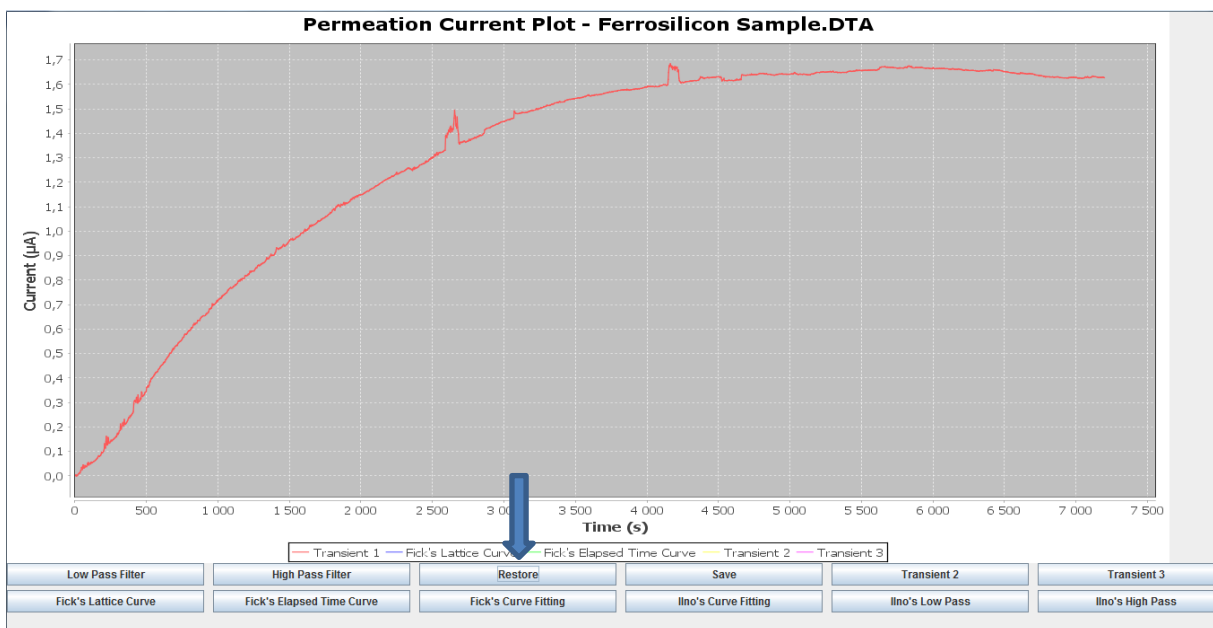


Display two extra transients in the chart. Not from same experiment, so it is a bad match depicted.



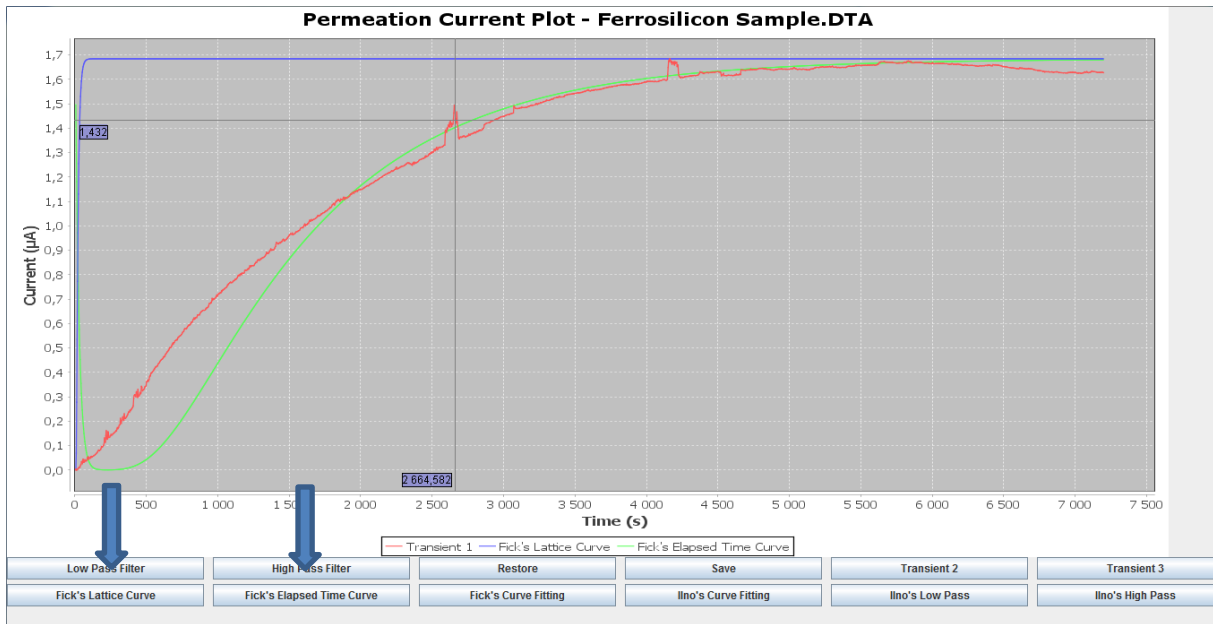
Step 9: Restore

By pressing the restore button, all other curves than the experiment data is removed.



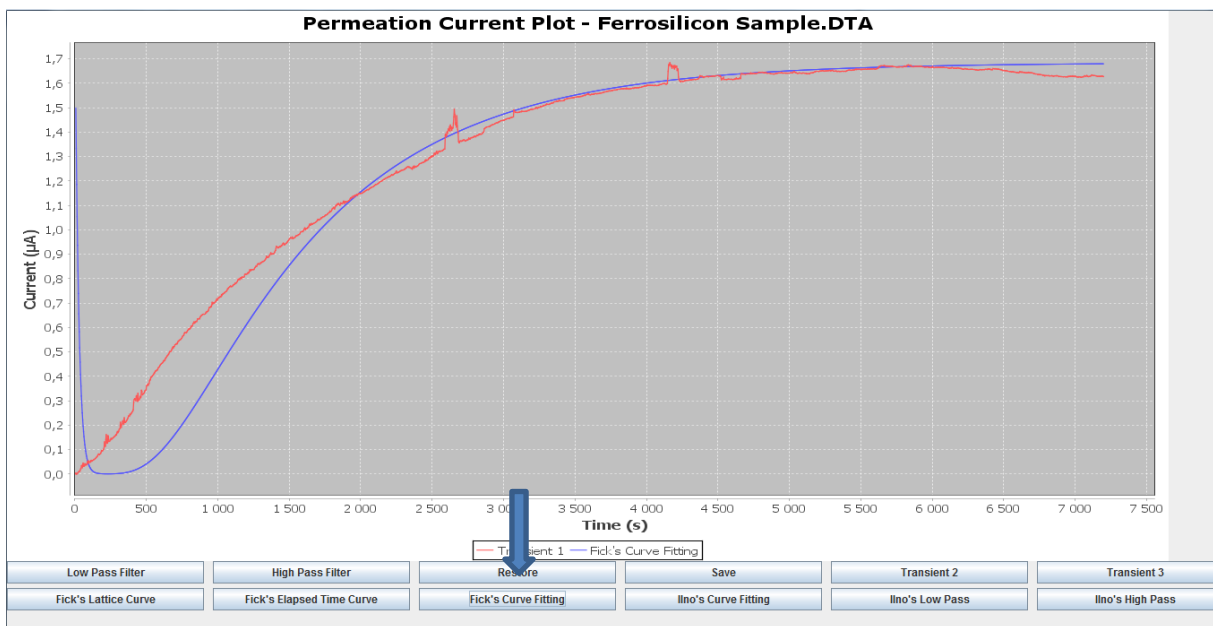
Step 10: Fick's Lattice and Elapsed Time Curve

Fick's lattice curve and elapsed time curve is added to the chart.



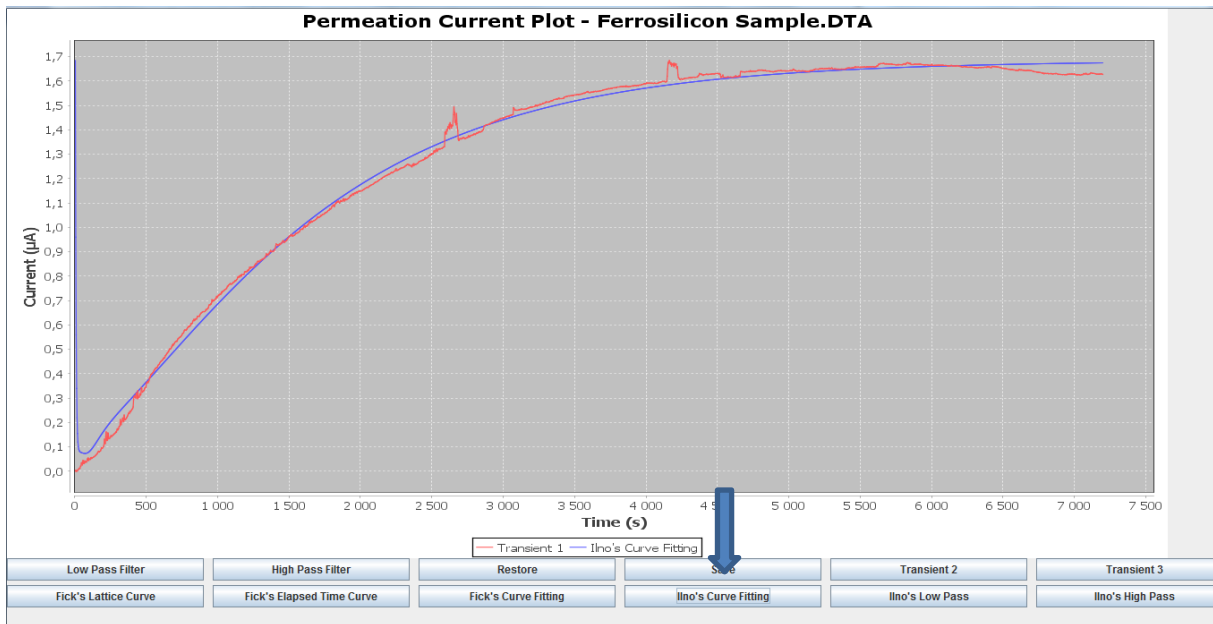
Step 11: Fick's Curve Fitting

Fick's curve fitting is performed and added to the chart.



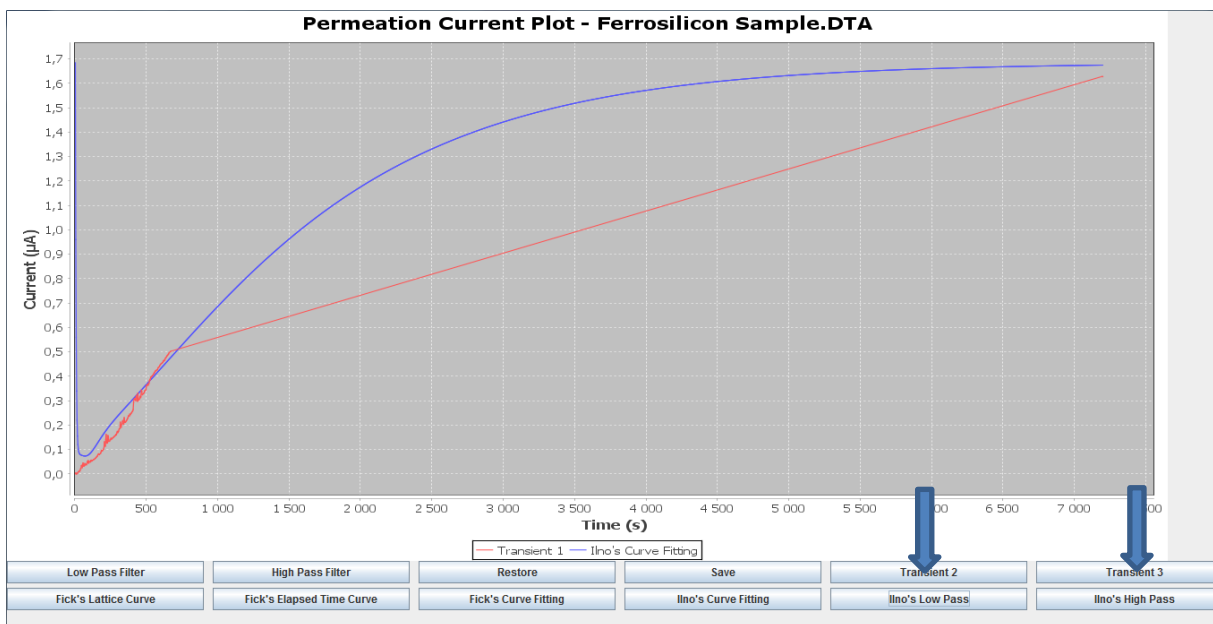
Step 12: Iino's Curve Fitting

Iino's curve fitting is performed and added to the chart. Use more runtime, determined by the amount of data.



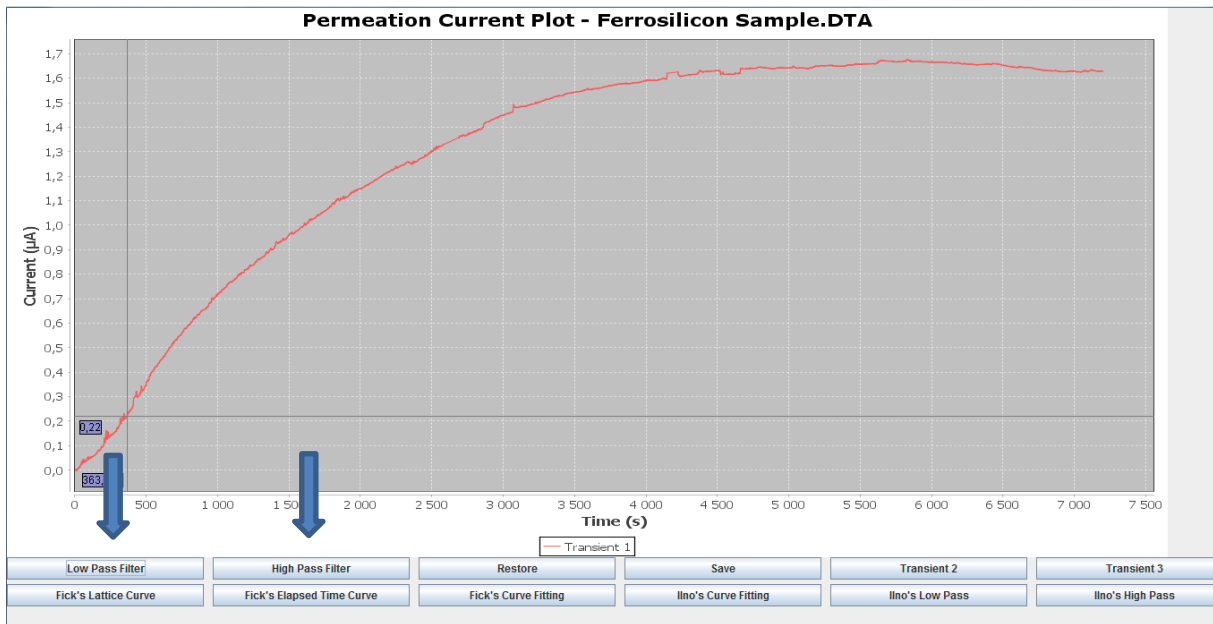
Step 13: Iino's filter

Iino's filter applied, after Iino's fitting has been added. Removing too much data in this case.



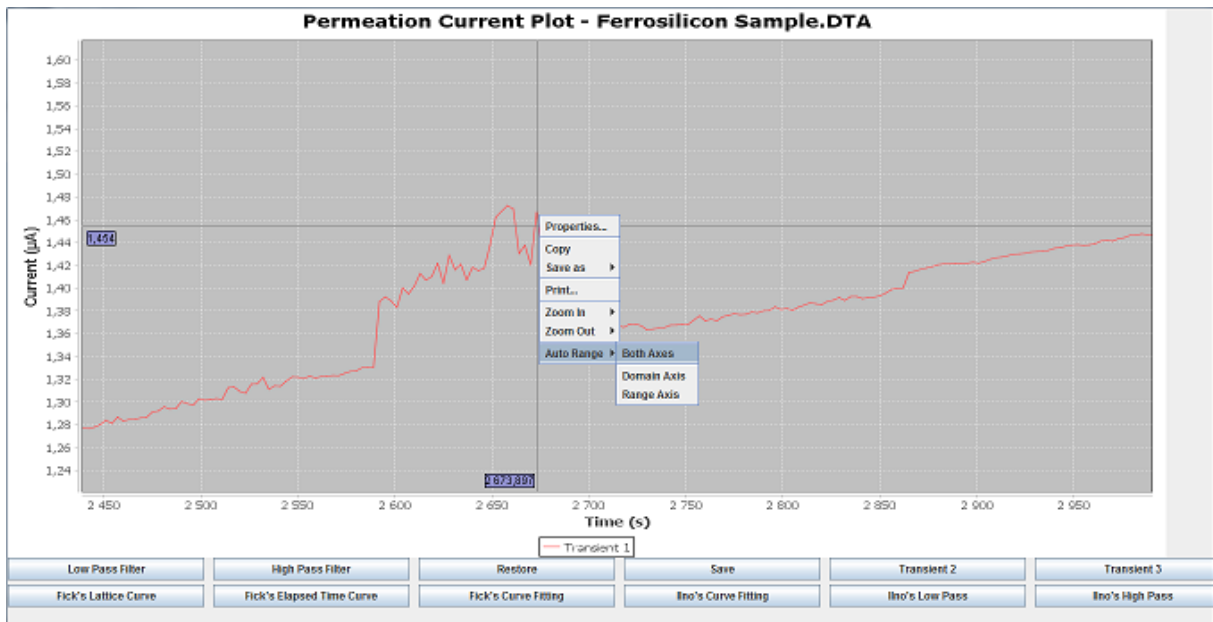
Step 14: Custom Pass Filter

Custom filter applied, which removes a good amount of data, after multiple button presses.



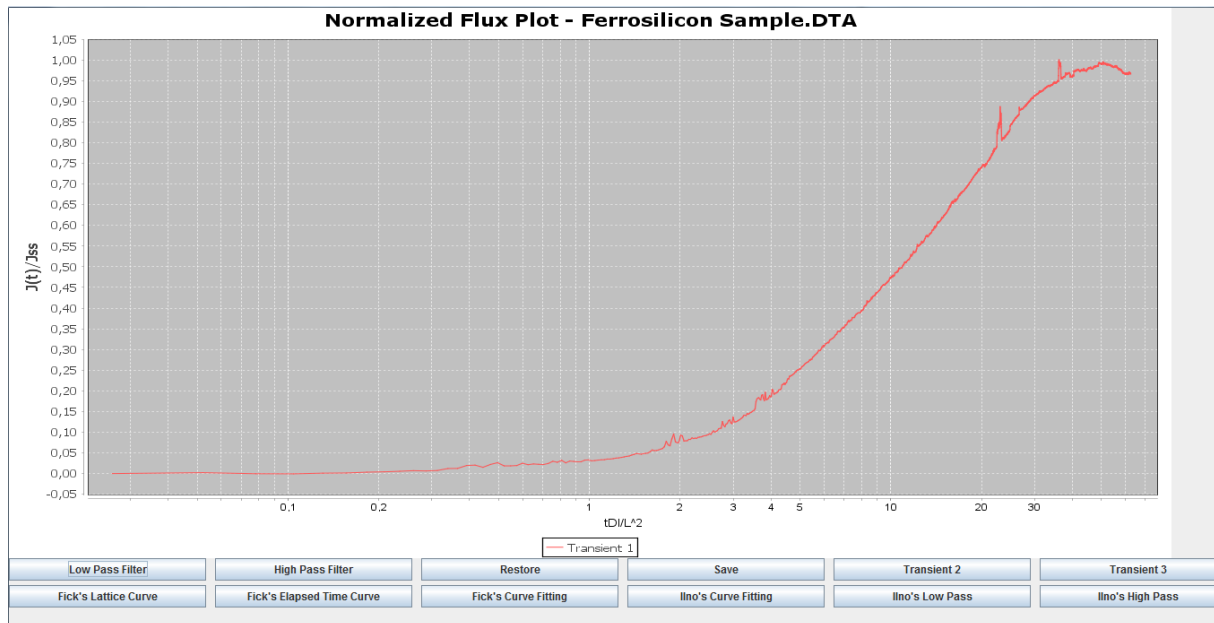
Step 15: Zooming and Mouse Clicking

By pressing the left-mouse button and dragging a rectangle around a section of the chart, the GUI will zoom into this area. By right clicking, and then selecting Auto-Range -> Both Axes, the view will go back to the original. In the pop up window appearing when right clicking, the user will be able to copy and save the chart as well. By double clicking the right-mouse button, when pointing at a data point, the data point will be removed.



Step 16: Permeation Chart

By pressing the “Normalized Flux Chart” button from step 5, the permeation chart window below will pop up. The same properties as in Step 6 are applied. This plot has a logarithmic x-axis.



Step 17: Update Button

When one of the charts is opened, and modifications or curve fittings are performed to the experiment data, the update button can be pressed in the main menu, displaying results and saving modifications. If chart window is closed before update button is pressed, the modifications and results obtained will be lost.

Nr.	Time	Current	Current - Backgro...	Normalized Flux	Normalized Time
0.0	3.0	5.06294E-6	0.0	0.0	0.026064873
1.0	6.0	5.0666E-6	3.6598067E-9	0.002173243	0.052129745
2.0	9.0	5.06228E-6	-6.6029315E-10	-3.920911E-4	0.07819463
3.0	12.0	5.06184E-6	-1.1000338E-9	-6.5321516E-4	0.10425949
4.0	15.0	5.06462E-6	1.6798367E-9	9.9751E-4	0.13032436
5.0	18.0	5.06539E-6	2.449724E-9	0.0014546795	0.15638927
6.0	21.0	5.06865E-6	5.7098077E-9	0.0033905618	0.18245412
7.0	24.0	5.07009E-6	7.1499926E-9	0.004245763	0.20851898
8.0	27.0	5.07232E-6	9.380074E-9	0.0055700163	0.23458388
9.0	30.0	5.07481E-6	1.1869815E-8	0.0070484583	0.26064873
10.0	33.0	5.07358E-6	1.0639724E-8	0.0063180136	0.28671363
11.0	36.0	5.0754E-6	1.2460077E-8	0.0073989644	0.31277853
12.0	39.0	5.08343E-6	2.0490006E-8	0.012167245	0.3388434
13.0	42.0	5.08391E-6	2.0969765E-8	0.012452133	0.36490825
14.0	45.0	5.09577E-6	3.283003E-8	0.019494921	0.39097315
15.0	48.0	5.09741E-6	3.446985E-8	0.020468667	0.41703796
16.0	51.0	5.08848E-6	2.5539975E-8	0.015165988	0.4431029
17.0	54.0	5.10006E-6	3.7120117E-8	0.022042435	0.46916777
18.0	57.0	5.10711E-6	4.4170065E-8	0.026228787	0.4952326
19.0	60.0	5.09419E-6	3.1249783E-8	0.018556548	0.52129745
20.0	63.0	5.09433E-6	3.1389845E-8	0.018639721	0.5473624
21.0	66.0	5.09563E-6	3.2689968E-8	0.01941175	0.57342726
22.0	69.0	5.10488E-6	4.1939984E-8	0.024904538	0.59949213
23.0	72.0	5.09907E-6	3.613013E-8	0.021454565	0.62555707
24.0	75.0	5.10214E-6	3.920013E-8	0.023277573	0.65162194
25.0	78.0	5.10066E-6	3.771993E-8	0.02239861	0.6776868
26.0	81.0	5.09983E-6	3.6890015E-8	0.021905797	0.7037516
27.0	84.0	5.10394E-6	4.100002E-8	0.024346374	0.7298165
28.0	87.0	5.11297E-6	5.002994E-8	0.029708464	0.7558814
29.0	90.0	5.10885E-6	4.590993E-8	0.027261943	0.7819463
30.0	93.0	5.11686E-6	5.3919848E-8	0.03201834	0.80801123
31.0	96.0	5.1067E-6	4.3759883E-8	0.025985217	0.8340759
32.0	99.0	5.11378E-6	5.0839844E-8	0.030189395	0.860141
33.0	102.0	5.11235E-6	4.941012E-8	0.029340405	0.8862058
34.0	105.0	5.11078E-6	4.7839876E-8	0.028407974	0.9122707
35.0	108.0	5.11112E-6	4.8180027E-8	0.02860996	0.93833554
36.0	111.0	5.11758E-6	5.4639713E-8	0.03244581	0.9644004
37.0	114.0	5.11862E-6	5.567972E-8	0.033063382	0.9904652
38.0	117.0	5.11481E-6	5.1869847E-8	0.030801026	1.0165303
39.0	120.0	5.11597E-6	5.3029908E-8	0.031489886	1.0425949
40.0	123.0	5.11785E-6	5.4909833E-8	0.03260621	1.06866

0.1

50

5.06294E-6

RESULTS

index 586

DI 8.688293E-5

imax 1.6840299E-6

DI/L^2 15.300082

ttag 1760.9998

Deff 9.464322E-7

Co(mol/cm^3) 4.1912915E-7

Co(g/cm^3) 4.2244028E-7

Co(ppm) 0.053473454

Calculate

Permeation Current Chart

Normalized Flux Chart

CHART RESULTS

Fick's Fit Deff 9.2843214E-7

lIno's Fit Deff 4.5746433E-6

lIno's Kappa 1.0E-4

lIno's Lambda 22.0

lIno's My 6.29999999999999945

lIno's Residual 0.3790419101715088

lIno's Runtime 2

Update

Appendix C: Application Editions

Displaying all editions of the application, date uploaded, and the modifications made.

Edit #	Date	Changes
1	06.02.2015	<ul style="list-style-type: none">- Changed charts into JFreeChart components- Made <i>ScrollView</i> component into table
2	17.02.2015	<ul style="list-style-type: none">- Made crosshairs to show in charts where the cursor points in coherence with both axis.
3	25.02.2015	<ul style="list-style-type: none">- Displaying maximal current- Changed specimen areal from 4.9 to 4.4- Changed name of initial noise to background current
4	02.03.2015	<ul style="list-style-type: none">- Added thickness input text field- Started low pass filter implementation, button removes current graph
5	03.03.2015	<ul style="list-style-type: none">- Low pass, high pass, and restore button implemented for current and permeation graph- Results mediocre, needs better filtering function

6	10.03.2015	<ul style="list-style-type: none"> - Downloaded Papyrus, and used it to make a class diagram - More comments made to code, making it easier to understand
7	18.03.2015	<ul style="list-style-type: none"> - Made save and write function in class <i>CurrentChartModel</i>, to save data series, and write multiple in same plot. - Needs buttons for the two methods above
8	20.03.2015	<ul style="list-style-type: none"> - Added buttons to add two more transients, and save the first transient for both charts - Added Fick's curve for the permeation chart
9	27.04.2015	<ul style="list-style-type: none"> - Added Fick's curve for current and permeation chart - Fick's curve is now based on earlier found diffusion coefficient
10	29.04.2015	<ul style="list-style-type: none"> - Added numerical approach to Fick's curve, using the least squares method
11	08.05.2015	<ul style="list-style-type: none"> - Added method for Iino's approach (almost finished)

		- Added buttons for Fick's and Iino's numerical approaches
12	09.05.2015	- Working on numerical approach to Iino's method - Diffusion coefficient part working, my coefficient under investigation
13	11.05.2015	- Implemented several <i>ArrayLists</i> , to iterate through more my values and diffusion coefficients at the same time - Some problem with the printing
14	12.05.2015	- Finished all methods which increase parameters - No reason to increase kappa - Need to increase speed of analysis
15	14.05.2015	- Started to redefine variables locally instead of globally to reduce storage use - Efficiency of Iino's method increased by 80%
16	15.05.2015	- Removed Iino's curve for predefined diffusion coefficient

		- Made button for Iino's curve fit
17	16.05.2015	- Finished buttons for Fick's curve, Fick's elapsed time and Fick's fit for both current and permeation chart - problems with Fick's lattice in both charts, and Iino's in current chart - Made chart result table
18	19.05.2015	- Fick's lattice problems and Iino's problems fixed in both charts - Filters added for Iino's method, buttons in both charts added - New sample data gives problems for Iino's method, need to define boundaries
19	21.05.2015	- Added boundaries applicable for both samples
20	22.05.2015	- Analyzing different boundary conditions - Fitting bigger piece of the curve - Big runtime problem
21	23.05.2015	- Defining boundary and initial conditions in an array,

		and making them dynamic through three graph generations, for the Iino method permeation chart
22	24.05.2015	<ul style="list-style-type: none"> - All functionalities enabled for current chart as well - Commenting finished up - Iino's high filter repaired
23	25.05.2015	<ul style="list-style-type: none"> - Name of file included in frames - Names changed to more intuitive names - Concentration computing bug fixed - Iino's time included
24	26.05.2015	<ul style="list-style-type: none"> - Implemented double click DUI noise remover - Update field updates all data after noise removal - Iino changed to IIno
25	27.05.2015	- Update button, only updates charts that are open, changes that are not updated before chart windows are closed will be lost
26	28.05.2015	- Names of chart buttons, and titles over charts changed to

		<p>more appropriate names</p> <ul style="list-style-type: none"> - Timer for current chart fixed
27	29.05.2015	<ul style="list-style-type: none"> - Flags in <i>ResultView</i> for flux and current running implemented - Float variable obstructing current chart Iino low pass filter changed to double
28	03.06.2015	<ul style="list-style-type: none"> - Some fields converted to local variables, and every field declared either public or private - Setters and getters implemented for private fields - Residual threshold increased in normalized flux chart to fit complex experiment data
29	05.06.2015	<ul style="list-style-type: none"> - Fixed Iino curve print out length
30	06.06.2015	<ul style="list-style-type: none"> - Names of methods changed to more sensible ones
31	07.06.2015	<ul style="list-style-type: none"> - Changed name of methods and fields from Iino to Iino
32	08.06.2015	<ul style="list-style-type: none"> - Fixed method and field names

Appendix D: Hope Data

The list in this appendix contains data received from Hope which she performed during her master thesis [36], using the application developed in this work. Single and double, specifies how the material have been emptied for hydrogen, either by extraction from either sides, or only one side. BM and HAZ are short for Base Material and Heat Affected Zone, respectively, and specify the materials properties. Quotient is Iino's D_{eff} Divided by the elapsed time D_{eff} .

Material	Temp	Specs	$\mu\text{A}/\text{cm}^2$	Trans	D_{eff}	Iino's D_{eff}	Quotient	Lambda	My
FeSi	30	Single	-150	1	3.61E-07	1.75E-06	4.85	7	1.6
				2	4.01E-07	1.69E-06	4.21	7	1.6
				3	4.17E-07	1.76E-06	4.22	8	1.9
			-10	1	1.95E-07	9.74E-07	4.99	49	11.2
				2	2.44E-07	1.22E-06	5.00	49	10.8
				3	2.25E-08	1.12E-06	4.98	49	10.9
		Double	-150	1	7.93E-07	2.97E-06	3.75	5	1
				2	7.62E-07	3.17E-06	4.16	6	1.3
				3	7.80E-07	3.27E-06	4.19	8	1.8
	50	Single	-150	1	6.02E-07	2.96E-06	4.92	14	3.4
				2	6.35E-07	3.33E-06	5.24	16	3.7
				3	Noisy				
			-10	1	4.73E-07	2.96E-06	6.26	12	2.4
				2	4.16E-07	1.93E-06	4.64	9	2.1
				3	3.24E-07	3.12E-06	9.63	12	3.1
			-100	1	6.63E-07	2.56E-06	3.86	5	1
				2	Noisy				
				3	Noisy				
			-50	1	4.93E-07	2.44E-06	4.95	10	2.3
				2	5.96E-07	2.98E-06	5.00	11	2.4
				3	5.59E-07	2.64E-06	4.72	9	2.1
		Double	-150	1	1.47E-06	6.13E-06	4.17	9	2.1
				2	1.55E-06	6.44E-06	4.15	9	2.1

				3	1.43E-06	5.73E-06	4.01	8	1.9
	75	Single	-150	1	1.31E-06	6.94E-06	5.30	19	4.6
				2	9.85E-07	5.71E-06	5.80	27	6.3
				3	8.61E-07	4.75E-06	5.52	26	6.3
		Double	-150	1	3.90E-06	1.75E-05	4.49	17	4.2
				2	Noisy				
				3	2.61E-06	8.61E-06	3.30	4	0.8
X70	30	BM1	Undefined	1	2.00E-06	8.59E-06	4.30	12	2.9
				2	2.05E-06	8.46E-06	4.13	10	2.4
				3	2.14E-06	8.70E-06	4.07	10	2.4
		HAZ1		1	1.75E-06	7.48E-06	4.27	14	3.3
				2	1.13E-06	6.90E-06	6.11	26	5.5
				3	1.09E-06	5.00E-06	4.59	10	2.4
		BM2		1	2.23E-06	8.21E-06	3.68	8	1.8
				2	3.32E-06	1.59E-05	4.79	23	5.5
				3	3.29E-06	1.49E-05	4.53	19	4.6
	50	BM1	1	9.57E-06	5.22E-05	5.45	890	2025	
			2	Noisy					
			3	5.15E-06	1.55E-05	3.01	4	0.8	
		HAZ1	1	Noisy					
			2	1.71E-06	8.36E-06	4.89	12	2.8	
			3	2.59E-06	1.29E-05	4.98	16	3.7	
	75	BM1	1	Noisy					
			2	7.61E-06	3.68E-05	4.84	13	3	
			3	9.90E-06	4.53E-05	4.58	15	3.5	
		HAZ1	1	6.08E-06	3.18E-05	5.23	28	6.6	
			2	6.91E-06	3.39E-05	4.91	27	6.4	
			3	Noisy					
			1	Noisy					
			2	5.12E-06	2.13E-05	4.16	12	3	
			3	6.44E-06	3.44E-05	5.34	91	20.8	